A biophysical study of the mechanotransduction of cells in controlled multi-dimensional microenvironments

Ng, Soon Seng

2011

Ng, S. S. (2011). A biophysical study of the mechanotransduction of cells in controlled multi-dimensional microenvironments. Doctoral thesis, Nanyang Technological University, Singapore.

https://hdl.handle.net/10356/47727

https://doi.org/10.32657/10356/47727

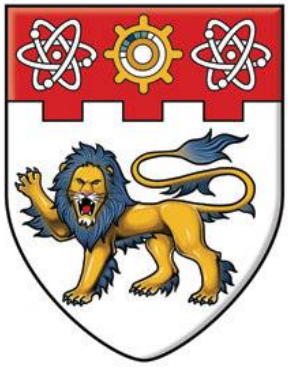

NANYANG TECHNOLOGICAL UNIVERSITY

A BIOPHYSICAL STUDY OF MECHANOTRANSDUCTION OF CELLS IN CONTROLLED MULTI-DIMENSIONAL MICROENVIRONMENTS

NG SOON SENG

SCHOOL OF CHEMICAL AND BIOMEDICAL ENGINEERING

2011

A Biophysical Study of the Mechanotransduction of Cells in Controlled Multi-dimensional Microenvironments

NG SOON SENG

School of Chemical and Biomedical Engineering

A thesis submitted to the Nanyang Technological University
in partial fulfilment of the requirement for the degree of
Doctor of Philosophy

2011

To my grandmother (Kam Har), grandfather (Chew Keong), mother (Peck Kew),
and father (Fook Ming)

ACKNOWLEDGMENTS

I am deeply indebted to my thesis advisor, Assoc. Prof. Vincent Chan, who has guided me throughout my thesis with his patience and knowledge whilst giving me the freedom to develop in my own way. Without his inspiration and encouragement, it would not be possible for me to complete this dissertation. Besides,I sincerely thank my co-supervisor, Assoc. Prof. Mary Chan, who has given me enormous research idea in the field of cardiovascular tissue engineering.

I have been granted the opportunities to collaborate with several excellent researchers; working with them was a fun and life-long memorable experience. Firstly, I attributed my first publication to Assoc. Prof. Li chuan from National Central Univerisity, Taiwan, in sharing his knowledge in finite element method generously and correcting the manuscript uncountable times. Secondly, I thank Assoc. Prof. Wang Dong-An and his Ph.D. student Mr. Su Kai, for providing their excellent chondrocyte culture system for the biomechanical analysis of three-dimensional microenvironment.I'm indeed grateful for their insightful comments and fruitful discussion which improved the clarity of my research.

I want to extend my gratitude to our research team for helping me to establish my experiments and workplace, they are Ms. Chen Beiyi, Mr. He Tao, and Mr. Li Xi. They were always there to help me in every single aspect that I could possibly encounter. My appreciation also extends to all the staffs and phD colleagues from various laboratories. I want to thank them for all their help, support, and valuable advice. Especially I am obliged to Dr. Poon Yin Fun, Ms.

Cao Ye, Ms. Liu Yunxiao, Mr. Xiong Yun, Dr. Chen Long Qing, Dr. Shahrzad, Dr. Gavin, and Mr. Li Peng.I also would like to say thanks to all other colleagues who are generous to lend me their equipments, to give me the trainings and to share with me their experimental skills.

Most important of all, I am indebted to my grandparents and parents who provide me with everything throughout my life.

ABSTRACT

Cells are mechanically coupled to the surrounding microenvironment which acts as local physical cues for triggering cells to carry fundamental activities. In the quest of understanding mechanotransduction of cells, it is essential to reveal the biocomplexity paradigm underlying cellular behaviors which are believed to be derived from the collective interactions among multiple signaling pathways. However, the study of cellular biomechanics is significantly impaired due to the great difficulties in developing characterization methods for probing mechanical responses in the sub-cellular level. Therefore the main objective of my thesis is to develop biophysical techniques for probing the biomechanical responses of cells in different culture systems and for facilitating the development of innovative and robust tissue-engineered platforms.

Cell traction force microscopy (CTFM) has been recently developed to measure traction force generated by cell towards a deformable support. Cell traction force is a direct representative parameter of intracellular contractility established by the dynamic force equilibrium between cell and microenvironment. The implementation of micro-characterization by atomic force microscopy, Mooney-Rivilin constitutive law as the material model, and finite element method (FEM) in the force computation allowed us to analyze the three-dimensional (3D) stresses with higher accuracy and efficiency compared with previously reported methods.

The shape of the vascular smooth muscle cells (SMCs) have been known as the fundamental characteristics of the vasoactivity in cardiovascular physiology. In

order to investigate the effects of cells shape on cell traction force distribution, micro-contact printing technique and microchanneled scaffolds were introduced in the fabrication of highly controlled cell culture systems. It was found that the cell spreading area was linearly related to the overall intensity of traction force, whereas the cell elongation factor was governing the orientation of traction force. SMCs with high aspect ratio exhibited highly regulated force orientation along the cell long axis due to the organization of stress fiber and the preferential membrane extension along the cell long axis. SMCs seeded on microchanneled scaffold were first appeared as synthetic and proliferative and adopted contractile phenotypes upon confluence. Due to the microtopographic features, SMCs seeded at the edges of microchannels adopted elongated morphology and established significant traction force due to the extra dimensionality provided by microwalls. The forces were found to be propagated from the edge to the centre of microchannels via the cell-cell interactions to promote contractile phenotype and cell alignment at confluence. The effects of microtopographic features on the collective traction force in the formation of aligned cell sheet were first demonstrated to study the biophysical interactions among multiple cells and microenvironment.

Lastly, the encapsulated chondrocytes in the 3D hydrogel were observed to exhibit abundant neo-tissue outgrowth at the edge of the hydrogel, this phenomenon was thus termed as “edge flourish” (EF). In order to fully elucidate EF phenomenon in the cartilage tissue engineering, in-depth biomechanical characterizations of such phenomenon are needed. Histological staining, 3D multiple-particle tracking assay, and newly developed surface tension

characterization assay were introduced to elucidate the mechanobiological activities of EF phenomenon. This phenomenon was shown to be driven by the oriented outgrowth of chondrocytic isogenous groups located along the edge of hydrogel. The isogenous groupsexhibited directed outgrowth towards the surface of the hydrogel and gradually generated substantial surface tension on the interface of hydrogel and medium. Ultimately, the encapsulated chondrocytes closest to the hydrogel/medium interface sprouted out of the hydrogel spontaneouslyto form a layer of rich proliferative and chondrocytic extracellular matrix secretive chondrocytes at the surface of hydrogel. The in-depth understandings of neo-tissue formation in 3D microenvironment are expected to inspire the innovative hydrogel scaffold for cartilage or bone tissue engineering.

TABLE OF CONTENTS

LIST OF TABLES

LIST OF FIGURES

LIST OF ABBREVIATIONS

2D	Two-dimensional
3D	Three-dimensional
A.R.	Aspect Ratio
AFM	Atomic Force Microscopy
BIS	Bis-acrylamide
BSA	Bovine Serum Albumin
c-AMP	Cyclic-adenosine Monophosphate
CCM	Chondrocyte Culture Medium
CTFM	Cell Traction Force Microscopy
DIC	Digital Image Correlation
DMEM	Dulbecco’s Modified Eagle Medium
DRIE	Deep Reactive Ion Etching
EC	Endothelial Cell
ECM	Extracellular Matrix
EDTA	Ethylenediaminetetraacetic Acid
EF	Edge Flourish
F-actin	Fibrous Actin
FAK	Focal Adhesion Kinase
FBS	Fetal Bovine Serum
FEM	Finite Element Method
FFT	Fast Fourier Transform

FITC	Fluorescein Isothiocyanate
FT	Fourier Transform
FTTC	Fourier Transform Traction Cytometry
GAG	Glycosaminoglcan
GTPase	Guanosine Triphosphatase
HEPES	4-(2-hydroxyethyl)-piperazine-1-ethanesulfonic acid
LINC	Linker of Nucleoskeleton and Cytoskeleton
MAPK	Mitogen-activated Protein Kinase
mRNA	Messenger Ribonucleic Acid
MSC	Mesenchymal Stem Cell
NEAA	Nonessential Amino Acid
PAG	Polyacrylamide Gel
PBS	Phosphate-buffered Saline
PCM	Pericellular Matrix
PDGF	Platelet-derive Growth Factor
PDMS	Poly(dimethyl siloxane)
PIV	Particle Image Velocimetry
PTCC	Phase Transfer Cell Culture
RMS	Root-mean-square
RNA	Ribonucleic Acid
ROCK	Rho-associated protein kinase
SMC	Smooth Muscle Cell
Sulfo-SANPAH	Sulfosuccinimidyl-6(4’-azido-2’-nitrophenylamino) Hexanoate

TEMED	N,N,N′,N′-Tetramethylethylenediamine
TGF β	Transforming Growth Factor-β
μCP	Micro-contact Printing

Chapter 1 Introduction

1.1 Background

The advancement in molecular biology has given valuable insights into the intracellular mechanism of cell signalingin response to various biochemical cues and revolutionized the fundamental research of life sciences. In the quest of discovering discrete events that contribute to the mechanism of cellular activity, it is clear that the investigation of biochemical signal transduction alone could not complete the entire puzzle. Therefore the current focus in biology and medicine is shifting from reductionism to a more integrativeparadigm where the collective interactions among multiple components including mechanical forces are put into consideration. Mechanical forces experienced by living organisms varied from whole-body forces like gravity and musculoskeletal movement to tissue-specific forces like shear stress on blood vessel and compressive stress on cartilage [1-3]. The ability of cells in sensing and reacting to mechanical forces via a cascade of intracellular signaling is defined as mechanotransduction.

In contrast to the early understanding of intracellular structures where cell is filled with viscous protoplasm, cell is actually supported by architectural framework known as cytoskeleton[4].Cytoskeletal framework enables mechanochemical transduction by linking the external mechanical forces with the internal force within cell through ‘tensegrity’ principle. This dynamic force equilibrium known as isometric tension or prestress is balanced by cytoskeleton, extracellular matrix (ECM), and transmembrane protein. By forming the isometric tension, cells are able to react actively towards the

external forces by rearranging the cytoskeletal and nucleoskeletal organization in order to reestablish the force equilibrium[5, 6].The reestablishment of intracellular organization is found to trigger multiple signaling transductions and in turn regulate the cellular activities [7, 8].Therefore, this is the primary motivation for scientist to study the pre-dominant driving forces which is known as cell traction force anchoring between cell and external environment in mechanobiology.

With the growing interests in mechanobiology, much attention has been given to the bio-mechanistic studies of cell and tissue responsesin native microenvironment with different structural cues. In tissue engineering, the combination of cell, scaffold, and soluble cues alone is insufficient in reproducing the *in vivo*tissue-specific phenotypes that contribute to the particular biological functions[9]. In contrast, the seamless integration of cells with their surrounding microenvironment is critical to the development of tissue with specialized physiological functions. Numerous studies have suggested that the force balance generated by the cells with their local microenvironment plays an important role in dictating the intracellular structure and 3Dtissue organization and thus regulating the cellular phenotypes and tissue behaviors [10-13]. While the study of biochemical signal transduction is relatively matured, the study of mechanical cues from the physical microenvironment is significantly impaired due to the practical difficulties in fabricating the mechanical signals in sub-cellular level. Recent advances in microfabrication technique have contributed to the development of *in vitro* culture systems that recapitulate the micron- and nanoscale parameters that define the physical microenvironmental characteristics [14]. This enables us to perform systematic analysis to unfold the essential components that assemble the biocomplexity of mechanobiology

with a well-controlled microenvironment.

1.2 Objective and Scope

The overall goal of my PhD project is to develop a direct quantitative assay to characterize the cellular mechanobiological responses in various cell culture systems from two-dimensional (2D) constraint to microtopographical features and 3D matrix. The developed models in this thesis are expected to facilitate the characterization of mechanotransduction in a more efficient and thorough approach, as well as to provide a fundamental cellular understanding for the development of more innovative and robust tissue engineered models.

The specific aims of this thesis arelisted as follows:

1. To develop an improvised biophysical assay based on cell traction force microscopy with the aim of incorporating the hyperelastic properties of substratum into the finite element analysis to increase the accuracy and efficiency of the traction force calculation.
2. To manipulate the cell spreading and adhesion using micro-contact printing technique to study the mechanotransduction of vascular SMCs under different geometric constraints.
3. To characterize the collective behaviours of multiple vascular smooth muscle cells in the formation of highly aligned cell sheet with contractile phenotypic characteristicsdue to the present of microtopographical features that are crucial in the cardiovascular tissue engineering.

4. To study the biomechanics of the encapsulated chondrocytes in the 3D culture system in the purpose of promoting cell proliferation and chondrocytic ECM secretion that are crucial in the cartilage regeneration.

1.3 Outline

This thesis is divided into six chapters. In Chapter One, the background of the mechanobiology is provided and the objectives and the outlines of this thesis are described. Chapter Two contains the literature reviews of the development of mechanobiology, in particular, the significance of mechanobiology in different disciplines, and the current direction of the bio-mechanistic studyof cells in different microenvironments. In Chapter Three, the drawbacks of the current approach in CTFM are discussed in detail and the respective solutions are proposed. In brief, the ultra-sensitive micromechanical characterization and the FEM are developed to analyze the cell traction force using the hyperelastic model (Mooney-Rivlin) in 3D approach. In Chapter Four, the newly developed CTFM assay is incorporated with different nanolithography techniques to study the vascular SMCbiomechanics in different geometric constraints for discovering the role of cell morphology in vasoactivity. The micro-contact printing (μCP) technique is utilized in the ECM protein conjugation in order to manipulate the cell shape on a 2D surface. In addition, the hot-embossing technique is used to fabricate 3D scaffold that provides the microtopographical features to direct the cell alignment. Chapter Four extends the mechanotransduction study from 2D platform to 3D matrix. Bio-mechanistic study of encapsulated chondrocytes in agarose hydrogel is carried out to investigate the ‘edge flourish’ phenomenon. Several biophysical assays are developed to characterize the real time cell proliferation

distribution, 3D cell movement, and mechanical interaction between the encapsulated cells and hydrogel surface. In the last chapter, conclusions are made and possible future work is discussed.

Chapter 2 Literature Review

2.1 Tensegrity-based cytoskeletal framework

The physical structure of the eukaryotic cell is supported by the molecular framework known as cytoskeleton. Unlike the protoplasmic model that was proposed century ago, where the structure of cell was assumed to be like an elastic balloon filled with viscous fluid, the cytoskeleton model is supported by three different filaments known as microfilaments, intermediate filaments, and microtubules. With the development of immunobiology and electron microscopy, the architectural organization of the interconnected cytoskeletal filaments was revealed [15, 16]. The microtubules are the thickest cytoskeletal filaments composed of α- and β-tubulin dimmers in the bundle of hollow cylindrical filaments. These thick filaments are served as the basic structural components in resisting compression in the intracellular environment and involved in many cellular activities such as cytokinesis, vesicular transport, and mitosis. The intermediate filamentsare the most prominent cytoskeletal components in cell which withstand the major mechanical stresses experienced by the individual cell. Generally, there are five different types of intermediate filaments in the cytoplasm and nucleoplasm of all cell types. One notable type of intermediate filaments is the Type V intermediate filament, also known as lamin, that span across the inner nuclear membrane. This filamentous structure on the inner nuclear membrane is a vital medium for the transmission of mechanical forces in mechanochemical transduction. Lastly, microfilaments in conjunction with myosin filaments are responsible in the generation of tensile forces. The combination of microfilaments (actin filaments) and myosin is known

as stress fiber and is critical in many cellular activities such as muscle contraction, motility, and cytokinesis.

In protoplasmic model, cells are assumed to withstand external mechanical forces and maintain the cell shape by outward pressure originated from the viscous fluid within an elastic membrane. Recently, an architectural concept known as ‘tensegrity’ (tensional integrity) was proposed by Ingber *et al.* to model the tensional prestress sustaining the shape and structure of living organisms [5, 6, 17, 18]. Fuller *et al.* first described the tensegrity as a building principle that stabilizes shape and structure by isometric tension. The tensegrity framework is distinguished by the way forces are distributed and balanced within the network of structure. Tensegrity framework consists of a network of continuous cables which is always under tensional prestress and distributed throughout the structure, this tensed network is stabilized by incorporating local discontinuous compression components and the anchorage sites as shown in Fig. 2.1 [19]. As a result, the mechanical stabilization of the cell structure is maintained by the isometric tensional prestress that make it resilient towards shape distortion.

Several studies have revealed that the tensegrity model correctly describes the cytoskeletal framework that contributes tothe sustainability of the shape and structure of cell. Three types of cytoskeletal filaments together with the anchorage sites in cells are mechanically integrated using the tensegrity model to form an interconnected molecular network. The tensile forces generated by the actin and myosin filaments are distributed throughout the cells and counterbalanced by several compression components, most notably the microtubules and the anchorage sites on the cell membrane. The presence of prestressed fibers in cell has been recently proven by biophysical study using laser

nanoscissor and fluorescent photobleaching methods [20]. Laser nanoscissor was used to sever a single stress fiber of a well spread endothelial cell on elastic substrate. Both ends of the severed stress fiber were observed to retract towards the opposite direction immediately just like the way tensed cable behaves after being cut open. Furthermore, the group demonstrated that the disruption of a single stress fiber compromised the force balance of the entire cell, and triggered the cytoskeleton remodeling which resulted in significant changes in cell shape [20]. This result supported that the interconnected cytoskeletal network was under isometric tension prior to the disruption. The inwards tensile forces spanning across the cell surface via the distribution of stress fibers enables the cell to spread out. This is particularly important for anchorage-dependent cells because they first establish physical attachment with the substrate in order to perform critical cell activities such as proliferation, differentiation, migration, etc [21-28]. Moreover, the prestressed tensegrity state in cell provides a stabilized structure that is able to resist distortion against the external mechanical forcers as well as to offer immediate respond towards mechanical forces in mechanotransduction.

(a) (b)

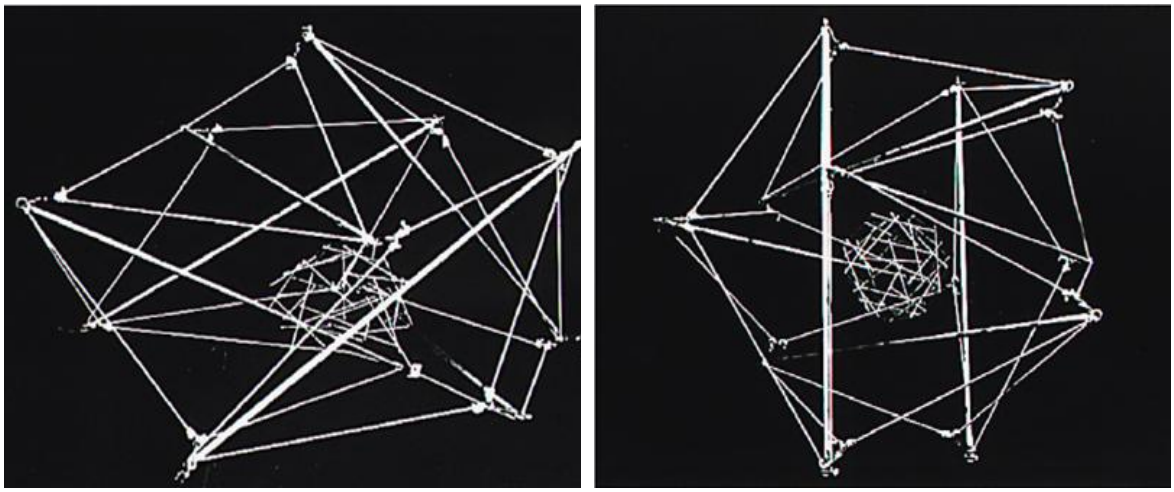

Fig. 2.1 The tensegrity model was built to represent the internal architecture of eukaryotic cell. The anchorage-dependent cell that is attached to the rigid substrate exhibits fibroblast-like morphology. The well spread morphology is coordinated by the elastic thin cords that represent the tensional stress fibers and the rigid thick strunts that represent the compressive microtubules. The nucleus shown in the centre of the structure appears to be polarized due to the tensional continuity in the structure (a). The detached anchorage-dependent cell exhibits rounded morphology due to the lost on anchorage sites with ECM and well distributed tensional stress generated by the tensegrity model (b).

2.2Tensegrity architecture and mechanotransduction

The cytoskeletal framework is physically connected with the transmembrane proteins that are exposed to the external microenvironment at one end, and nuclear anchoring structure known as LINC (linker of nucleoskeleton and cytoskeleton) complex at another end[29-31]. Thus it is plausible to assume that the influences of external mechanical forces arenot just limited to the activation of membrane associated signaling

pathway, but rather propagated to the cytoplasm as well as nucleoplasm to activate the mechanochemical conversion in distant location due to the force induced cytoskeletal rearrangements [32, 33].

The long distance force propagation as mentioned above is only valid under the tensegrity model where the cyto- or nucleoskeletal filaments are interconnected under isometric tension. In the tensegrity model, the applied force from the cell surface concentrates and channels along the stiffened filaments owing to isometric tension. In contrast, the applied external force traveling in the viscous protoplasmic model dissipates rapidly against the reciprocal of the squared distance because the input energy must be equally distributed in homogeneous cytosol [31, 34-36]. The mechanochemical conversion at distant site is believed to be initiated by the conformational changes of the signaling molecules immobilized along the cbackbone of the cytoskeleton in response to the force along the direction of prestressed filaments.In particular, focal adhesion kinase (FAK) and Rho GTPases that are critical in mechano-regulated signaling transduction[22, 37-41].The molecular conformational changes induced by force alter the biochemical properties of the immobilized molecules in ECM and eventually modify the self-assembly of regulatory complexes that are involved in protein and gene expressions [13, 39-46].

Recent studies have revealed that most messenger RNA (mRNA) are specifically immobilized along the backbone of actin filament where mRNA would be released from cytoskeleton using the actin depolymerizing drug [47]. With the use of antibodytagging and electron microscopy, majority of poly (A) mRNA and polyribosomes could be visualized at the cytoskeletal microcompartment that is specialized for translation [48].

These findings strongly suggest that the remodeling of cytoskeleton due to the alteration of isometric tension in response to the external mechanical forces mayregulate the translation of the immobilized mRNA. Once the cells attach to the ECM coated microbeads, the mechanical interaction between the integrin and ECM ligand activates the formation of focal adhesion complex that serves as the physical linkage between cytoskeleton and ECM. In order to establish the isometric tension needed for cell spreading, the cytoskeletal structure is rearranged according to the tensegrity principle. As a result, the rearrangement of cytoskeleton and establishment of prestress promote the formation of the specialized microcompartment that is contributed to the poly (A) mRNA and polyribosomes immobilization and eventually modulate the local gene expression [49].

This direct mechanochemical transduction between cell and external environment is particularly interesting because it provides a more efficient way in transmitting information than the conventionalparadigms based on chemical diffusion and vesicular transport. Furthermore, this signaling model suggests that multiple signaling components can be activated simultaneously by mechanical forces. It provides another perspective on the complex system of cell mechanical behaviors where the cell fate (e.g. differentiation, proliferation, migration) is governed by a collective network interactions among chemical (gene and protein) and mechanical signals known as biocomplexity [50].

2.3Contribution of tensegrity prestress in tissue engineering

Tissue engineering has emerged as the most promising technology in regeneration

medicine where both biology and engineering principles are integrated in the development of engineered tissue equivalents that are aimed to repair, preserve, and enchance tissue functions [51, 52]. One of the fundamental aspects of tissue engineering is the elucidation of the driving forces underlying the growth and development of organisms. It is essential to understand the principle of tissue regeneration in order to engineer an artificial tissue that is able to address the acute shortage of organ transplants [53]. Cell, scaffold, and growth factor are three basic components in tissue engineering. Scaffold provides solid support for cell seeding and the foundation for subsequent cell growth and tissue formation. The mechanical properties of scaffold are critical in the determination of cell fates as the cell senses the mechanical force of the local surroundings and responses accordingly. For instance, mesenchymal stem cell (MSC) relies on the matrix rigidity to determine the lineage fate, the resultant cell fates can be varied from adipogenesis to osteogenesis depending on the scaffold used in the *in vitro* culture[54].

Despite numerous in-depth studies have reportedthe effect adhesive proteins, structural topography, surface chemistry, mechanical properties,and 3D architecture of biomaterial scaffold on cell regeneration, the resultant engineered tissue still falls short in replicating the native tissue functionalityunder *in vivo* environment. Several studies have looked beyond the aforementioned three basic components of tissue engineering and discovered that the missing link to achieve functional engineered tissue equivalents appears to be the mechanical forces from the microenvironment [43, 55]. In order regenerate or engineer functional cells and tissues that are sustainable under *in vivo* environment after transplantation, bioreactor is used in the *in vitro* culture to expose the

developing tissue to appropriate physical stimuli. For instances, perfumed column is designed to control the flow of the medium recirculation to provide the appropriate hydrodynamic shear stress needed in the development of vascular tissue [2].

During epithelial morphogenesis, MSCdepends on the local mechanical cues to determine the specialized growth patterns that eventually give rise to functional tissue. Although soluble factors such as growth factors and generic substrates are vital in the tissue development, yet they do not provide the essential global cue for the formation of functional 3D tissue with unique mechanical properties. Further mechanistic studies of tissue formation revealed that cell heavily relies on the activity and structure of the anchorage formation platform called ‘basement membrane’ to determine the pattern of tissue morphogenesis. Basement membrane is a thin sheet of epithelial ECM matrix formed by the molecular network of various cell-derived ECM proteins such as laminin, collagen, fibronectin, and proteoglycans [56, 57]. In general, tissue morphogenesis like epithelial bud formation was believed to be driven by the anisotropic growth directed by local cell proliferation. However, recent collective cell studies have demonstrated the process of morphogenesis is initiated by the formation of new basement membrane and then followed by the increases in local cell proliferation [58]. The formation of new basement membrane is resulted from local variation of ECM mechanics caused by spatial ECM remodeling. The cells react to the ECM mechanics variation by reorganizing the internal cytoskeletal architecture in order to reestablish the prestress state according to the tensegrity principle. As a consequence, the reestablishment of tensegrity model leads to the specialized cell growth pattern for tissue formation. ECM remodeling in basement membrane is regulated by the ECM turnover rate, where the ECM synthesis rate is higher

than ECM degradation rate which in turn allows the basement membrane to alter its mechanical properties constantly [58].

In the epithelial organ development, metalloproteinases occurred at selective regions where the degradation rate of ECM is accelerated and resulted in thinner and higher compliance basement membrane. In order to sustain the dynamic force equilibrium between cells and ECM, the cell-generated traction force pulls the thin and elastic basement membrane apart in order to maintain the overall isometric tension. As a result, the adhesive cells are elongated together with the stretched basement membrane. The elongated cells are more sensitive towards the soluble mitogens and prone to proliferation and ECM deposition. Since the elongated cells are associated with higher ECM turnover rate and prone to exhibit higher proliferation than the neighboring cells, the mechanical imbalance across the cell-cell junctions may in turn contributes to the spatial variation in cell phenotypes and growth as detected in early embryogenesis [59]. The greater local ECM deposition and cell proliferation lead to lateral extension of compliance basement membrane by folding outwards to form bud-liked structure. This epithelial-mesenchymal interactions observed in the embryogenesis is persistent in the adult tissues where the basement membrane is subjected to constant turnover event in order to retain their ability in morphogenesis.

2.4Contribution of tensegrity prestress in cancer study

Gene mutation and chromatic abnormalities have beenextensively studied for a few decades because the development of cancer is known to be resulted from progressive accumulation of genetically mutated cells. This has driven the focus of cancer research

towards the identification of critical cancerous genes and proteins which eventually lead to the drug development targeting the specific cancerous molecules. However, switching cell behaviors and states are not simply regulated by a linear signaling pathway, but a multiple signaling pathway that requires network of molecular interaction with high level of cross talk known as biocomplexity[5, 50, 60]. As a consequence, some developed cancer drugs in the market that only inhibit a linear signaling pathway associated cancer development lead to severe complexities and side effects. Since the switching of cell behaviors and states are found to be altered by the multiple signaling pathway, mechanical forces that are able to initiate such complex pathway through the tensegrity principle might play an important role in the development of malignant tissue. For instance, several studies showed that the implantation of a piece of rigid metal in animal model triggered the cancer formation, whereas the introduction of the same metal in powder form did not cause cancer formation [61]. Thus, it is essential to consider the role of the epigenetic factors such as structural complexity and mechanical forces in the future development of cancer therapeutic strategies.

One of the epigenetic factors of cancer formation is the properties of ECM. It has been confirmed that cellular behavior such as growth, differentiation, motility and apoptosis can be altered by mechanical forces via the reestablishment of prestress state under the variation of ECM mechanics and proteins[26-28, 62-65].During the early stage of epithelial cancer development, the hyperplastic cells appear to have lost the ability to regulate proliferation and ECM deposition in response to the ECM mechanical variation. Instead of reestablishing their intracellular organization to accommodate the mechanical variation of ECM resulted from a thinner and higher compliance basement membrane,

they develop into a pile of cells known as neoplasia that had lost the ability in regulating cell division and in responding to normal stimuli. Deregulation of cell proliferation alone is not sufficient to develop malignant tissue, other major factors such as the induction of angiogenesis and ability to migrate into blood stream or lymphatic are critical in cancer formation. In the study of multi-step tumorigenesis, the expression of oncogene in the β-cells of pancreatic islet alone did not induce tumor formation. Rather the induction of angiogenesis or neovascularization on the surrounding stroma transformed hyperplasia to neoplasia and might eventually become metastasis if the integrity of basement membrane was compromised [66].

As mentioned above, the neoplasia formation is activated by the induction of angiogenesis and the malignant tissue is initiated by the alteration of the mechanical integrity at the basement membrane. During tissue morphogenesis under high ECM turnover rate induced by metalloproteinases, appropriate cell division and ECM deposition facilitate the formation of bud-liked structure. In contrast, the basement membrane of the cancerous cells is observed to udnergo thickening, reduplication, loosening, and discontinuity. All these would eventually lead to the complete disintegration of basement membrane and enable the cancerous cells to invade the nearby blood streams and lymphatics, thereby metastasize to distant organs[67]. Due to the aforementioned mechanical factors such as ECM mechanics and stroma connective structure involved in the development of cancer tissue, a highly provocative idea was proposed that cancers can be reverted to normal tissues or be quiescent, differentiate, or die, if provided with the correct collection of complex signals, as conveyed by embryonic tissues or other micro-environmental cues as shown in Fig. 2.2 [68].

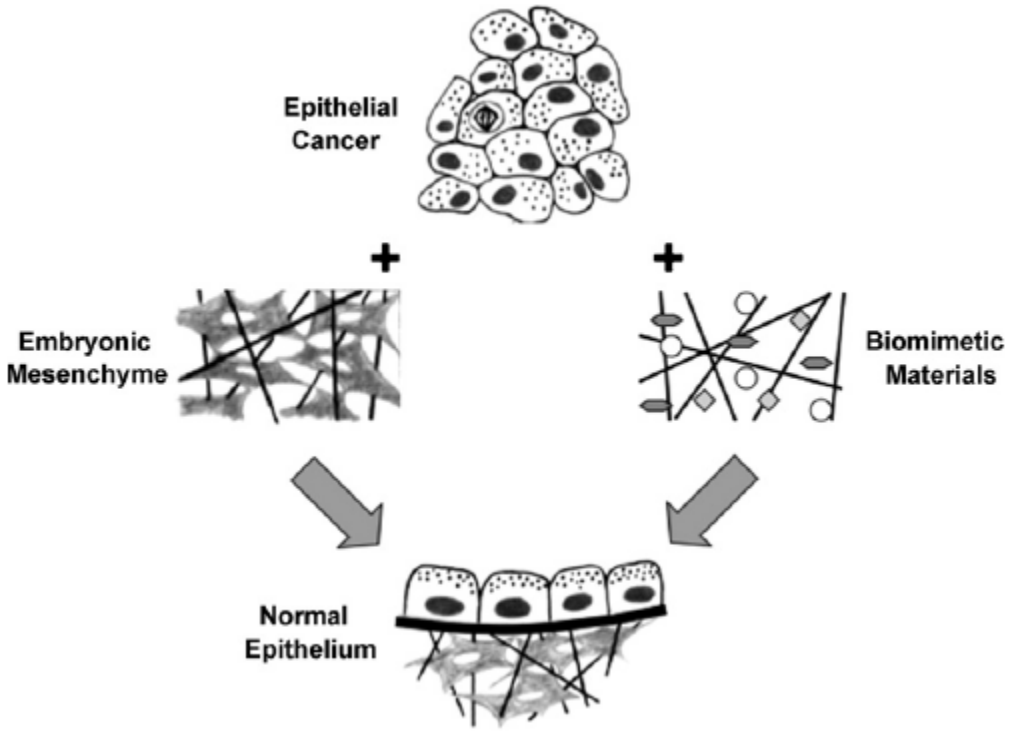

Fig. 2.2 An engineering solution to cancer. Epithelial tumor cells have proved to be reversible using embryonic mesenchyme as basement to restore normal epithelial cells as shown in the left diagram. Synthetic biomimetic materials which mimic the embryonic mesenchyme are the future potential of cancer therapy as shown in the right diagram [67].

2.5Cell traction force

In order to survive, anchorage-dependent cells such as SMCsundergo complex mechanical interactions with the microenvironment and neighboring cells through the formation of focal adhesions and other adhesive structures [23, 64, 69-74]. Various studies showed that once cells attached to a substrate, dynamic force equilibrium among the intracellular cytoskeletal organization, focal adhesions, and ECM is established

instantaneously to generate isometric tension.The internal isometric tension or prestress is the predominant element in cell tensegrity model and it is the major determinant of cell mechanics. In order to establish the tensegrity force balance, compression bearing components acting in opposite direction are needed to maintain the cell shape and structural stability. Several studies have revealed that the degree of cell spreading is dependent on the stiffness of local ECM region acting against the cell generated traction forces in order to stabilize the tensegrity structure[65, 75, 76]. The isometric tension balanced by the tensegrity-based interactions among stress fibers, cell adhesions, and microtubules can be visualized by seeding cells on the substrate with high compliance.In fact, the surface deformation caused by the inward traction forces generated by attached cells is used to quantify prestress within individual adherent cells [77-80].

The inward traction force experienced by the ECM substrate is a bi-directional reciprocal force generated by intracellular acto-myosin. Cell traction force represents the dynamic force equilibrium of the adherent cell with its local ECM mechanics and structure according to the tensegrity principle. Although it does not represent the biochemical reaction of the living cell, yet it does provide a platform to evaluate the state of the internal isometric tension which is responsible for the mechanotransduction. As mentioned above, the state of isometric tension dictates the sensitivity of cells towards the mechanotransduction because the external mechanical forces are imposed on the preexisting force balance. The level of conformational changes caused by the force balance alteration is mediated by the prestressed filaments are the basis of the respective downstream biochemical reaction. More specifically, the modulation is carried out by biochemical molecules through actomyosin interactions and conformational changes in

cytoskeletal architecture. For example, the changes in traction force can activate the integrin-dependent molecules such as RhoGTPase, talin 1, FAK, which then trigger a cascade of signaling pathway and eventually alter gene expressions [81-85].

It is believed that in-depth study of the mechanical interactions that occur at the cell-ECM interface is one of the crucial keys in understanding mechanotransduction. Cell traction forces are generated between cells and the surrounding environment hence they are also known to be an important driving force in multi-cellular processes such as embryogenesis, tissue formation, wound healing, and metastasis [86]. The measurement of cell traction forces involved in mechanotransduction allows scientists to study the bio-mimetic progress of morphogenesis *in vitro* and to monitor the cell behavior under various environmental stimulations. ECMs such as basement membranes are the crucialsignalsin promoting tissue renewal and providing physical interaction between epithelial and mesenchymal cells for epithelial tissues formation in embryo [67]. In addition, alterations in ECM mechanics are found to be mediating cell phenotypes, signaling pathway, gene expression, and the secretions of soluble growth factors through the regulations of cell traction forces [63, 73]. This observation coincided with the process of embryogenesis where the cells grow, migrate, pull, and stretch against one another in a specific region through the generated traction force.

By measuring cell traction forces in various conditions, we can trace the cell signaling pathway from the fundamental factors underlying the cause of many physiological and pathological events in native microenvironments. Fig. 2.3 shows the cellular processes in sensing and responding the external environment through the generation of cell traction force. These mechanical interactionsprovide physical

mechanisms for various basic cell activities such as adhesion, migration, communication, proliferation, and differentiation. Such activities are then collectively drive many biological functions likeembryogenesis, tissue morphogenesis, tumor metastasis, wound healing, etc [8].

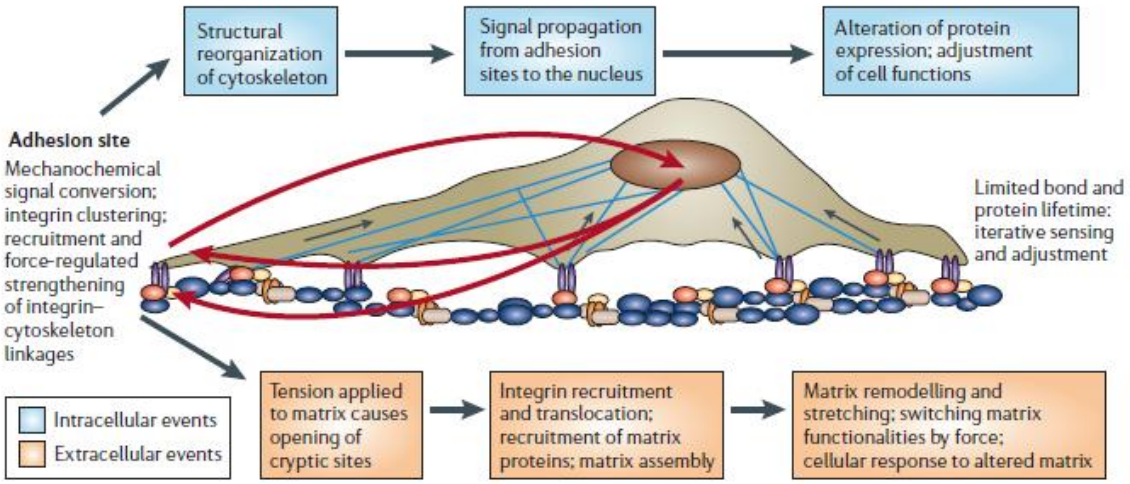

Fig. 2.3 Cellular process of mechano-sensing and responses [87].

2.6 Cell traction force microscopyassay

Unlike the conventional study of biochemical transduction, mechanotransduction is relatively new. The characterization of mechanotransduction requires the integrative knowledge from different expertise across medicine, molecular biology, bioengineering, and software engineering. Therefore, innovative techniquescapable of probing the biophysical activities of cell as well as the intracellular activities under well controlled mechanical cues are challenging. The pioneers in the measurement of cell traction forces are Harris*et al.*, who started the first generation of traction forces measurement in 1980 [77, 88]. They used thin film of silicone rubber as a substrate to detect mechanical forces

exerted by the seeding cells. The degree of cell wrinkling on the surface that caused by cell traction forces has been used as the quantitative measurement for the cell traction force map [77]. However, Barton and Taylor discovered that the wrinkle approach as mentioned above was hard to draw conclusion on the cell traction force measurement due to the highly intricate wrinkle-force correlation and the low resolution of traction force map [79]. In 1994, the second generation of traction force measurement assay was developed by Lee *et al*.to measurethe traction forces generated by rapidly moving cells. Lee *et al*.applied silicone substrate with embedded small beads as markers for tracing the gel deformation that was caused by cell traction forces. The direct quantitative method as mentioned above is known as 'elastic substratum method' [78]. This approach is suboptimal because of irreversible deformation of silicone caused by viscous component and low degree of cell adhesion. Nonetheless, the approach propelled the development of cell traction forcemeasurement. In 1999, Wang and Dembo developed a method called cell traction force microscopy. This method is similar to that developed by Lee et a,the main difference between the two techniques was the substitution of silicon substrate with polyacrylamide gel (PAG) [80]. PAG possesses many advantages over silicone because itselasticity can be easily tuned for all kinds of cell by changingthe reaction condition of arylamide polymerization. Furthermore, cell adhesion on PAG is not significant without the conjugation of adhesive ligands, hence it is a perfect model system for studying mechanotransduction in a highly controlled and defined environment.

In CTFM, the fluorescent microbeads embedded underneath the PAG surface serve as the markers to trace gel deformation under the influences of cell traction force. The displacement vector field is obtained according to the movement of embedded

microbeads. In the computation of cell traction force, Dembo and Wang first assumed that PAG is an infinite half-space substrate with linear elastic properties. By utilizing the linear elastic model associated with the characterization of PAG's Young's modulus, the estimated surface displacement $u(i)$can be used to calculate the corresponding traction force $F(j)$ via an integral transform, $u(i) = \int dr' G(r)F(j)$. This inverse problem can be solved by the forward model formulated earlier by Pelham and Wang [89, 90]. The 2D Green's compliance tensor $G(r)$in the integral transform can be determined by applying a simple yet elegant solution called Boussinesq theory. By assuming the displacement of the surface is infinitely significant than the thickness of substratum, the Boussinesq solution for the displacement $r_x = x_i - x_j$, $r_y = y_i - y_j$ caused by a point surface force can be expressed as $G(r) = \frac{1+\gamma}{\pi E r^3}\begin{bmatrix}(1-\gamma)r^2 + \gamma r_x^2 & \gamma r_x r_y \\ \gamma r_x r_y & (1-\gamma)r^2 + \gamma r_y^2\end{bmatrix}$, where $\gamma$is Poisson's ration, E is the Young'smodulus of the substratum, and $r = \left(r_x - r_y\right)$[80]. They first divided the projected area of the cell into quadrilaterals using paving algorithm and only considered the displacement within the cell boundary as a constraint. The computation of cell traction forcefrom fluorescent bead displacementsposed by Dembo and Wang is subjected toill-posed due to the calculation of inverse problem. Therefore, explicit regularizations are required to constraint the recovery system from yielding large variation solution due to the minor perturbation (e.g. noise) from the estimated displacement field [72]. Heavy explicit regularization such as smoothing and mapping algorithms were introduced to regularly estimate the parameters of traction force under a constraint approach. A more recent and simplified computation approach established by Butler *et al.* utilizes Fourier transform (FT) to convert the complicating Fredholm integral into a simple multiplication [91]. Force and displacement vector maps are located on the

respective nodes which can be viewed as an implicit form of regularization, where the high frequency components has been limited to avoid unrealistic solution due to ill-posed condition like microscopic noises. The key difference is that Fourier transform traction cytometry(FTTC) works in the Fourier space for the Fredholm integral, it requires no smoothing operation and hence less complex computation. In addition, FTTC is either bound constrained or unconstrained way to determine the cellular traction force.

Even though Boussinesq solution is generally utilized in the computation of cell traction force, yet it is found to be error-prone because the thickness of the substratum is not infinite compared with the surface deformation. Yang *et al.* evaluated such error by using 3D FEM analysis. A point force was used as the boundary condition on a discretized model composed of elements with similar mechanical properties and degree of freedom as the real time substratum in the cell traction force microscopy. Models with different gel thickness varied from 1000 μm to 70 μm were built to evaluate the mechanical responses towards the point force on the surface according to the thickness of substratum. When the gel thickness was higher than 1000 μm, the mechanical responses obtained from the FEM analysis and Boussinesq solution were identical as expected. When the thickness was reduced from 1000 μm to 70 μm, the Boussinesq solution revealed significant larger induced displacement in comparison with FEM analysis, and the rate of decay was found to be 1/r faster in Boussinesq solution. The result indicates that the conventional cell traction force computation lead to a solution which is significantly higher than the actual traction force [92]. Therefore, the assumption of finite half-space adopted by Dembo and Wang might result in substantial errors in the computation of cell traction force because the thickness of the gel is recommended not to

be more than 500 μm in order to prevent involuntary bulk lateral vibration.

Furthermore, the CTFM highly depends on the mechanical responses of substratum towards the influences of cell traction force. Thus it is critical for us to determine the precise characterization of the PAG mechanical properties. To date, linear elastic model is widely used to describe the deformation of PAG caused by cell traction force. Linear elastic properties were assumed in force calculation; hence the Young's modulus and Poisson's ratio are the only critical mechanical factors in the computation of cell traction force. However, the linear elastic model is too idealized for the mechanical properties of PAG. This assumption of linear elasticity is only valid if the substrate is behaves like Hookean material (e.g. steel, concrete) and the deformation of substrate is infinitely small compared to unity. In several experimental studies, the stress-strain relation of most hydrogel such as gelatin pork skin, poly(L-lysine)/hyaluronic acid, carotid arteries ,and poly(dimethylsiloxane) is found to be nonlinear[93-98]. In addition, Boudou *et al.* proposed an original formulation of the nonlinear strain energy function of PAG using micropipette aspiration technique and FEM on the small strain domain [99]. They further evaluated the implication of linear and hyperelastic model in cell traction force computation by comparing the results constructed by their nonlinear elastic model with the conventional approach developed by Dembo and Wang. The comparison showed that the linear elastic model significantly underestimated traction forces for substrate displacements larger than 2 μm.

2.7 Cell traction force on micro-contact printing

The studies of mechanotransduction have revealed that the transition of cellular activities

and states are resulted from a complex cascade of multiple intracellular signaling pathways known as biocomplexity. This reaction requires interplay between the biochemical and mechanical cues in order to fulfill the activation of several fundamental protein and gene expressions. For example, modulating the expression of Rho and Rho-associated protein kinase (ROCK) proteins which occupy both the upstream and downstream of major force transduction signaling pathways, the endothelial budding morphogenesis and angiogenesis can be either stimulated by enhancing the Rho and ROCK activity or inhibited by suppression the cytoskeletal tension [100]. Therefore, it is concluded that the variation of cell fates in embryogenesis and adult morphogenesis is closely regulated by the isometric tension or prestress established by the 3D intracellular architectural network. The reestablishment of isometric tension based on the tensegrity principle initiated by the mechanical signal such as cell shape distortion plays an important role in many cellular activities such as differentiation, migration, and mitosis [63, 101-105]. In general, cell shape is the basic indicator in the evaluation of the anchorage dependent cell characteristics during cell culture because the degree of cell spreading determines the major cellular activities. For instance, unhealthy anchorage dependent cell undergoes apoptosis by retracting cell boundary to form a rounded morphology before detaching due to the relaxation of the internal tensile stress[102].

While there is no doubt that the cellular activity affects the cell shape and structure; several studies had shown that cell shape can in turn determine the cellularbehaviors through the feedback mechanisms. For instance, the expression of cyclic-adenosine monophosphate (c-AMP) which is the regulator of intracellular signaling transduction is linearly proportional to the degree of cell spreading under the

same mechanical force [10]. Furthermore, the cells with higher spreading area are more sensitive towards induced stress in promoting proliferation, whereas the cells with smaller spreading area are more sensitive towards apoptosis [99, 106]. These studies further highlight the complex relationship between the intracellular molecular events and global cellular phenotypes.Hence it is suggested that the large scale cell shape and size distortion are able to influence the complex signal integration that ultimately alter the gene and protein expression.

Although it is apparent that the interplay among the cytoskeleton and adhesive ligands in the microenvironment is one of the major determinants of cellular activities, yet the understanding of the corresponding mechanotransduction remains unknown due to the difficulty in manipulating the native microenvironment in sub-cellular level.To understand the influences of the adhesive microenvironment on cellular activities, it is advisable to break down the complex environmental conditions into several simplifiedmodel systems and carry the study in a highly controlled manner.In native microenvironment, cells exhibit highly reproducible shape with specialized cytoskeletal organization that is ideal for their respective characteristics throughout the lifetime. In general, cells do not replicate the morphology and cytoskeletal organization of the native cells under *in vitro* culture due to the variations in geometric factors. As a consequence, the isotropic cytoskeletal architecture exhibited by the cell *in vitro* fails to sustain its characteristic phenotype and becomes pleomorphic [107]. In order to study the mechanotransduction of cells experienced in native microenvironment, it is essential to control thecell shape, to prevent cell movement, and to impose a reproducible shape for single cell study.

With the incorporation of nanolithographic technology known as micro-contact printing (μCP), scientists are able to control the pattern of the adhesive site with the precision down to micro- or nanometer scale. This precise ECM pattern fabricated by μCP produces a physical platform for the cell to attach. By doing so, researcher can manipulate the cell shape, cell-ECM interaction, cell alignment, cell-cell interaction, and even the local formation of focal adhesion. As a consequence, it is possible to study the individual contributions of various mechanical and biochemical cues that are involved in the mechanotransduction in a highly controlled manner.

Spatial distribution of cell traction force with specialized constraints provided by μCP revealed that the force generated by cell always concentrated on the acute corner regions with or without the presence of contractile agonist[24]. On the contrary, cell with round morphology did not exhibit any preferential spatial distribution of traction force, but higher traction force could be observed at the site where protrusion like lamellipodia, filopodia, or microspikes was formed [63, 108]. The overall magnitude of cell traction force has always been associated with the cell morphology in the past. Recently, a series of ECM islands with various area and shape produced by μCP revealed that cell traction force is indeed linearly correlated with the degree of cell spreading area. In addition, wide and well-spread human airway smooth muscle cell generates higher traction force than the cells with higher aspect ratio [109]. The study of cell shape associated activities revealed that the degree of cell spreading is linearly correlated with the cell proliferation due to the upregulation in the expression of platelet-derive growth factor (PDGF) and transforming growth factor-β (TGF β) [106]. In contrast to well-spread morphology, the elongated morphology is the optimal cell shape in the tendon morphogenesis, this is due

to the enhanced expression of the major tendon's component known as collagen type I against the degree of elongation [24].

These findings raised an important issue on how the cell shape defines the cell fate in a distinguished manner. One promising mechanism that contributes to this phenomenon is the multiple intracellular signaling transductions regulated by the tensegrity principle. The tensegrity principle that governs cell structure indicates that the manipulated cell shape caused by the spatial constraint of ECM pattern is balanced by the rearrangement of cytoskeletal architecture and redistribution of focal adhesion in order to achieve an isometric tension. Therefore, it is essential to discover the cytoskeletal organization and focal adhesion distribution of the cell with specific area and shape. The immunostaining showed that each individual cell shape is supported by different form of cytoskeletal structure (e.g. F-actin [24, 63, 110, 111], microtubule [112]), focal adhesion protein spatial distribution (e.g. vinculin [24, 63, 110, 113], paxilin), and ECM spatial distribution (e.g. fibronectin [63], collagen I). The ECM pattern is also contributed to the internal organization and polarity orientation of cell due to the rearrangement of cytoskeletal structure. This is because many associated proteins and organelles are physically immobilized on the actin filament and the microtubule is the major determinant in the spatial distribution of nucleus, centrosome, and Golgi apparatus [112]. In addition, 3D images from confocal microscopy revealed that the cell shape and area modulated the nucleus shape and volume, thus indicating a possible direct physical linkage between the cell shape distortion and gene expression [106]. By identifying the respective contribution of mechanical signals through the patterning of *in vitro* cells, it is possible to manufacture a regulatory engineered microenvironment that mimic the

characteristics and functions of tissue in native environment[114].

2.8 Mechanotransduction of vascular smooth muscle cells in microchannels

The study of single cell performed by μCP is a powerful tool to discover the mechanism of mechanotransduction with respect to the cellular shape and area. However, the single cell model itself cannot describe some situations such as the morphogenesis of blood vessels. In the general context of tissue development, cellular behaviors are collectively regulated by the intercellular biochemical and mechanical transmission rather than individual activities. As elaborated in the tensegrity contribution in the tissue morphogenesis, mechanical signals have been heavily incorporated in the development of tissue engineering. One of the much studied tissues in mechanotransduction is blood vessel due to the importance of hydrodynamic blood flow in vascular morphogenesis and physiology. In the development of the synthetic blood vessel, the appropriate mechanical properties and vasoactivity demonstrated by the engineered blood vessel are the critical requirements in the coronary artery bypass or peripheral vascular surgery.

Blood vessel comprises three major layers known as tunica intima (endothelial cell monolayer), tunica media (smooth muscle cell multi-layer), and tunica adventitia (connective tissue) as shown in Fig. 2.4[115]. The tunica intima refers to the inner wall of blood vessel which is constructed by a monolayer of endothelial cell (EC). This layer is directly exposed to the shear stress from the hydrodynamic blood flow and served as the mediator in transmitting biochemical and mechanical signals into the tunica media. The degree of shear stress transmitted to the tunica media is measured as blood pressure because it is resisted by the circumferential stretching normal to the vessel wall. The

coordinate circumferential stretching and releasing mechanism is known vasoactivity of blood vessel and is governed by the thick layer of vascular SMC called tunica media. This thick multi-layer is the major vasoelastic component of the blood vessel and is actively responsible in controlling the diameter of the inner blood vessel according to the myogenic effect to keep the blood flow constant. This constriction and dilation mechanism is important in the cardiovascular physiology because the inconsistent blood flow will result in arteriolosclerosis and restenosis [116]. As a result, this specific layer has been heavily subjected to the bio-mechanical study in the quest on achieving a functional and durable engineered blood vessel.

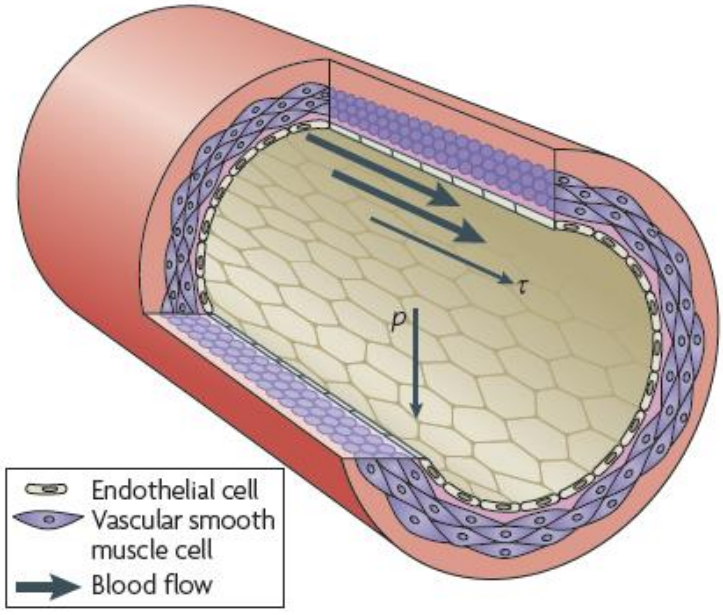

Fig. 2.4A cross-section of an artery blood vessel[115]. A monolayer of endothelial cell forms the inner wall of lumen with the alignment parallel to the blood flow. This thin layer is defined as tunica intima and is directly exposed to the shear stress τ. The middle part with several layers of circumferentially aligned smooth muscle cells is defined as tunica media. This layer is the predominant component in vasoactivity where it generates

circumferential constriction and dilation mechanism to resist the blood pressure ρ. The outmost layer is known as tunica adventitia which is entirely formed by connective tissue and is absent in capillaries.

The primary characteristic of tunica media is the circumferentially alignment of contractile SMCs normal to the blood flow, it governs the vasoactivity of the blood vessel by generating appropriate contractile force, thereby sustaining vascular physiology. Vascular smooth muscle cells in native blood vessel exhibit elongated morphology known as contractile SMCs. They have slower proliferation and ECM secretion rate as compared to the synthetic SMCs that exhibit fibroblast-like morphology. However, the contractile SMCs are critical in generating contractile forces which are important in the vasoactivity. Therefore, in the early stage of tissue engineering, SMCs with synthetic phenotype are in favor due to their rapid extension in cell number and ECM production for the replacement of biodegradable scaffold [117] . In the later stage, the synthetic SMCs must switch to the contractile and quiescent phenotype to produce critical vasoactivity in functional engineered blood vessel as well as prevent wall thickening and narrowing of vessel lumen [1]. As a result, scaffold that supports phenotype switch either by controlled drug release or functional topography is highly demanded in the field of cardiovascular tissue engineering.

The effects of scaffold on tissue engineering are critical as it is one of the three major components in the development of engineered tissue equivalent. Scaffold provides the mechanical properties and physical platform for cell seeding under aggressive *in vivo* microenvironment during tissue regeneration. In addition, physical platform also provides

the necessary spatial constraint to direct the specific tissue development. Therefore, many studies have been directed to the manufacture of the optimal scaffold for tissue engineering. Microfabrication technologies have been applied to produce 2D micropatterned surface and 3D topographical features on scaffold to facilitate the development of tissue with appropriate phenotype switch [28, 62, 118-121]. For instance, deep microchannels manufactured by hot embossing lithography allow the SMCs to develop into a layer of highly aligned cell sheet with contractile expression upon confluence. During the early cell seeding, SMCs adopted the synthetic phenotype to provide substantial cell proliferation and ECM production. As the cultured cells approached confluent state, the morphology of smooth muscle cells shifted from fibroblast-like characteristic towards elongated shape, and adopted the contractile phenotypic characteristics. Such coordinated collective alignment and phenotypes appeared to have an important role in the vasoactivity of a functional blood vessel as the contractile proteins were upregulated in the expression of α-actin proteincalponin, smoothelin, and myosin heavy chain [122, 123].

2.9 Mechanotransduction of encapsulated cells in the three-dimensional microenvironment

With the increased recognition in mechanotransduction, it is important to extend our knowledge from 2D geometry to 3D matrix. Studies have shown that the dimensionality of the microenvironment played an important role in the development of the transmembrane compartment which regulates the bilateral signal transduction between cell and ECM [114, 124]. For instance, FAK that is served as the major mediator

protein in 2D mechanotransduction was found to be down-regulated in 3D microenvironment based on its activation of mitogen-activated protein kinase (MAPK) [125]. However, the associated phosphorylation of other mediator protein such as paxillin remains unchanged [124].Therefore, it is not surprised to discover that cells adopt distinct mechanotransduction signaling model in different dimensional culture system.

The mechanotransduction study of encapsulated cells in 3D culture system is particularly important because most of the tissue formation is inevitably initiated and developed in the 3D microenvironment such as cartilage tissue. The native cartilage structure is supported by collagenous fibrils and aggrecan matrix[126]. In cartilage regeneration, hydrogels are the most commonly used synthetic 3D scaffolds in providing appropriate mechanical signals for the formation of functional cartilage [127-130]. The mechanical properties of the hydrogel can be easily tuned by adjusting the degree of polymer cross-linking and water content in order to precisely mimic the native cartilage microenvironment. In addition, due to the inability of the adult hyaline cartilage in self-regeneration after sustaining trauma, the hydrogel injectability is a promising cell delivery-based therapeutic for *in situ* cartilage regeneration [131].

The bio-mechanical behaviors of the encapsulated chondrocytes have been extensively probed *in vitro* using 3D culture system in order to optimize the ability of hydrogel in promoting functional cartilage regeneration. An ideal hydrogel provides mechanical and structural support to guide cell proliferation and ECM secretion. It has been reported that chondrocytes adopt two distinct morphologies and behaviors in different environmental factors such as dimensionality and rigidity. Under the same biochemical signals, differentiated chondrocytes exhibit typical spherical morphology on

3D matrix which is distinctive from the fibroblast-like morphology on the 2D surface [132]. The cultured chondrocytes on 2D surface undergo dedifferentiation that associated with phenotypic change as well as inability in producing cartilaginous ECM [133, 134]. This phenomenon is consistent with the MSCs-based cartilage regeneration, where the chondrogenesis of MSCs is determined by the dimensionality and rigidity of culture system. Results showed that the MSCs cultured in 3D scaffolds demonstrated significant cartilaginous gene expression like Collagen II, aggracen, and Collagen X, while the MSCs cultured on 2D film showed little or no detection of cartilaginous gene expression [135]. These chondrocytic characteristics are important in the cartilage tissue regeneration because the lack of cartilaginous ECM production may substantially weaken the structural integrity of regenerated tissue.Interestingly, several studies reported that the dedifferentiated chondrocytes from the 2D culture system could be reversed to the chondrocytic phenotype under the appropriate 3D culture system such as agarose [136], alginate [137, 138], Collagen I hydrogel [139, 140], and Collagen II hydrogel [141]. Nevertheless, the lost of chondrocytic characteristic due to the dedifferentiation effect is remained as the substantial obstacle in cartilage tissue engineering.

Furthermore, the tissue regeneration rate has to match the hydrogel degradation rate in order to produce an integrated regenerated tissue. However, the cell proliferation is still greatly limited in hydrogel scaffold due to the significantly lack of space [142]. Although the size of pores inside hydrogel can be expended to allow higher cell occupation, yet the overall structural integrity of hydrogel will be compromised and the phenotype of the encapsulated chondrocytes will be altered. Therefore, a better understanding in biomechanical behaviors of the encapsulated chondrocyte in needed to

develop an innovative hydrogel that is capable of providing optimal signals to facilitate the cell proliferation, as well as to match the tissue regeneration rate with hydrogel degradation rate. The mechanism of how cells sense the dimensionality of its microenvironment and then respond appropriately with distinctive morphology and mechanotransduction is remained to be discovered. However, it is believed that the unique cellular responses towards different dimensionality might be due to the fundamental differences in cell-ECM communication that is regulated by tensegrity principle. This is a valid hypothesis because the observed differences in cellular morphology and adhesion proteins are the basic component of tensegrity model that is closely associated with cellular mechanotransduction.

Chapter 3 Experimental and numerical determination of cellular traction force on polymeric hydrogel

3.1 Introduction

Most cells undergo complex mechanical interactions with the environment and neighboring cells through the formation of focal adhesions and other adhesive structures [23, 64, 69-74]. These mechanical interactions provide physical mechanisms for various basic cellular activities such as adhesion, migration, communication, proliferation and differentiation. Such activities collectively drive embryogenesis, tissue morphogenesis, tumor metastasis, wound healing, etc [8]. Though cellular adhesion is commonly recognized, yet only few mechanical factors have been elucidated in a quantitative manner due to practical difficulties in both theories and experiments to characterize the interfacial interactions. Among various interactions, cell traction force has been shown important in cellular functions [78, 79, 143]. Such traction is essentially bi-directional, reciprocal, and dynamic across the interface between cell and ECM. Most cells can modulate the traction force dynamically according to the extracellular signals to maintain the cell homeostasis and to initiate cellular activities. More specifically, the modulation is carried out by acto-myosin interactions and conformational changes in cytoskeletal architecture. For example, the changes in traction force can activate the integrin-dependent molecules such as RhoGTPase, talin 1, FAK, which then trigger a cascade of signaling pathway and alter gene expressions [81-85]. One renowned mechanotransduction theory called ‘tensegrity’ indicates that the changes in cytoskeletal

3D architecture caused by mechanical signals could be transmitted to the nucleus via a direct mechanical link from ECM to nuclear chromatin [5]. These studies purposefully signal the necessity of a direct and rigorous measurement of cell traction force at cell-substrate interface for characterizing the biological mechanocahemical feedback controls in cellular functions.

The microscopy approach in reconstructing traction forces was pioneered by Harris *et al.,* who first applied the deformable silicone substrata to probe traction forces qualitatively by the wrinkling assay [77, 144]. The complex relation between force and deformation (wrinkle) and the low resolution of wrinkling assay made the quantitative measurement difficult. A more direct characterization of non-wrinkling silicone with embedded particles as indicators of deformation was later developed by Lee *et al.*[78]. However, the viscosity of the substrata used in Lee's study led to irreversible deformation and poor conditions for cell adhesion. Dembo and Wang further developed traction force microscopy by using the substrata prepared from PAG with embedded fluorescent beads [80, 145]. PAG has the advantages over other materials because of its tunable mechanical compliance through the change of reaction condition for acrylamide polymerization. Furthermore, cell adhesion on PAG is insignificant without the conjugating of adhesive ligands. Hence PAG is ideal for studying mechanotransduction through the quantitative determination of tractions on PAG surface induced by cells. In addition to PAG,PDMS is another commonly utilized material in the study of cellular force.

The calculation of cellular traction forcevia the displacements of fluorescent bead is an inverse problem which can be ill-posed and thussome regularization (constraint with Lagrange multiplier) are needed [72]. Here the inverse problem means the following:

Assuming beads' displacement is obtained from the Fredholm integral of force with Green's function as a kernel, i.e.,$u(r) = \int dr' G(r - r') F(r')$,the task is to search the force $F(r')$ which yields the minimum difference between the calculated and measured displacements with presumed mechanical properties. Such numerical process is an optimization problem and constraints on the force $F(r')$ are needed to avoid unrealistic solution as well as numerical divergence. This inverse problem can be solved by the forward model formulated earlier by Pelham and Wang [89, 90]. More recently, Dembo and Wang [80, 145] employed the Boussinesq solution to approximately determine the 2D Green's compliance tensor $G(r - r')$ for cases when the thickness of substratum is much larger than the maximum marker displacement (~1μm/70μm). However, the determination of the Greens' tensor is complicate and the beads displacement is heavily dependent on the image resolution. More challenges lies in the finding of force distribution. Generally some smoothing operations are included when calculating the Fredholm integral because force $F(r')$ is highly sensitive to small changes in displacement $u(r)$ and one-to-one mapping may not exist between them. A remedy proposed by Butler *et al.*[91]using FTTC is more efficient than directly applying Boussinesq solution to find $G(r - r')$. The key difference is that FTTC works out the Fredholm integralin the Fourier space instead of the real space; it thus requires no smoothing operation and hence less complex computation. It should be noted that FTTC is formulated by either (a) bound constrained (a mixed boundary value problem in which the displacements under the cell being specified using the measurement, and zero tractions outside the cell boundary), or (b) unconstrained (specifying all displacements using the measurement; no tractions specified) to determine the cellular traction force.

In general, approaches based upon Boussinesq solution and Fredholm integral restricts the substratum material to be linear elastic. They also required some specific mappings of displacement field on the substratum surface. These devices are set up for mathematical convenience to determine $G(r-r')$and avoid ill-posed issues. A more robust approach for such mapping is digital image correlation (DIC), originally developed by Yang *et al.* and Chu *et al.*[92, 146] and a more modern version by Brock *et al.* and Berfield *et al.*[147, 148]. In this technique, a statistical correlation function among different parts of a digital image pair is employed to measure the movement of objects in the images. DIC was extensively used in many studies of bioimaging for probing cell mobility and cytoskeleton dynamics [92, 108, 149, 150]. Another interesting issue is that Boussinesq solution assumes the substratum to be an infinite half-space. Such assumption can be accurately achieved only if the displacement field by traction force is small compared to the substratum's lateral dimensions and thickness. For a medium with low elastic modulus like PAG, a small deformation is hard to guarantee and if its thickness exceeds 100μm, the substratum can be easily deformed by its own weight. One practical way to circumvent this limitation is to analyze the 3Dhydrogel by FEM [92, 108, 149, 150]. The measured displacement field from experiments is directly applied as boundary conditions without using any specific mapping as seen in other methods.

In this study, rat aorta SMCswere chosen as model for probing cell traction force on a PAG substratum. The study was carried out in two steps. First, AFM was used to characterize the stiffness of PAG film. Secondly, the deformation images of PAG substratum induced by cell traction are probed by fluorescence microcopy. The deformation was measured by the relative position of displaced fluorescent latex beads

via particle image velocimetry (PIV). The measured displacement field was then input as boundary conditions for the subsequent FEM simulation. In the simulation, a non-linear (Mooney-Rivilin) material model was employed and the optimal range of PAG mechanical properties was investigated as well.

3.2 Materialsand Experiments

3.2.1 Preparation of activated glass coverslips

PAG was immobilized on activated coverslip surface in order to prevent the gel from floating off during CTFM assay. The surface activation procedure used herein is developed by Alpin and Hughes [151]. Glass coverslips (Φ31.4mm, 0.17mm thickness, Willco) were first sterilized by briefly putting through the inner flame of Bunsen burner. Then 0.1N NaOH was smeared on its surface and dried under nitrogen stream. Then 3-aminopropyltrimethoxysilane (Sigma, St. Louis, MO) was loaded evenly on the coverslips and incubated for 5 minutes. The coverslips were washed with distilled water thoroughly and then covered by 0.5% glutaraldehyde in phosphate-buffered saline (PBS, Sigma) for 30 minutes. After this, the coverslips were again washed extensively with distilled water and stored in the 4^{o}C refrigerator up to 48 hours for later use. The resulted aldehyde groups () on coverslips' surfaces will form strong covalent bonds with PAG (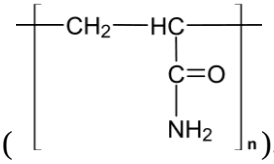).

3.2.2 Preparation of polyacrylamide sheets

PAGsheetswere prepared by preparing 8% v/v acrylamide (40% w/v, Sigma), 0.1% v/v N,N'-Methylene bis-acrylamide (BIS, 2% w/v, Sigma) in distilled water . The solution was degassed for 30 minutes with nitrogen in order to optimize the polymerization. Then ultrasonicated 0.2μm fluorescent latex beads (fluorescein isothiocyanate (FITC)-labeled, Invitrogen) at 1/1000 volume concentration were added to the solution. Another 1/2000 of N,N,N′,N′-Tetramethylethylenediamine (TEMED, Sigma) and 1/200 of ammonium persulfate (10% w/v, Sigma) in volume concentration were also added as initiators and catalysts to trigger free radical polymerization of acrylamide. To prepare a thin sheet of PAG, a small amount of mixture was dropped onto the activated coverslips and immediately overlaid with a piece of inert plastic sheet. The coverslips were then placed up-side-down to allow the fluorescent latex beads precipitating down to the surface of hydrogel sheet. This polymerization process has to be at least 30 minutes to allow beads to settle down [143, 152-154].

The thickness of PAGsheet was estimated from the initial volume of polymer solution applied onto the coverslip and the area of the gel. The actual thickness of the swollen gel was measured by a microscope with focus ranges from the glass surface up to the gel surface. The thickness of gel under swollen condition is estimated to be 70μm on average.

3.2.3 Conjugation of collagen to the polyacrylamide surface

PAG is highly hydrophilic and chemically inert. Therefore, a photoactivatable heterobifunctional reagent, sulfosuccinimidyl-6(4'-azido-2'-nitrophenylamino) hexanoate (Sigma), also known as sulfo-SANPAH, was used as the molecular bridge to link the cell

ECM proteins (1mg/ml collagentype I) to PAG[152]. Sulfo-SANPAH comprises phenylazide groups at one end which reacts nonspecifically with PAG under UV irradiation, and sulfosuccinimidyl groups at the other end can react with primary amines in the ECM proteins [153].

3.2.4 Cell culture

Rat aorta smooth muscle cells (SMCs, A7r5 rat fibroblast, ATCC) were cultured in high glucose Dulbecco's modified eagle medium (DMEM) supplemented with 10% fetal bovine serum (FBS), 5mg/ml penicillin and 5mg/ml streptomycin (Invitrogen Inc.). Cells were maintained at 37^{o}C in humidified atmosphere with 95% air and 5% carbon dioxide. The culture medium was changed every two days, and cells were subcultured at least once a week. Before every experiment, cells were detached from the culture flask by adding 5.3mM trypsin-EDTA solution in 1X PBS. The cell suspension was transferred to a 15ml Falcon tube and then centrifuged at 1500rpm for 5 minutes. After centrifuge, trypsin was removed and remaining cell pellets were re-suspended in the DMEM supplemented with 10% FBS. The cells were then plated onto PAG surface at a density of 13cells/mm^2 for traction force microscopy. All experiments conducted in this study using cells before tenth passage. After 24 hours of seeding, healthy cells found at a distance of at least 200μm away from the edges of PAG substratum were chosen for cellular traction force measurement. This is to avoid the edges effect and minimize cell-cell interactions.

3.2.5 Live cell traction force microscopy

Live cell microscopy was performed on an inverted light microscope (Olympus IX71) using LUCPlanFLN 40x/0.60 Ph2 objective (Olympus) on a motorized stage

(BioPoint 2, Ludl Electronic Products). PAG substratum on modified coverslip seeded with cells was mounted onto microscope perfusion chamber where the desirable environmental parameters were controlled. Throughout the experiment, temperature of the chamber was maintained at 37^{o}C using Tempcontrol 37-2 Digital and Heating Unit (Leica). 5% Carbon dioxide and the humidity of the microscope stage were controlled by humidifier system (CTI-Controller 3700, Leica). Photos were taken on the cells with phase-contrast optics to visualize the cell shape and location, and with fluorescein illuminating at 490nm to excite the fluorescent beads with emission at 515nm. In order to assess the displacement of beads under the null-force condition, culture medium was removed and trypsin was added to detach the cells from PAG surface. Once the trypsinization was completed, both phase-contrast and fluorescent images were taken again at the proximal location to obtain beads' positions for assuming the gel to return to its initial state without cells. The set of images shot after the removal of cells are termed as "null-forces" images.

3.2.6 Image processing the displacement field on substratum surface

A particle image velocimetry program coded in MATLAB (MatPIV) was used to quantify the displacement of microbeads induced by the cell traction force. PIV calculates the average movement of many nearby particles inside a small window directly from a *pair* of digital images taken at two contiguous instants. Theories behind this numerical process will be discussed later.

3.2.7 Characterization of elastic mechanical properties of PAG substratum

It has to measure the mechanical properties of PAG before the traction force

analyses. The measurement was carried out by the atomic force microscope (AFM, Asylum Research, model MFP-3D) with water immersion capability for a flat, homogeneous, PAG substratum with average thickness of 70μm under swollen condition [155, 156]. A contact mode with spring constant of 36mN/m was applied via the silicon nitride cantilevers (Sharpened Microlevers, Crest Technologies). Both the velocity of cantilever and indentation depth were carefully controlled during the test. In addition, the unloaded cantilevers were calibrated before the test to measure the thermally induced motion of gels under water immersion, which was automatically discounted from measurements in the indentation test.

3.3 Results

3.3.1 Estimate on the elasticity of PAG substratum

Fig. 3.1 shows the schematic details of AFM indentation and the *force-indentation* relation, from which we can have the following *indentation-deflection* relation [155]

$$z - z_o = d - d_o + \sqrt{\frac{k(d - d_o)}{(2/\pi)[E/(1-\upsilon^2)]\tan(\alpha)}} \qquad (3\text{-}1)$$

where $k = \frac{3E_{\mathrm{SiN}}I}{L^3}$ is the stiffness of silicon nitride cantilever. This equation is used to determine the elasticity of substratum (E) by fitting the *indentation-deflection* curves from AFM measurement. Example of the AFM measurements on a flat, homogeneous PAG substratum under swollen conditions is shown in Fig. 3.2 where a full cycle of loading and unloading process is presented by the indentation-deflection ($z - z_o$ vs. $d - d_o$) curve. For a small deflection of cantilever, the relation between the applied force

F and indentation depth δ on an elastic medium is presumed to be the Hertzian contact via[155, 157]

$$F = \frac{2}{\pi}\frac{E\delta^2}{(1-\nu^2)}\tan\alpha \qquad (3\text{-}2)$$

where E is elastic modulus, ν is Poisson's ratio of polymer, and α is the half-cone angle of cantilever tip.

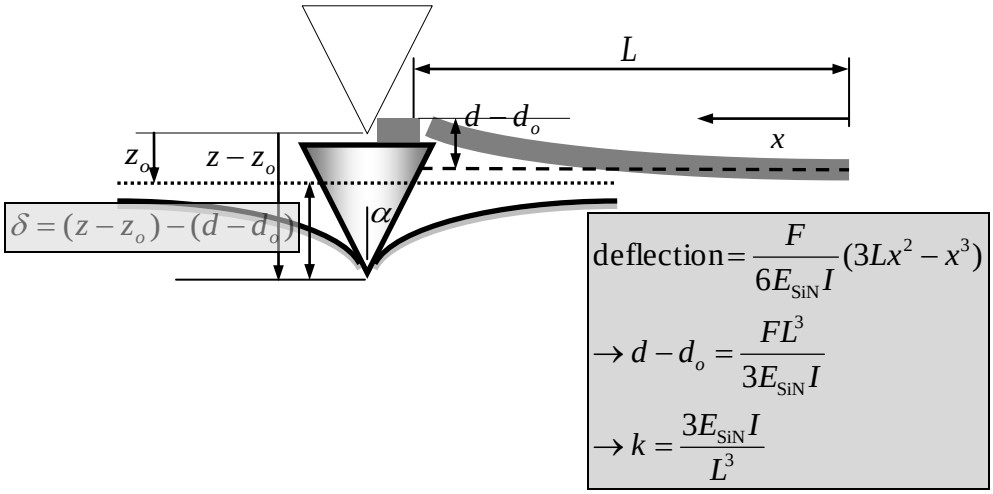

Fig. 3.1 A schematic representation of AFM indentation and indentation-deflection relation.

Due to its high content of water, PAG is almost incompressible and thus its Poisson's ratio is close to 0.5 [158]. The initial deflection and height of cantilever, d_o and z_o can be located directly from the experimental curves. Therefore, slope of any two points on the curve can be used to calculate the value of E from Eq. 3-1 [155, 156, 159-162]. However, the choice of points is too arbitrary. In order to yield an accurate estimate, an optimization approach was employed. By iteratively specifying different E in Eq. 3-1 to calculate z at every d from the measured data, the average difference (L_2 norm)

between $z^{experimental}$ and $z^{calculated}$ along the loading force curve can be minimized when an optimal elastic modulus is found. This approach ensures every point along the experimental loading force curve was taken into account in the determination of optimal *E* value. Fig. 3.2 presented one example result of the AFM measurements and the optimal $E = 44$ kPa. In the 3rd and 4th quadrant of Fig. 3.2 also demonstrates adhesion between the tip and PAG around 200~800pN (lower inset, force-indentation curve). There were totally five measurements taken at different locations on a PAG and the range of optimal value was found between 32 and 44 kPa. Fig. 3.3 gives those optimal Young's moduli and their corresponding minimum errors. With the *t*-test on the mean value of average (39.2 kPa) and χ-test on the variance (4.6 kPa) of Young's modulus, we can determine the 95% confidence interval of Young's modulus (Table 3-1). The interval gives us a confirmation on the estimated modulus as marked on the abscissa in Fig. 3.3.

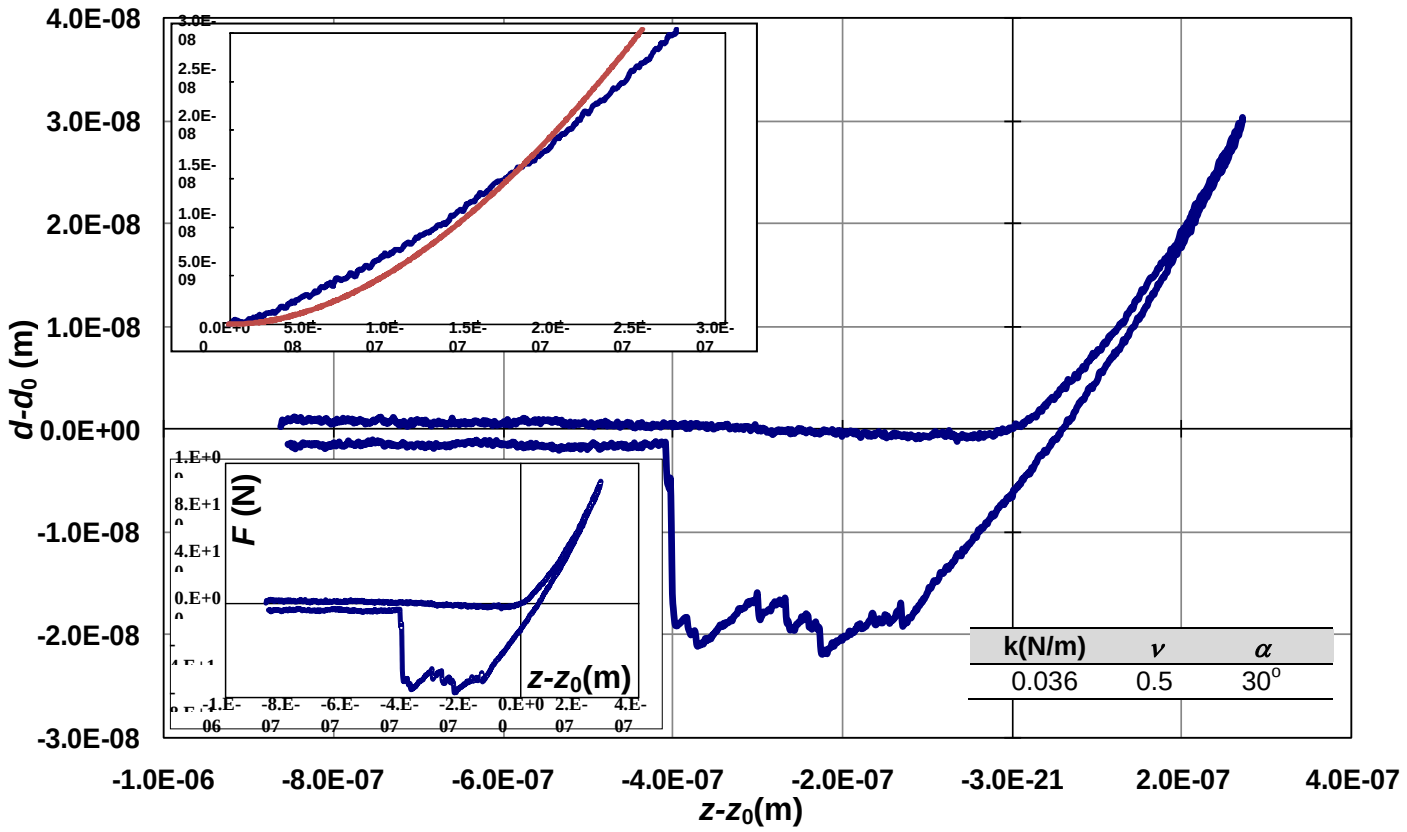

Fig.3.2 Experimental measure of AFM indentation curve for PAG substratum using contact mode. Corresponding force on the cantilever tip and an optimal fitting of loading result using Eq. (3-1) with the value $E = 44$ kPa are shown in the insets.

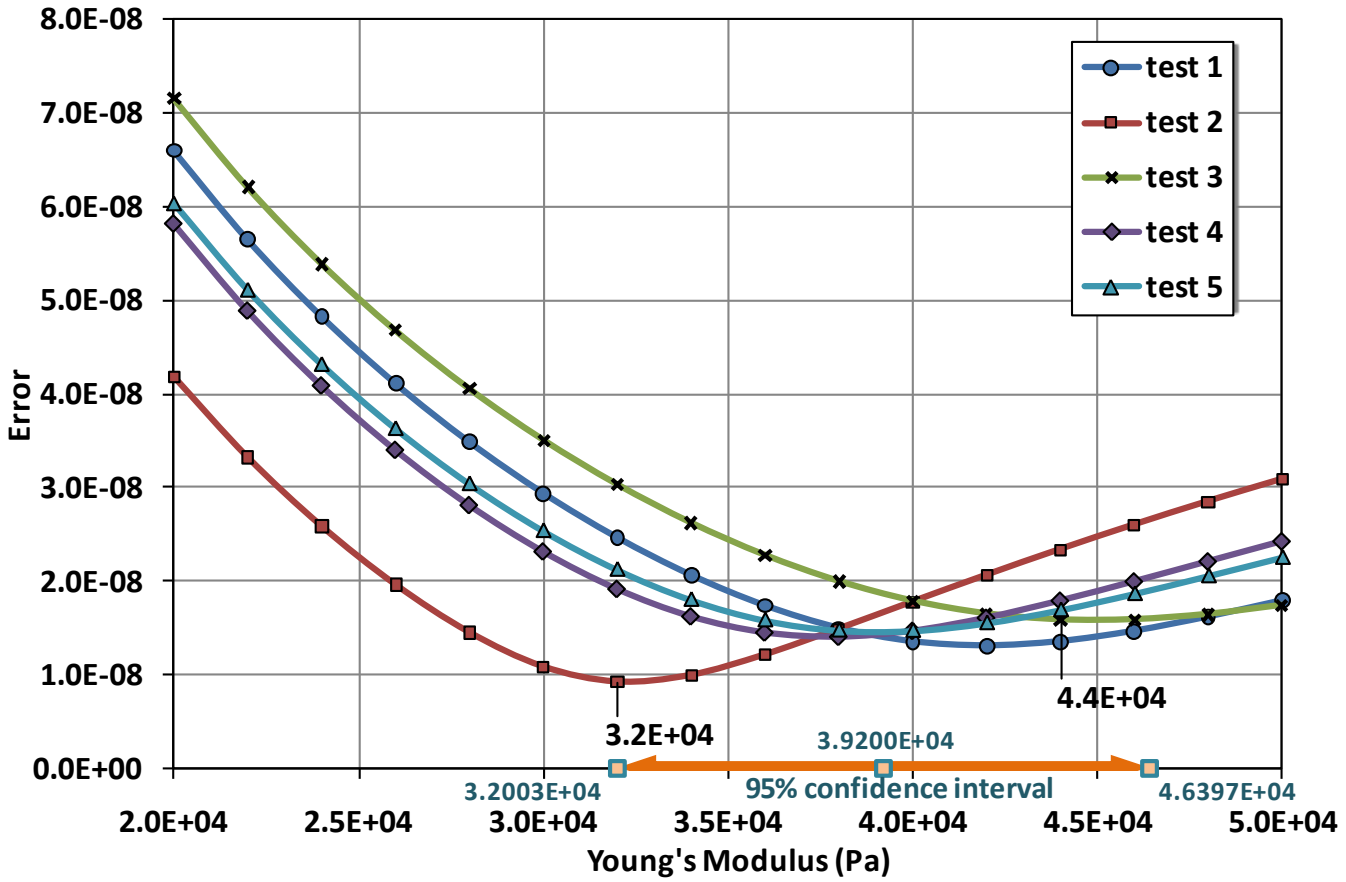

Fig.3.3 Errors between the calculated and experimental measures of AFM indentation for PAG substratum using contact mode.

The attainable minimum errors fall in the range between 32kPa and 44 kPa. (Fig.3.2 is the result of test 3). The confidence interval was calculated based on two-tailed test in Table 3-1.

t-test on the mean of Young's modulus from AFM					
Deg. Freedom	**Xn (sample mean)**	**Sn (sample std. dev.)**	**Significant level**	**$t_{0.05}$**	**$YE_{95\%\ confidence}$**
5	3.92E+04	4.60E+03	0.0500	3.4954E+00	4.6397E+04
					3.2003E+04

χ-test on the variance of Young's modulus from AFM					
Deg. Freedom	**Xn (sample mean)**	**Sn (sample std. dev.)**	**Significant level**	**$\chi_{0.975}$/ $\chi_{0.025}$**	**$YE_{95\%\ confidence}$**
5	3.92E+04	4.60E+03	0.0500	1.2833E+01	2.6788E+01
				8.3121E-01	1.0526E+02

Table 3-1 Two-tailed t-test and χ -test on the mean and variance of Young's modulus estimated from AFM.

3.3.2 Hyperelasticity of PAG substratum

To quantitatively assess the mechanical response of PAG induced by cell traction, numerical analysis is conducted following the experimental set up. The ensuing goal was to examine the contact between PAG substratum and cells. The basic mechanical properties for the proceeding analysis included the Young's modulus (E) and Poisson's ratio (γ). As mentioned previously, Poisson's ratio shall be assumed 0.5 under the assumption of incompressibility for PAG[158]. A more realistic material model, the Mooney-Rivilin constitutive relation was used for the simulation. Mooney-Rivilin constitutive law was applied in numerous studies of rubber-like or synthetic and natural polymeric materials, e.g. gelatin pork skin, poly(L-lysine)/hyaluronic acid, carotid arteries , poly(dimethylsiloxane) [163-168]. The formulation of Mooney-Rivilin is based upon the theories of hyperelasticity. Hyperelasticity refers to materials that are able to recover completely from a finite deformation to their undeformed state. This material model assumes a special form of the strain energy function W as follows [163-168]

$$W = c_{10}(\bar{I}_1 - 3) + c_{01}(\bar{I}_2 - 3) + \frac{\kappa}{2}(\bar{I}_3^2 - 1)^2 \qquad (3\text{-}3)$$

where c_{10}, c_{01} and κ are empirical material constants; $\bar{I}_i$ are reduced strain invariants, each defined as

$$\bar{I}_1 = I_1 I_3^{-1/3}, \qquad \bar{I}_2 = I_2 I_3^{-2/3}, \qquad \bar{I}_3 = I_3^{1/2} \qquad (3\text{-}4)$$

by the three invariants I_i of the Cauchy-Green strain tensor: $I_1 = C_{ii}$, $I_2 = \frac{1}{2}(I_1^2 - C_{ij}C_{ij})$ and $I_3 = \det(C_{ij})$. The Cauchy-Green strain tensor is calculated from the kinematic (strain-displacement) relation

$$C_{ij} = f_{ik} f_{jk}^{T} \tag{3-5}$$

where $f_{ik} = \partial x_i / \partial X_k$ is the deformation gradient, and X_k, x_i are components of the position vectors of a material point before and after deformation along direction i and k respectively. Overall, the strain energy W is a function of Cauchy-Green strain. Its first derivative yields

$$S_{ij} = 2\frac{\partial W}{\partial C_{ij}} \tag{3-6}$$

where S_{ij} is the second Piola-Kirhhoff stress tensor, representing the force per unit area in the undeformed body. In contrast to the commonly used Cauchy stress (σ_{kl}), which measures the force per unit area in the deformed body, the two stress measures are algebraically related to each other by the deformation gradient as

$$S_{ij} = J(f_{ik})^{-1}\sigma_{kl}(f_{lj})^{-\mathrm{T}} \tag{3-7}$$

where the superscript -1 and T represent the inverse and transpose of a tensor respectively, $J = \det(f_{ik})$ is Jacobiandeterminant.. The Cauchy stress (σ_{kl}) has to satisfy the equilibrium equations $\frac{\partial \sigma_{kl}}{\partial x_l} = 0$ in all three Cartesian coordinates directions. Eq. (3-5), (3-6) and (3-7) together would allow us to express the equilibrium equations in terms of deformation gradient and solve them numerically. Note that in Eq. (3-7), the material density is considered to be a constant throughout the deformation.

3.3.3 Connections among different mechanical properties

We have noticed that AFM data yields an optimal estimate on Young's modulus. It is thus necessary to discuss the connections among various material constants before the

implementation of FEM simulations. Assuming the incompressibility of PAG, Poisson's ratio is assigned to be 0.49 to avoid numerical singularity for linear elasticity, so does κ to be $0.7*10^{-3}$ to guarantee small effect from the volumetric change $(\bar{I}_3^2 - 1)^2$ in Mooney-Rivilin model. The connection between Young's modulus and c_{10}, c_{01} comes from the uniaxial tension when the Cauchy-Green strain tensor reduces to one single component – the stretch ratio λ and then the following expression can be found [164, 165, 167]

$$\lim_{\lambda \to 1} \frac{\partial \sigma_{11}}{\partial \lambda} = 6(c_{10} + c_{01}) \tag{3-8}$$

In other words, the Young's modulus corresponds to the *initial* slope of stress-strain curve for Mooney-Rivilin materials under uniaxial tension. This argument leads to the following relation between the *initial* shear modulus μ and c_{10}, c_{01}

$$\mu = \frac{E}{2(1+\nu)} = 2(c_{10} + c_{01}) \tag{3-9}$$

Obviously, either Eq. 3-8 or 3-9 can be used to estimate c_{10}, c_{01} based on the measured Young's modulus from the AFM measurement. In general, Young's modulus and c_{10}, c_{01} are not necessarily related to each other. We can always conduct a stand-alone study on chosen polymeric materials for their hyperelastic properties whenever needed [163].

3.3.4 Displacement field on PAG surface under cellular traction force

The experimental design to investigate the adhesion of a single cell on PAG surface is shown in Fig. 3.4, where the traction forces are transmitted from the cell to the gel surface via transmembrane molecules such as integrins. The embedded fluorescent microbeads just beneath the gel surface are used as markers to track the gel deformation

caused by cell traction force. The measurement of displacement field of the microbeads is obtained from a pair of images, one shows the original position of beadswithout cell on top and the other is under the presence of cell. The quantitative numbers of displacement field is obtained by the PIV in which a cross-correlation function is introduced to derive the local motion of microbeads statistically [169]. Once the displacement field is determined, the mechanical stresses and strains can be analyzed by well established numerical approach such as finite element method.

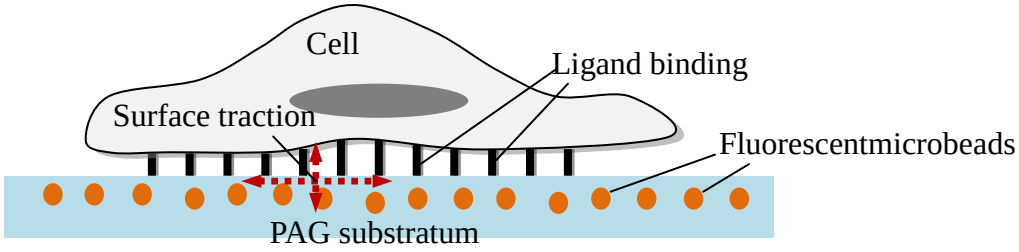

Fig. 3.4 Schematic representation of cell ligand bond to a PAG substratum.

The phase contrast image of a SMC was shown in Fig. 3.5(a). Prior to quantify the microbeads' displacement field, it is important to overlay the pair of fluorescent images before and after trypsinization to correct the misalignment due to the drift of sample on the motorized stage and to minimize systematic errors [79, 91, 152, 170]. It is also necessary to take several fluorescent images at different focal planes in the same region in order to prevent mismatching of the image pairs. This is because the two images from before and after trypsinization might not be taken at the same focal plane. Fig. 3.5(b) shows the fluorescence images at the same location in Fig. 3.5(a). Fig. 3.5(b) shows the two overlaid images before and after trypsinization (force-loaded and null-force). Each dot represents one 0.2μm fluorescent bead. Moreover, pseudo-colors were

applied to the fluorescent beads which appear *green* when SMCs were present (force-loaded), and *red* when SMCs were absent (null-force). When two images overlaid, beads with zero displacement before and after trypsinization is shown by *yellow* dots whereas a pair of nearby red and green dots indicate the embedded bead was displaced by a distance. For reader's reference, the cell boundary was also marked by the white dash lines traced from Fig. 3.5(a).

Fig. 3.5(b) shows that more green and red dots appear underneath the cell area and almost all yellow dots are found at distance further away from cell body. In other words, cell traction is a highly localized effect concentrating in the area occupied by cells. A careful examination demonstrates that more green and red dots tend to be around the cell peripheries rather than the interior of the cell body. This may be caused by the cellular movement via focal adhesions that are typically distributed at the edges of cells[149, 171, 172]. Fig. 3.5(b) contains over a few thousands of beads in the images, thus it is advisable to determine the bead displacement statistically on groups of beads rather than individual one. Therefore PIV is implemented through the method DIC to reckon the displacement of beads based on the following cross-correlation function:

$$C(u_i, v_i, \frac{\partial u_{ij}}{\partial X_i}, \frac{\partial u_{ij}}{\partial Y_i}, \frac{\partial v_{ij}}{\partial X_i}, \frac{\partial v_{ij}}{\partial Y_i}) = \frac{\sum_{i=1}^{N}\sum_{j=1}^{N}[f_1(X_i, Y_j) - \bar{f}_1][f_2(X_i + \Delta X, Y_j + \Delta Y) - \bar{f}_2]}{\sqrt{\sum_{i=1}^{N}\sum_{j=1}^{N}[f_1(X_i, Y_j) - \bar{f}_1]^2}\sqrt{\sum_{i=1}^{N}\sum_{j=1}^{N}[f_2(X_i + \Delta X, Y_j + \Delta Y) - \bar{f}_2]^2}} \tag{3-10}$$

The relation between the pixels (X_i, Y_j) and $(X_i + \Delta X, Y_j + \Delta Y)$ in two images is

$$\begin{aligned} X_i + \Delta X &= X_i + u_{ij} + \frac{\partial u_{ij}}{\partial X_i}\Delta X + \frac{\partial u_{ij}}{\partial Y_i}\Delta Y \\ Y_j + \Delta Y &= Y_j + v_{ij} + \frac{\partial v_{ij}}{\partial X_i}\Delta X + \frac{\partial v_{ij}}{\partial Y_i}\Delta Y \end{aligned} \tag{3-11}$$

where u_{ij}, v_{ij} are x- and y-displacement of the (i, j) pixel point; N is the pixel number (size) inside the interrogation window; $f_1(X_i, Y_j)$ and $f_2(X_i, Y_j)$ are intensity of image at pixel point (i, j) in each image; $\bar{f}_1$, $\bar{f}_2$ represent the average value of $f_1(X_i, Y_j)$ and $f_2(X_i, Y_j)$ in each window; $\Delta X, \Delta Y$ are the shift (or overlap) of the interrogation window between two images.

The value of C is between 0 and 1, the higher the value of C, the more closely related between the images at (X_i, Y_j) and $(X_i + \Delta X, Y_j + \Delta Y)$. Therefore, the objective is to numerically search a location in the second image that is most consistent with the one in the first image, i.e. finding the location with maximum C. Note that the search for maximum C is on all six variables $(u_i, v_i, \frac{\partial u_{ij}}{\partial X_i}, \frac{\partial u_{ij}}{\partial Y_i}, \frac{\partial v_{ij}}{\partial X_i}, \frac{\partial v_{ij}}{\partial Y_i})$. To expedite the computation, a common practice is to calculate the numerator terms in Eq. 3-10 by Fast Fourier Transform (FFT). Also, the iterative calculation should cover the whole image for at least one time [173]. A free program MatPIV distributed under the GNU general public license was adopted for our study [174-177]. This program has functions to remove the spurious vectors and interpolate missing vectors by Kriging method [178-180]. Both vectors are due to the background noises or defocus of images. The image for displacement field computed by PIV is shown in Fig. 3.5(c) by green arrows for the pair of fluorescence images in Fig. 3.5(b). Fig. 3.5(c) was processed with a further removal and interpolation to establish a well defined displacement field, which is ready for FEM analyses as the input data.

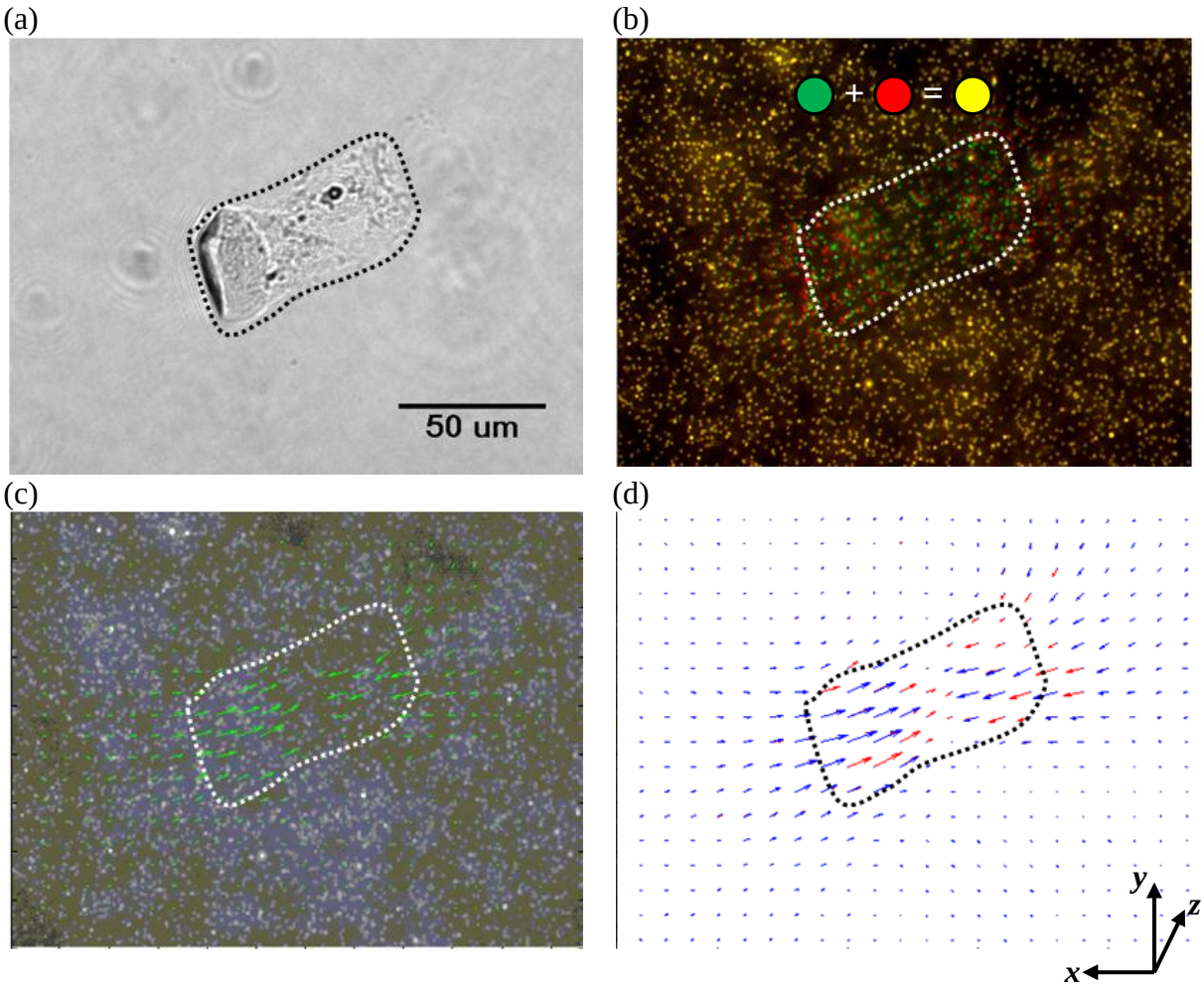

Fig. 3.5 Tangential deformation of PAG surface caused by cell traction force on the XY plane. (a) A phase-contrast image of rat aorta smooth muscle cell, cultured on the flexible PAG covered with collagen type I. (b) Overlaid fluorescent images of the 0.2μm microbeads embedded underneath the surface of PAG. The fluorescent image is taken at the same field of view as in (a). (c) Bead displacement (pixel) vector field computed from two fluorescent images taken before and after cell detachment. (d) Post-processed bead displacement (pixel) vector map from (c). The missing vectors are interpolated and shown in red arrows.

3.3.5 Finite element analysis of experimental results

The deformation and stress analysis of PAG sheet is implemented by the FEM software ANSYS®11. Starting with the geometry of PAG with dimension of 445.74μm×327.75μm×18.35μm, the whole domain (PAG substratum) was discretized by isoparametric, 20-node brick element SOLID186 (Fig. 3.6). The boundary conditions were specified displacements from PIV results, as shown in Fig. 3.5(c), at corresponding nodes on the surface underneath the cell. The nodes on the bottom of substratum were fixed because PAGwas immobilized on the coverslip. The specified displacement field on xy plane is shown in Fig. 3.7 where both contour and vector plots are presented in comparison with the PIV calculated bead displacement field shown in Fig. 3.5(c). The vector plot is particularly illustrative for the xy displacements between the two fluorescent images before and after cell detachment from PAG. In other words, we successfully demonstrated that the planar deformation of gel, which was obtained experimentally and analyzed quantitatively by the PIV image processing of microbeads' movement, can be directly used as input (boundary conditions) for subsequent FEM analysis.

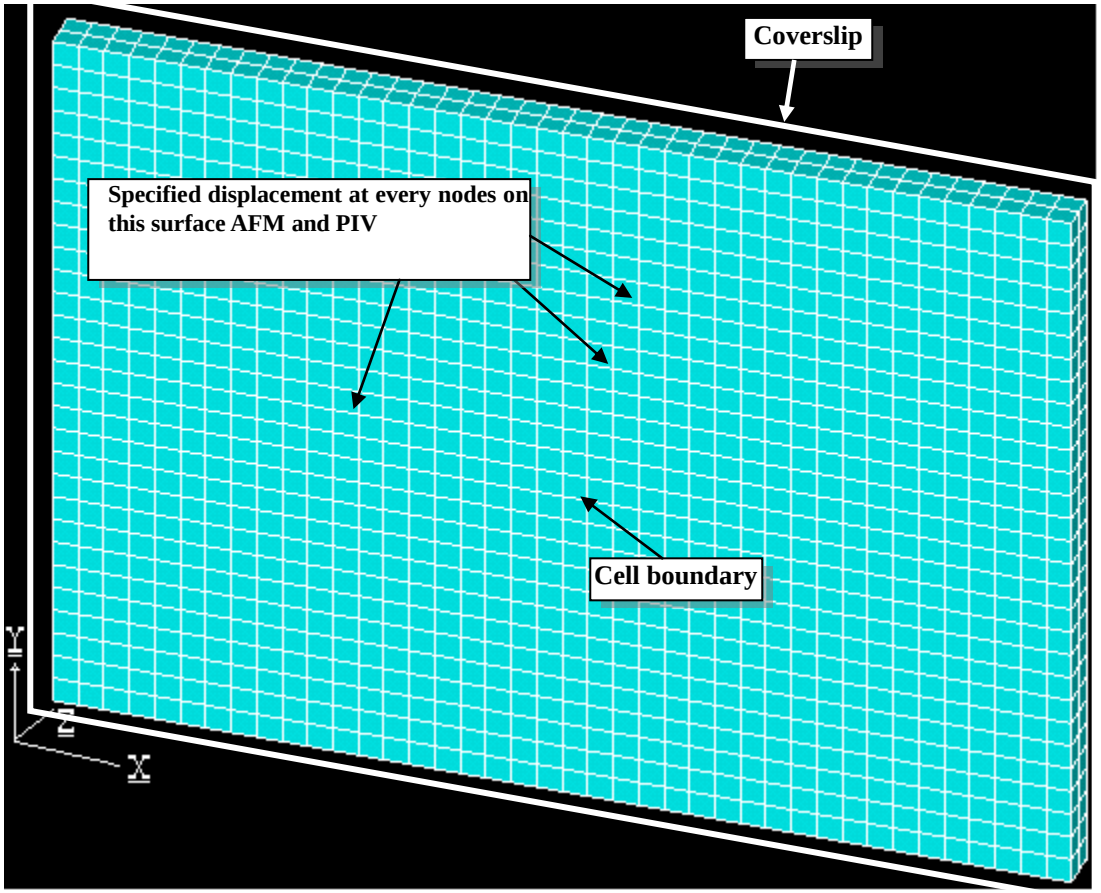

Fig. 3.6 Coordinates and geometry of PAG with dimension of 445.74μm×327.75μm×18.35μm for FEM analysis. The boundary conditions were specified displacements at corresponding nodes, generated from the PIV calculations on the movement of silica beads as shown in Fig.3.2(d). The bottom of substrate was fixed because of its attachment to cover slip.

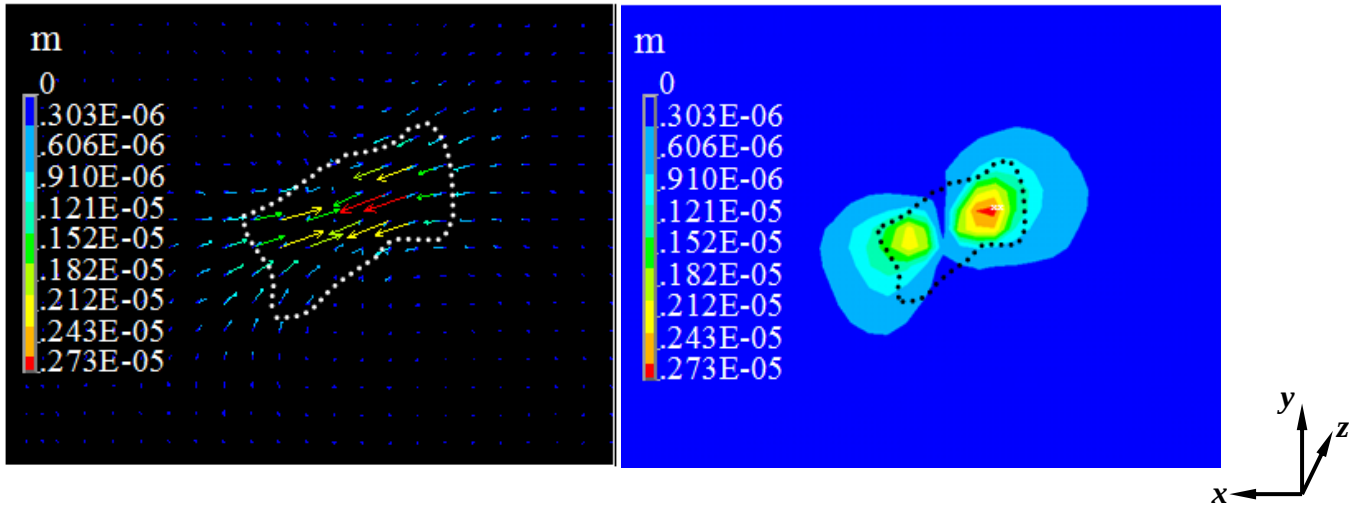

Fig. 3.7 Tangential (*x*-*y*) displacement field induced by SMCs from PIV calculations and specified for FEM analysis. Both the contour and vector plots are presented for a comparison with Fig.3.5(c). Dotted lines are the boundary of SMC.

Fig. 3.8 demonstrates an example results of vertical (z) displacement and three stresses on the gel surface under cell traction. The choice of Young's modulus of linear elasticity is 39.2kPa, the mean value of AFM measures from Fig. 3.3. Corresponding values of $C_{10} = C_{01} = 3.267$ kPa are estimated from Eq. (3-9) presuming that the initial slope of stress-strain curve is 39.2kPa. The equal values of C_{10} and C_{01} implies an equal contribution to the strain energy by principal and deviatoric strains ($\bar{I}_1$, $\bar{I}_2$). Fig. 3.8(a) shows the calculated vertical displacement u_z with a selected line of deformation profiles (insets of Fig. 3.8(a)). The Mooney-Rivilin model predicted that PAG surface to be sagged at the center and bulged around the edge within the area underneath cell. This result is consistent with the phenomena of focal adhesions where a high concentration of integrins appears around the edge of cell at protrusions like lamellipodia or hairlike filopodia to drive its motion. The cellular traction exerted by cells thus pulls the PAGsurface upwards. Focal adhesions are served as the physical linkages between cells and ECM to sense and transmit cellular traction force in order to regulate the movement of the cell[181-183].

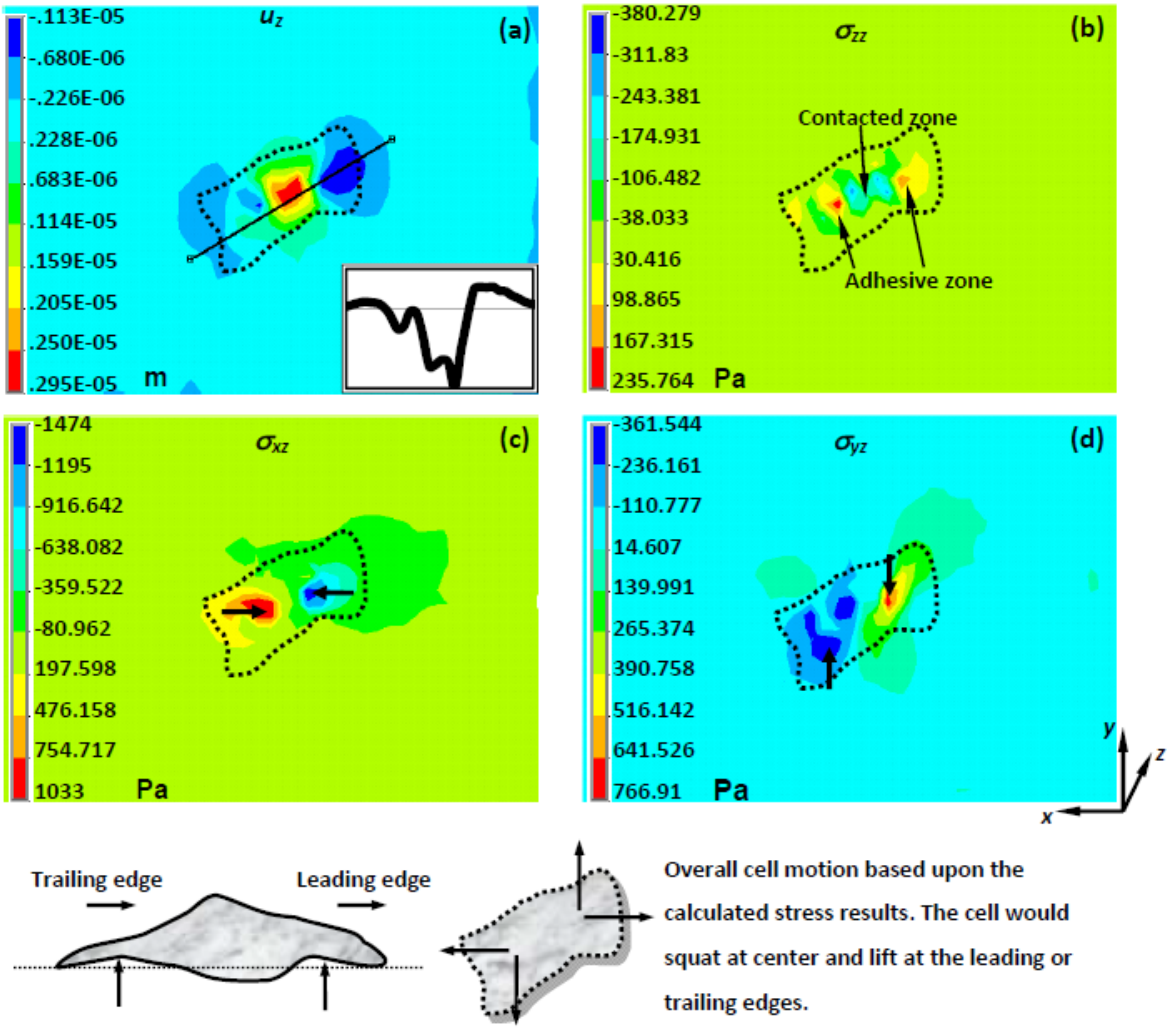

Fig. 3.8 Displacement and stress contour for linear elastic$E$= 39.2kPa (left column), and nonlinear elastic model, C_{10}= C_{01}= 3.267 kPa (right column).Profile of vertical deformation beneath the cell across the selected line is indicated in the insets of (a).

We further checked on the numerical values of displacement fields in Fig. 3.8(a) and compared them to the results from some other studies. In our results, the range of u_x, u_y was -1.13~2.95μm,Studies used as the references to evaluate our models are listed in the following: u_x and u_y: 0.20~1.20μm, u_z: -0.64~0.39μm by Hur et al[184]; u_x and u_y: 0.50~3.00 μm by Bulter et al[91]; u_x and u_y: 0.20~1.40μm by Yang et al.[92]

The corresponding normal and shear stresses simulated by the initial condition and boundary conditions (e.g. PIV displacement fields, mechanical properties of PAG)were simulated by FEM, the respective stress profile areshown in Fig. 3.8(b-d). Directions of shear stresses are indicated by arrows shown in figures. Both σ_{xz} and σ_{xy} help to indicate the direction of cellular motion. One noticeable result is from the normal stress σ_{zz} that regions of contact and adhesive locate at cell's center and margin respectively. If combining the results of u_z, we found that cell would squat or crouch at its center and haul up its leading and trailing edges in order to move. Note that although cell pressed down the substratum at its center, the adhesion still exists in the contact region simply because of the presence of integrins on the cell's bottom surface. The adhesion was overwhelmed by contact pressure and thus results σ_{zz} to become negative. This example case demonstrates that FEM simulation can provide an insight into the experimental results of traction force microscopy.

3.4 Discussion

3.4.1 Consistency check on finite element analysis

The FEM analysis shown in the previous section should be further examined for its numerical consistency on the contact region. Consider two bodies in contact, the contact stress (both normal and shear) exists only within the contact region. Outside the region, surfaces of both bodies are traction free. Assuming a point $\mathbf{x}$ locates outside contact region Ω, the traction free condition can be expressed generally as

$\boldsymbol{\sigma} \cdot \mathbf{n} = \sigma_{ij} n_j = 0$ for $\mathbf{x} \notin \Omega$

where $\mathbf{n}$ is the normal vector of the surface. For the case of PAG substratum underneath cells, the normal direction is in the $-z$ direction, thus $\mathbf{n} = (0,0,-1)$. This leads to the condition that $\sigma_{zz} = 0$, $\sigma_{xz} = 0$ and $\sigma_{yz} = 0$ on the surface of PAG outside contact region. In the current FEM analysis, there is no specified area of contact and therefore whether the traction free condition can be met outside the contact region is unknown. In order to identify the contact region, the following process was implemented: (1) converting the contrast microscopic image into black-white scale and filter out noises; also creating an equal size black-white map as a template for FEM nodal information. The pixel values of these two maps are denoted as $f^{\exp eriment}(\mathbf{x}_i)$ and $f^{FEM}(\mathbf{x}_i)$ respectively; (2) picking up an threshold value c so that $\sigma_{ij}(\mathbf{x}_i) = 0$ if $c(\sigma_{ij}(\mathbf{x}_i))_{\min} \le \sigma_{ij}(\mathbf{x}_i) \le c(\sigma_{ij}(\mathbf{x}_i))_{\max}$; (3) specifying $f^{FEM}(\mathbf{x}_i) = 0$ if correspondingly $\sigma_{ij}(\mathbf{x}_i) = 0$; (4) calculating the difference $\sum_{\mathbf{x}_i} f^{\exp eriment}(\mathbf{x}) - f^{FEM}(\mathbf{x})$. These process will be iterated until the minimum of the difference was obtained for a selected value of c. In summary, the fore mentioned process can be compactly expressed as

$$\begin{aligned} &\min\{\sum f^{\exp eriment}(\mathbf{x}) - f^{FEM}(\mathbf{x})\} \\ &\text{s.t.} \\ &\inf/\sup\{c \mid \sigma_{ij}(\mathbf{x}) = 0 \text{ if } c(\sigma_{ij}(\mathbf{x}))_{\min} \le \sigma_{ij}(\mathbf{x}) \le c(\sigma_{ij}(\mathbf{x}))_{\max}\} \end{aligned} \quad (3\text{-}12)$$

Fig. 3.9 presents the result of detection contact region by comparing the FEM map with the contrast microscopic image for different Mooney-Rivilin constants. It seems that the threshold value c converges to a constant for all three stress components when c_{10} or c_{01} is larger than 10kPa, which covers the estimated value based on average Young's

modulus from AFM. The contact region identified by FEM map plausibly fits the contrast microscopic image.

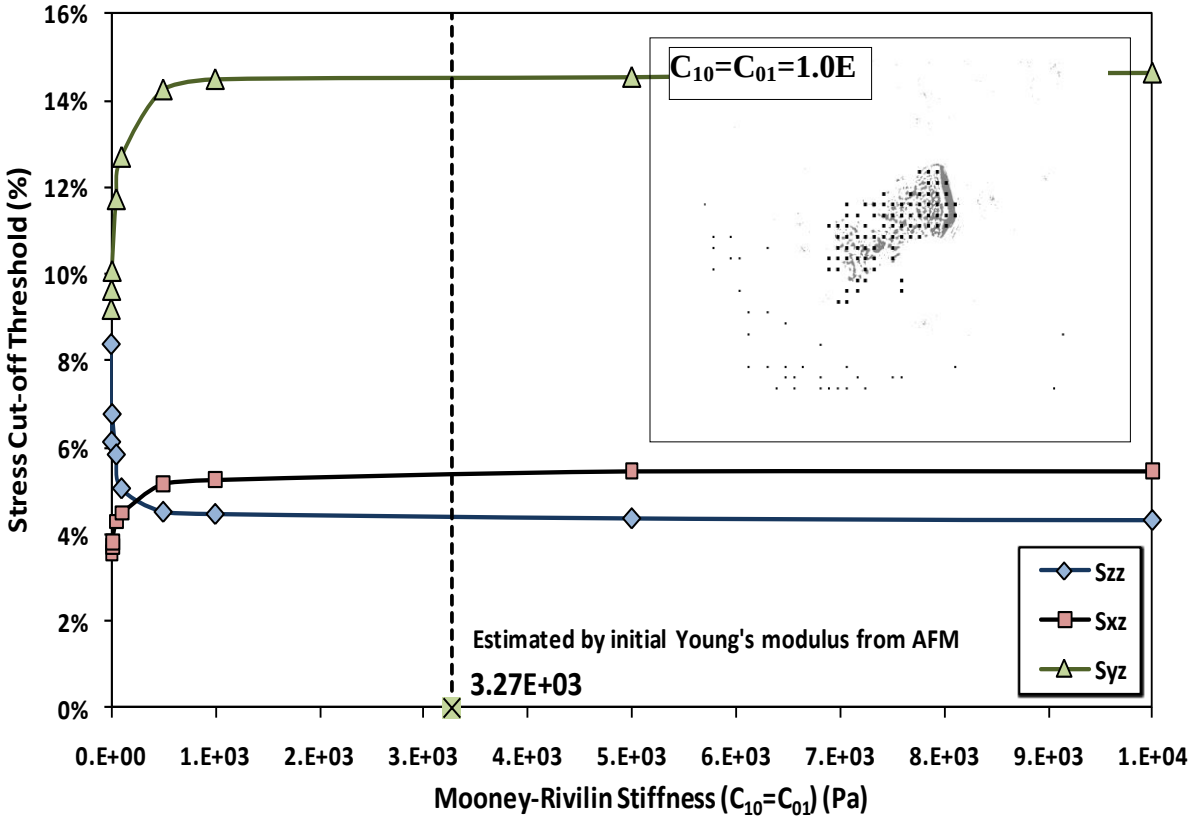

Fig. 3.9 Contact region detection by the cut-off threshold on FEM nodal stress to make a FEM map and then compared with the contrast microscopic image.

3.4.2 Traction force calculation finite element analysis

The shear stresses σ_{xz}, σ_{yz} and normal stresses σ_{zz} obtained from previous FEM analysis can be used to calculate the traction forces on PAG surface in the following the expressions:

$$\begin{aligned} Fx &= \iint_A -\sigma_{xz}(x,y)dxdy \\ Fy &= \iint_A -\sigma_{yz}(x,y)dxdy \\ Fz &= \iint_A \sigma_{zz}(x,y)dxdy \end{aligned} \tag{3-13}$$

where the area of integration is contained within the area underneath the boundary of cell. Since the values of stresses are at discrete nodes and the integration involves double integrals, numerical integration is necessary for the calculation. Simple trapezoidal rule is used for the calculation as the following example expressions [185]:

$$\iint_A \sigma_{xz}(x,y)dxdy = \int_c^d \int_a^b \sigma_{xz}(x,y)dxdy = T2D(\sigma,h,k) \tag{3-14}$$

where

$$T2D(\sigma,h,k) = \frac{1}{4}hk\left(\begin{array}{l} \sigma(a,c)+\sigma(b,c)+\sigma(a,d)+\sigma(b,d)+2\sum_{i=1}^{m-1}\sigma(x_i,c) \\ +2\sum_{i=1}^{m-1}\sigma(x_i,d)+2\sum_{j=1}^{n-1}\sigma(a,y_j)+2\sum_{j=1}^{n-1}\sigma(b,y_j)+4\sum_{j=1}^{n-1}\left(\sum_{i=1}^{m-1}\sigma(x_i,y_j\right)\end{array}\right) \tag{3-15}$$

h and k are intervals in x and y direction respectively.

$$h = \frac{b-a}{m},\ k = \frac{d-c}{n} \tag{3-16}$$

A uniformly discrete grid points were used for the calculation and these points are nodes

from FEM analysis. Following this numerical integration, we can determine traction forces in all three directions for different material constants (c_{10}, c_{01} for Mooney-Rivilin) as shown Fig. 3.9. Negative c_{10}, c_{01} were not included although they are allowable for certain classes of polymers [165-168].

The variation of traction forces in Fig. 3.10 demonstrates some interesting features. First, their magnitude increases as the PAG stiffens since a larger force is needed for a stiffer material in order to attain the same level of surface deformation. Secondly, the normal force F_z is found positive for positive c_{10}, c_{01} due to the slightly dominating contact pressure between cell and substratum. The F_z is around 1μN for the estimated $C_{10} = C_{01} = 3.267$ kPa. Lastly, the larger tangential force F_x than F_y implies a strong tendency of cell to move to the right. By a sheer luck, the image of a series of wavefront just to the right of cell was caught, which was evidently generated by the motion of cell. Fig. 3.11 provides some details of this observation. If the velocity of surface wave is equal to frequency×wavelength and the camera shutter speed is around 1/60-1/15 seconds then we estimate the wave velocity is about 9/(1/60-1/15)(1/s)×0.1898(μm)=0.0285-0.1139((μm/s). Such a speed looks like closer to the velocity generated by normal cells ((epithelial MCF-7) 0.003-0.1μm/s) [185] than by cancer cells (0.002-0.444μm/s(breast cancer cell), 0.0005-0.003μm/s (melanoma cells)) [185].

(a)

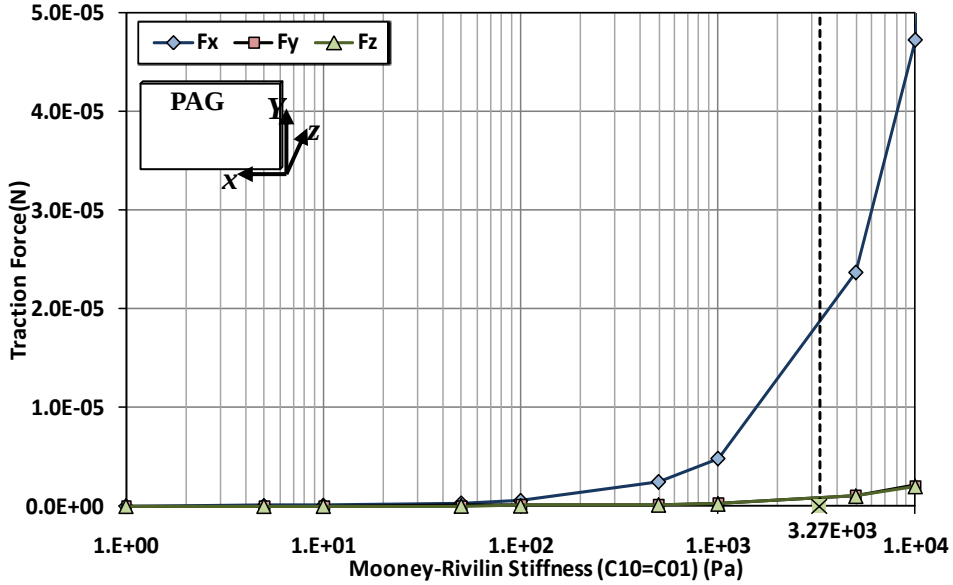

(b)

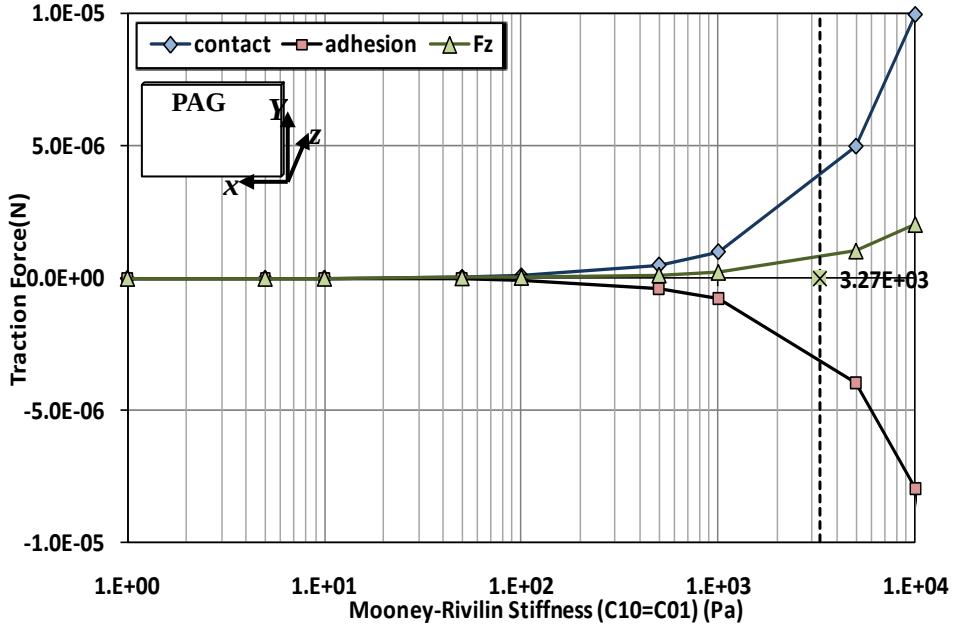

Fig.3.10Calculated tractions forces on PAG surface induced by cell as a function of different material constants. (a) is for all three forces in *x*, *y* and *z* direction. (b) is the breakdown of F_z into adhesion and contact pressure The positive values of F_z indicate that contact pressure slightly dominates over adhesion between cell and PAG sheet.

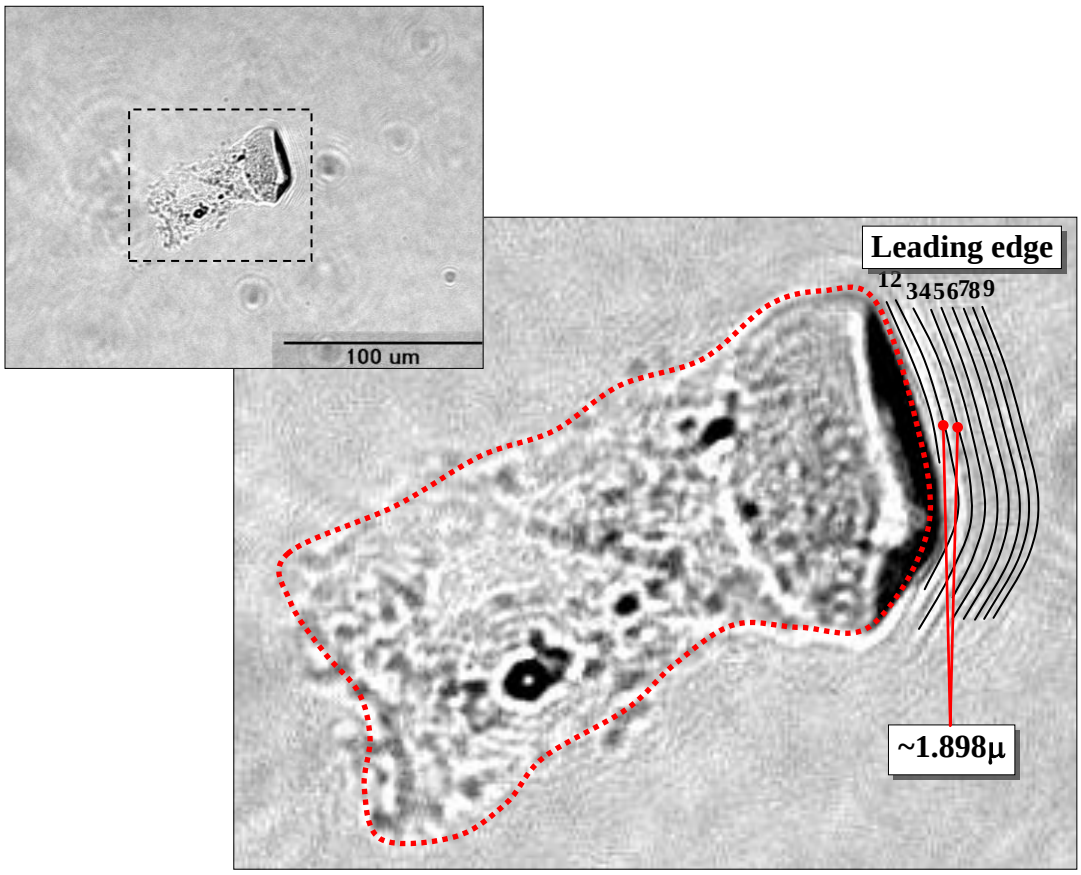

Fig.3.11 Ripples generated by the cell to move into its right. This may serve as an explanation for the larger horizontal force F_x in Fig. 3.9 from FEM analysis.

3.5 Conclusions

In conclusion, rat aorta smooth muscle cells were chosen for the study of cellular traction force on a PAG substratum. The PAG substratum was prepared to a desired concentration with chemically mixed fluorescent microbeads and immobilized on chemically activated coverslips. The traction forces between cells and PAG was marked by the movement of embedded fluorescent microbeads just beneath the gel surface, which portrayed the gel deformation caused by cell traction force. The measurement of displacement field was obtained from a pair of images, one showed the original position of beadswithout cell on top and the other was under the presence of cell. The displacement field was calculated

by the particle image velocimetry where a cross-correlation function of is introduced to derive the local motion of beads statistically. Once the displacement field was determined, the mechanical stresses and strains were analyzed by finite element method using the calculated displacement as boundary conditions. In the simulation part, a hyperelastic material model - Mooney-Rivilin were used to investigate the PAG mechanical response under cell traction force. Numerical results implied that cell moves on PAG substratum by pressing down its center while lifting its protrusions at leading and trailing edges. We also verified the FEM analyses by cross-examining it contact region with the microscopic photos to make sure their consistency. The total traction forces were calculated from FEM analyses to provide some insights into the cell traction microscopy. Most notably, the normal force F_z is found positive for positive c_{10}, c_{01} due to the slightly dominating contact pressure between cell and substratum. The F_z is around 1μN for the estimated $C_{10} = C_{01} = 3.267$ kPa. Lastly, the larger tangential force F_x than F_y implies a strong tendency of cell to move to the right. The measured tangential force is consistent with a series of wavefront on the phase contrast image just to the right of cell, which was evidently generated by the motion of cell. If the velocity of surface wave is equal to 0.0285-0.1139 μm/s. Such a speed looks like closer to the velocity generated by normal cells.

Chapter 4 The effect of two-dimensional constraints and microtopographic characteristics on cell traction force.

4.1 Introduction

It is well known that cell shape plays an important role in cellular activities such as adhesion, spreading, migration, proliferation, apoptosis, etc [186]. In the tensegrity model proposed by Ingber *et al.*[5, 6, 187], the cytoskeletal architecture of cell is in the state of isometric tension called prestress. The presence of prestress ensures instantaneous cellular mechanochemical responses towards extracellular mechanical forces. In the cytoplasm, the remodeling of cytoskeletal architecture activates a series of proteins that are physically immobilized on the cytoskeleton by stress-induced changes in molecular shape, position, or movement [31]. In addition, gene expression has found to be directly influenced by the alteration of prestress via the cytoskeleton-nucleoskeleton connections [188]. However, it is not known how the cell shape influences the contractility, which is governed bythe physical connections among the ECM, cytoskeleton, and nucleoskeleton.In this chapter, we developed two*in vitro* culture systems with different dimensionalities to investigate the role of cell shape in determining the contractility of vascular SMCs that has been proven to be important in vasoactivityin the cardiovascular physiology.

The use of soft-lithography known as μCP technique in cell culture system restricts the cell to spreadwithin a defined ECM islandswith controlled size and shape. The micro-patterned ECM island providesan elegant way in evaluating the role of cell

shape on cellular functions such as the proliferation, apoptosis, and differentiation. It has been shown that the increasing projected cell area leads to better cell proliferation while the decreasing cell area leads to apoptosis[106]. In addition, the elongation factor of the cell has been proven to regulate the differentiation of myotube by promoting dystrophone expression in C2C12 skeletal muscle cells [189]. Although such studies have successfully revealed the critical role of cell shape in cell functions, yet the mechanism of the cell morphological role is remained to be demonstrated. In addition, the cell shaped-dictated force balance manipulated by μCP can be served as the mechanosensory of the cell in the mechanotransduction[17, 74].Therefore, to reveal the correlationbetween cell shape andforce balance, it is essential to investigate the influences of cell size and shape on the cell traction forcein a controlled platform.

In previous studies, the combination of CTFM and μCP technique has demonstrated the linear relationship between cell traction force and spreading area[63, 73, 102]. However, only the size of the cell was controlled and the total magnitude of cell traction force was investigated. Fewer studies have been carried out whereby the aspect ratio of the cells wascontrolled to investigate the role of cell elongation factor in the generation of traction force. Tolić-Norrelykke *et al.*revealed that the cell-generated contractile forces were associated with cell shape where the wide and well-spread cells were observed to exert larger traction force than slim cells[190]. However, without the spatially confined microenvironment, it is difficult to correlate the cell shape and cell traction force in a quantitative approach. Li *et al.* manufactured specific cell-adhesive rectangular islands to constraint the cells in the same projected area but different aspect ratios[24]. They were able to demonstrate the total intensity of cell traction force was

decreased with the increasing cell aspect ratio. Due to the limit of previous CTFM models, they were not able to resolve the actual effect of cell aspect ratio in the orientation of cell traction force.

The cell elongation factor and the corresponding traction force orientation are particularly important in the cardiovascular tissue engineering. The major function of blood vessel is determined by the ability of the inner vessel wall to contract and relax coordinately with the dynamic blood flow. The functionality of cardiovascular tissue is thus governed by the vasoactivity of multiple vascular SMCs in the middle layer of blood vessel known as tunica media [1]. The study of single cell model performed by μCP is a powerful tool to discover the mechanism of mechanotransduction with respect to the cell shape and area. However, the single cell model itself cannot describe the collectivecell behaviors such as the vasoactivity of blood vessels. In native cardiovascular tissue, the vascular SMC activities are regulated by the collective behaviors via the intercellular biochemical and mechanical transition rather than individual initiation.Furthermore, the inability in coordinating contraction and dilation of internal diameter of vessel wall is the major cause in arteriolosclerosis and restenosis [116]. Therefore, it is important to discover the mechanism of cell contractility which is the major vasoelastic element in myogenic effect in order to provide the fundamental understanding for cardiovascular tissue engineering.

In this chapter, we reported the use of μCP technique to manufacture ECM islands with specific size and shape on PAG substrate. This powerful tool provides us a platform to study the mechanotransduction of single cell in a range of well controlled cell size and aspect ratio.In addition, scaffolds with microchannels assembled by discontinuous

microwalls were fabricated to provide microtopographic features for vascular SMC elongation and alignment. Anew developed FEM approach was applied in the traction force computation to yield several valuable insights of cell-generated mechanical signals such as traction force components in 3D Cartesian coordinate system. This allows us to study the orientation of cell generated contractile force in various cell morphologies.

4.2 Materials and methods

4.2.1 Cell culture

Primary vascular SMCs used in this chapter were obtained from human aorta. SMCs were cultured in high glucose DMEM supplemented with 10% FBS, 5mg/ml penicillin and 5mg/ml streptomycin (Invitrogen Inc.). The rest of the cell culture methodology was described in Chapter 3 (as seen in Section 3.2.4, Page 41).

4.2.2 PDMS stamp preparation and modification

Master silicon mold was made by a Surface Technology Systems deep reactive ion etching (DRIE) system. After etching, the silicon mold surface was passivated with a Teflon-like polymer for clean demolding. Poly(dimethyl siloxane) (PDMS, Sylgard 184 kit, Dow Corning) was prepared by thoroughly mixing two silicone components, 601A and 601B (Wacker Chemical) with the weight ratio of 10:1. After degassing the precursor in vacuum for 1 hour, the mixture was cast on the silicone mold and cured overnight at 80^{o}C. The polymerized PDMS was peeled off and cleaned in ultrasonic bath for 15 min in ethanol to remove the excessive monomers [24, 108, 111, 147, 191].

Surface chemistry is a critical parameter in carrying μCP because it determines the efficiency of ECM proteins transfer from PDMS stamps to targeted substrates and to secure the PDMS stamp at the desirable position throughout the printing process. The PDMS stamp surface is highly hydrophobic and inert to ECM proteins adsorption; hence it is not suitable to be used as a stamp. However, the interfacial properties of PDMS surface are readily modified to become highly hydrophilic by treating the surface with oxygen plasma.

4.2.3 Micro-contact printing on polyacrylamide gels

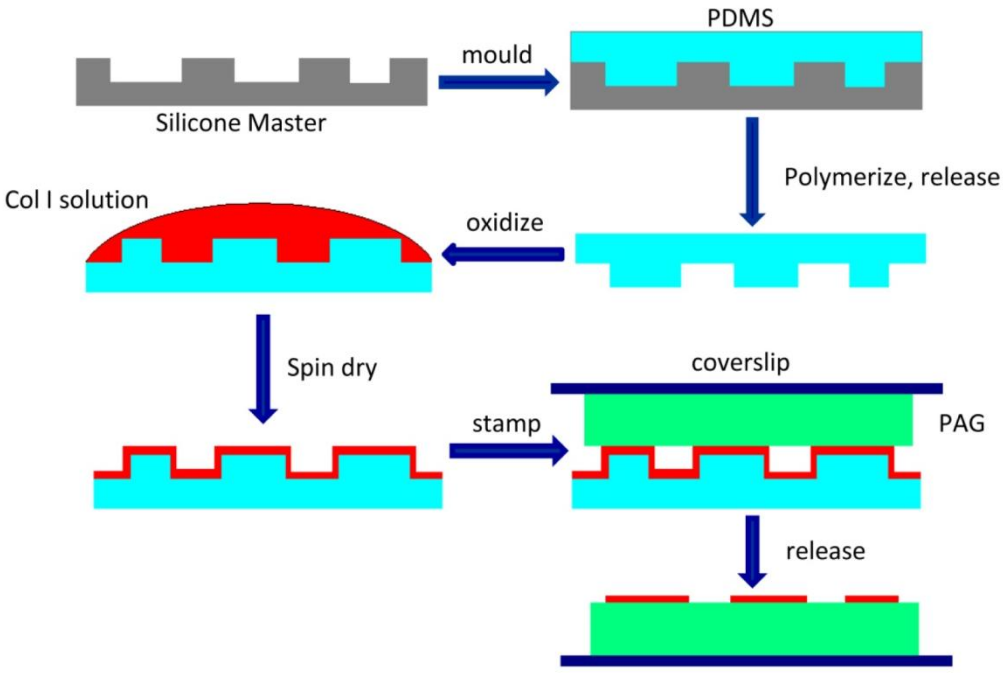

Fig. 4.1 Schematic illustration of the procedure used to stamp the micro-patterned collagen I islands on the surface of PAG. Refer to Materials and Methods for detailed description.

The surface of PAG was first activated by immersing in pure hydrazine hydrate (Sigma)

for three hours. The excessive hydrazine hydrate was washed in 5% glacial acetic acid (Sigma) in distilled water for one hour. The functionalized PAG sheet on coverslip can be stored at 4^{o}C with PBS up to 2 months. In order to covalently conjugate collagen I (Sigma) onto the hydrazine activated PAG surface, sodium periodate (Sigma) was added to oxidize collagen I. The oxidized collagen I exposed aldehyde group which is actively bonded with the hydrazine group on PAG surface. Collagen I was first solubilized in 0.1M acetic acid to the concentration of 1mg/ml. For oxidation, the diluted collagen solution was first diluted in 50mM sodium acetate buffer (Sigma) to 0.1mg/ml with pH 4.5. Lastly, 3.6mg/ml sodium periodate crystals (Sigma) was added in the diluted collagen I solution and incubated at room temperature for 30 minutes.

In order to performμCP, PDMS stamp was first covered with oxidized collagen solution for 45 minutes in room temperature. Due to the low surface energy and strong affinity to hydrophobic parts of molecules, a monolayer of collagen I protein was loosely attach to the surface of patterned PMDS. The PDMS stamp was then blew dried using nitrogen gas to remove excessive collagen solution and manually placed on the surface of activated PAG for 15 minutes. The stamp was pressed gently with tweezers to ensure close contact and lifted after 1 minute.

4.2.4 Fabrication of microchanneled scaffold

Microchannel array with discontinuous microwalls PDMS scaffold was fabricated using the exact procedure in Section 4.2.2. The microchannel with 300 μm of width was assembled by narrow microwalls with 60μm of height, 30μm of width, and 160 μm of length as shown in Fig 4.2. The microwalls were separated by a distance of 40μm, these empty regions in between the microwalls were found to enhance the rate of constrained

confluence by providing sufficient interaction among the cells in different microchannels [122].

In order to study the collective traction force of aligned and elongated SMCs, a thin layer of PAG with monolayer of fluorescent microbeads was coated on the PDMS surface as shown in Fig. 4.2(c). The microchanneled scaffold was first treated by Argon plasma to generate radicals on the PDMS surface. Although these radicals have a very short lifetime, they will subsequently react with air oxygen to form oxygen-rich species such as peroxide or hydroperoxide[192]. The peroxides will decompose to radicals under irradiation[193] or heating[194]. Therefore the life of plasma-generated radicals can be prolonged to initiate grafting polymerization. The PAG solution was prepared by mixing 10% v/v acrylamide (40% w/v, Sigma), 0.1% v/v N,N'-Methylene bis-acrylamide (BIS, 2% w/v, Sigma) in distilled water. The solution was degassed for 30 minutes with argon and added with pre-ultrasonicated 0.2μm fluorescent latex beads (fluorescein isothiocyanate (FITC)-labeled, Invitrogen) at 1/1000 volume concentration. The argon plasma treated PDMS scaffold was first exposed to air for 15 minutes for the formation of temporary peroxide layer on the surface. The degassed acrylamide solution mixture was then pipette to the surface of oxidized PDMS scaffold. The mixture was left under UV radiation for 15 minutes in order to deposit a thin layer of PAG on the PDMS surface. The PAG coated PDMS microchanneled scaffold was washed with PBS for 30 minutes to remove excessive acrylamide solution. The activation of PAG surface for the collagen I conjugation was illustrated in Section 3.2.3.

(a) (b)

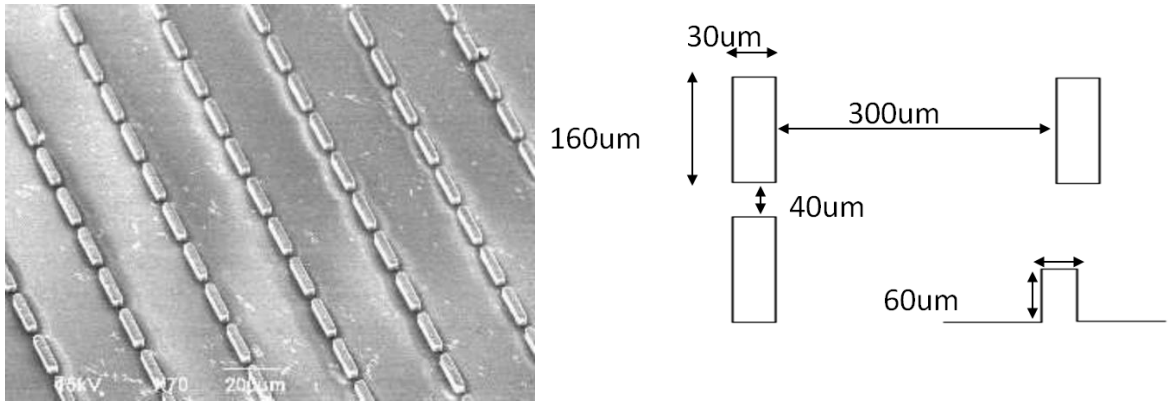

(c)

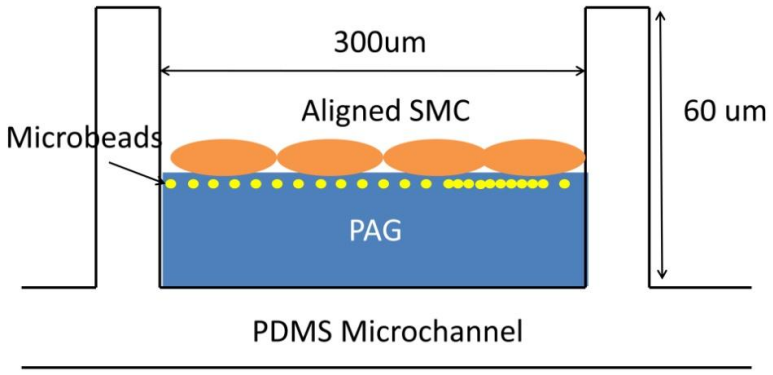

Fig. 4.2 Schematic illustration of microchanneled scaffold with discontinuous microwalls. (a) Scanning electron image of PDMS microchannel scaffold. (b) Geometry of microwalls. (c) Schematic illustration of PDMS microchanneled scaffold coated with a thin layer of fluorescent microbead embedded PAG.

4.2.5 Cell Traction Force Microscopy

The cell traction force microscopy assay was described in details in Chapter 3.

4.2.6Immunocytochemistry staining

SMCs were washed twice with prewarmed PBS to remove culture medium, covered with 3.7% paraformaldehyde for 30 minutes at room temperature to fix the cells, and washed twice with PBS again to remove excessive chemical. SMSs were then permeabilized by 0.05%Triton X-100 in 50mM glycine for 30 minutes and incubated with 10 μl/ml solution of Alexa Fluor 546 phalloidin (Invitrogen) for 30 minutes at room temperature. In order to prevent nonspecific staining with PAG substrate, 1% bovine serum albumin (BSA) was added to the staining solution. After incubation, the samples were washed rapidly with PBS for three times.

4.3 Results and discussion

4.3.1 Overall intensity of cell generated force

In order to study the mechanotransduction of cells under a range of spreading area and elongation, μCP technique was applied to fabricate the patterns of adhesive ligand on the otherwise nonadhesive PAG surface with well defined area, aspect ratio, and spacing. The SMCs seeded on the substrate were strictly confined within the area of the precoated adhesive islands. Therefore, one can manipulate the cell shape, cell-ECM interaction, and cell-cell interaction for studying various mechanical signals involved in the complex mechanotransduction in a highly controlled manner. The magnitude and spatial distribution of cell contractile force in various forms were measured using the newly optimized cell traction force microscopy as mentioned in the previous chapter. In brief, the contractile forces generated by cells are measured by analyzing stress-dependent

displacement of small fluorescent beads that are embedded in the flexible PAG substrate before and after the removal of cells from the substrate.

To directly study the influences of cell size on the cellular biomechanical responses, the cell generated forces and stresses were quantified over a population of cells with a range of different spreading area by using μCP technique. The cell size was evaluated in terms of the projected surface area occupied by the cells and the cellular biomechanical responses were evaluated by three different scalar representations of traction force field. In this study, we evaluated maximum shear stress (σ_{max}), root-mean-square of shear stress (σ_{rms}), and overall magnitude of tangential traction force ($\left|Fxy\right|$). $|Fxy|$ is the summation of the traction force magnitude at *x* and *y* axes according to the Cartesian coordinate of the model, $|Fxy| = \sqrt{|Fx|^2 + |Fy|^2}$. $\left|Fx\right|$ and $\left|Fy\right|$ are the integral of their respective shear stress magnitude over the area, $|Fx| = \iint \sqrt{\sigma_{xz}^2(x,y)}\, dxdy$ and$|Fy| = \iint \sqrt{\sigma_{yz}^2(x,y)}\, dxdy$,respectively, which are the integral of their respective shear stress over the area, where $\sigma(x,y) = \left[\sigma_{xz}(x,y), \sigma_{yz}(x,y)\right]$ is the continuous filed of shear stress vector defined at any position (x,y) within the cell.

Fig. 4.3shows that the maximum shear stress and root-mean-square shear stress exerted by cell to the underlying gel are linearly correlated with the cell spreading area. The best fit (R^2 value) of linear relationship among σ_{max} and σ_{rms} against projected cell area are 0.6272 and 0.6325, respectively. Interestingly, the overall magnitude of the tangential force generated by cell demonstrates tight linear relationship against the projected cell area, the R^2 value of the linear regression line is 0.9516. These findings are consistent with the several previous studies [195].

(a) (b)

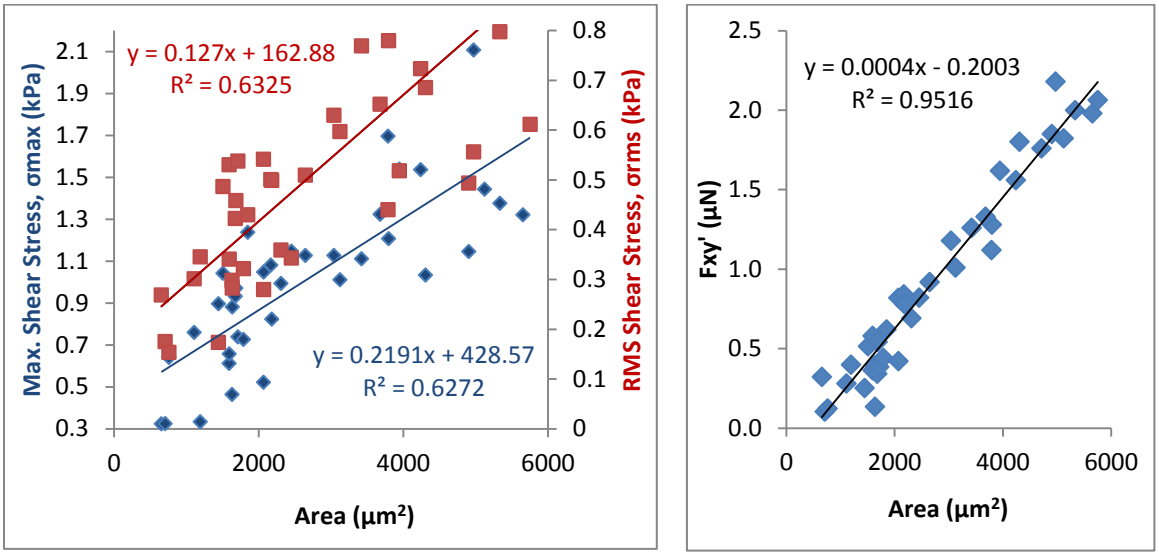

Fig. 4.3 Effect of projected cell area on the generated contractile force. (a) The maximum shear stress, σ_{max}. (♦) and root-mean-square shear stress, σ_{rms}. (■) generated by cell as a function of cell projected area, the respective linear regression line was fitted and displayed in blue ($\sigma_{max.}$) and red ($\sigma_{rms.}$). (b) The overall intensity of traction force experienced by substrate under the cell adhesion as a function of cell projected area.

4.3.2 Anisotropic force distribution in micro-patterned cells with different cell elongation factors

Cell elongation has been recently found to be one of the main phenotypic indicators in determining the biological functions of SMC. For instance, contractile SMC with elongated morphology exhibited significant vasoactivity by expressing substantial contractile proteins compared to the fibroblast-like morphology [1]. In our current study, the degree of cell elongation was quantified in term of cell aspect ratio, which is the ratio between the minor and the major axis (cell long axis) of the adherent cell. Cell aspect

ratio near 1 implies that the cell adopts either square-liked morphology, where value significantly larger than 1 implies that the cells are more polarized with spindle-shape morphology. In order to study the effect of cell aspect ratio as the global geometric cue on cellular mechanotransduction, cells were cultured on ECM-patterned surface and strictly confined within the ECM modified region with well defined shape and area. In contrast to projected area, cell aspect ratio did not establish a clear correlation with the overall magnitude of generated contractile force as shown in Fig. 4.4(a). Thereby, it can be concluded that the magnitude of the cell-generated contractile force is dominated by the degree of cell spreading. It is worthy to note that this finding is reproducible with other cell type such as human tendon fibroblasts studied by Wang et. al. [24].

In additional to the overall magnitude of the cell-generated contractile forces, the overall direction of contractile forces was found to be equally important in cellular activity. Recent studies had shown that cells controlled the direction of cell migration by generating anisotropic cell traction force to facilitate directional lamellipodia extension [63, 147]. Moreover, anisotropic cell traction force is important in regulating ECM protein expression, SMC differentiation, and tissue morphogenesis [24, 65, 147, 189]. In this study, the orientation of the tangential traction force was defined by the two force components acting on the substrate surface. The orientation of cell was the angular difference between the long axis of cell and the *x*-axis of the Cartesian coordinate model as shown in the inset of Fig. 4.4(b). This strong linear relationship (R^2= 0.9183) as mentioned above clearly illustrates that the orientation of cell traction force is closely related with the orientation of cell. As the orientation of overall traction force exerted by cells is one of the important characteristics of vascular SMC in cardiovascular myogenic

effect, to the best of our knowledge, no in-depth studies on cell aspect ratio effects on traction force direction have been reported to date. Therefore, it is worthy to investigate the role of cell aspect ratio in force orientation.

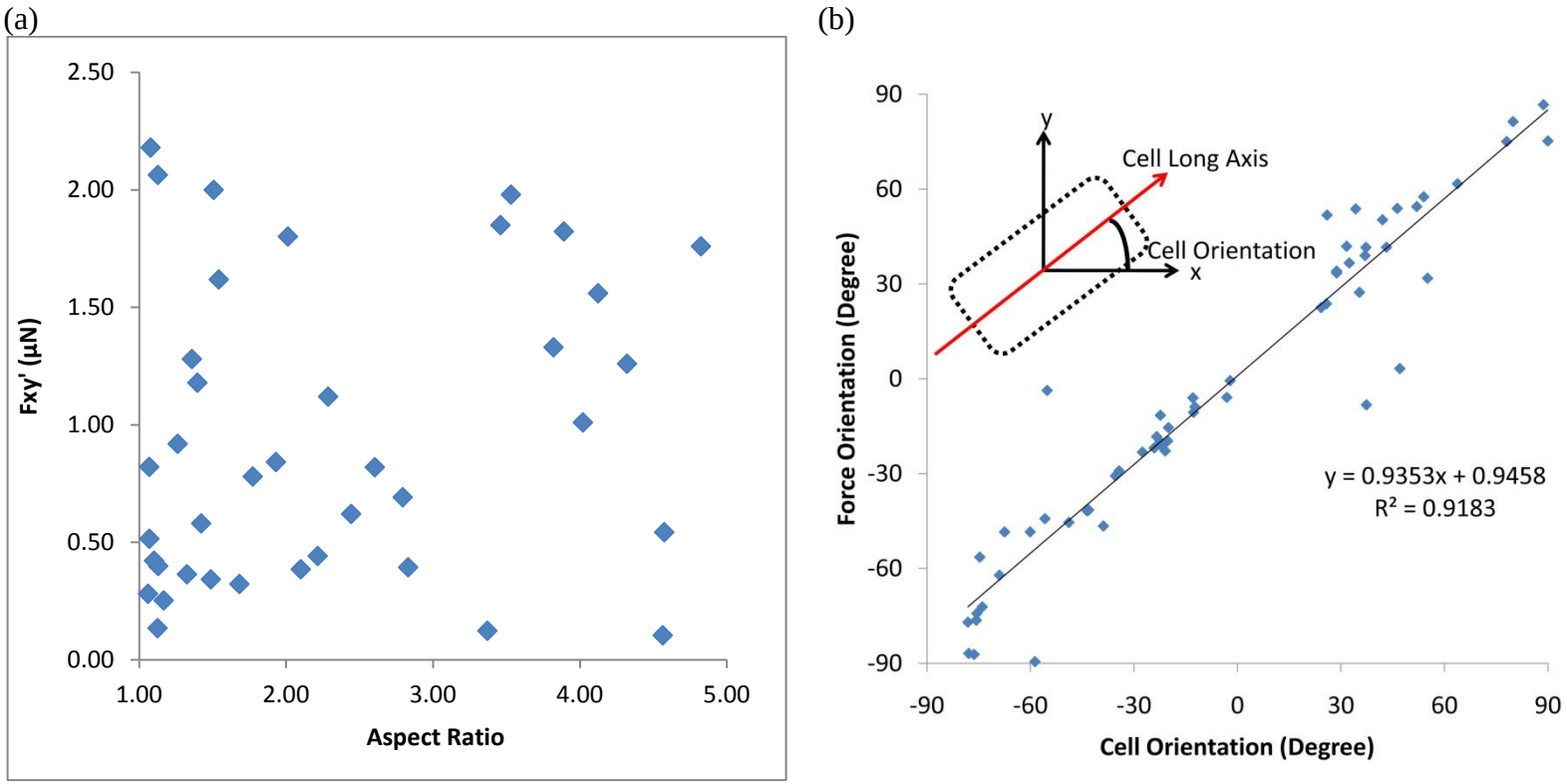

Fig. 4.4 The effects of cell aspect ratio on cell generated traction force. (a) The overall intensity of traction force experienced by substrate under the cell adhesion as a function of cell aspect ratio. The measurements showed no relationship between traction force intensity and cell aspect ratio. (b) The orientation of tangential force generated by cell is linearly related with the orientation of cell, the gradient of the regression line is 0.9353 with the R^2 value of 0.9183.

To elucidate the effect of cell aspect ratio on the orientation of generated contractile force, we measured the angular deviation between the cell long axis and the orientation of the tangential cell traction forces and defined it as θ value. Cell with low θ value implies close alignment between the orientation of generated tangential force and cell long axis; whereas the high θ value indicates large angular deviation between generated tangential force and cell long axis. Fig. 4.5(a) clearly demonstrates that the orientation of cell traction force was gradually aligned with the cell long axis against the increase of cell aspect ratio. Contractile-liked SMCs with high aspect ratio exhibited highly regulated behavior as the direction of cell traction is closely aligned with the cell long axis. In contrast, the fibroblast-liked SMCs with low aspect ratio value demonstrated random distribution of θ value in a broad range. The gradual constraint of cell traction force orientation with respect to cell long axis as shown in Fig. 4.4(a) indicates that the role of cell elongation in guiding the orientation of cell traction force.

To further interrogate the influences of cell aspect ratio on the angular deviation between cell long axis and tangential cell traction force, we classified the cells into three categories of interest according to their respective aspect ratios as shown in Fig. 4.5(b). Cells that confined within the ECM islands with the aspect ratio of 1.0 to 1.5 were defined as low aspect ratio, this group of cells represents the general fibroblast-liked SMCs in synthetic or proliferative state [196]. The median of the angular deviation (θ value) in the group of cells with the lowest range of aspect ratio was highest $\theta = 14.75 \pm 16.60^{o}$ (n= 15) among the three groups of cells herein. Cells that seeded on the ECM islands with moderate aspect ratio of 1.5 to 3.0 with $\theta = 6.10 \pm 5.65^{o}$ (n=20)represent the transition of SMCs from synthetic to contractile phenotypes. Lastly, the cells with the

aspect ratio ranging from 3 to 5 were defined as the high aspect ratio group. This group has an architecture that resembles the SMCs with contractile phenotypes that are commonly seen in the tunica media of blood vessel [1, 197]. The cells with high aspect ratio exhibited highly regulated behavior in the orientation of cell traction force, where the direction of the force was parallel to the cell long axis and with low error deviation, $\theta = 2.18 \pm 1.62^{o}$ (n=18). Although the force generated by the contractile vascular SMS in blood vessel is widely known to determine the major functionality of cardiovascular engineering, yet the orientation of contractility with respect to the cell elongation factor is less explored compared with the intensity of contractility. Therefore, the angular deviation was first defined in this study to facilitate the investigation of the correlation between cell aspect ratio the force orientation. These findings had given us the idea of how vascular SMC exhibit collective contraction and dilation when subjected blood pressure in the *in vivo* environment.

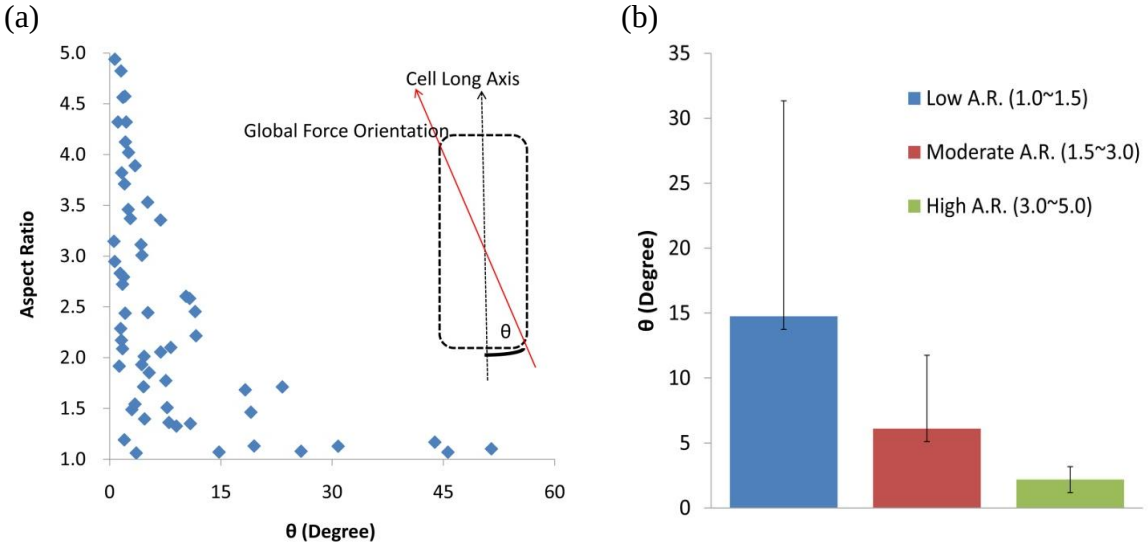

Fig. 4.5 Effect of cell aspect ratio on the orientation of generated contractile force. The graph shows the value of the deviation angle (θ) between the longest cell axis and the orientation of tangential cell traction force with respect to cell aspect ratio (a). The cells

were categorized into three major groups according to their aspect ratio. They are ‘low aspect ratio’ with the range of 1 to 1.5, ‘moderate aspect ratio’ with the range of 1.5 to 3, and ‘high aspect ratio’ with the range of 3 to 5. The mean and the standard deviation values are shown in each category (b).

4.3.3 Spatial distribution of PAG surface deformation caused by micropatterned SMCs

In order to further investigate the intricate correlation between cell aspect ratio and the orientation of cell traction force, representativeindividual cells from three groups shown inFig. 4.5(b) were chosen for examining the spatial distribution and magnitude of tangential deformation whichmay contribute to the trend of θ. It is found that the spatial distribution of cell traction force was governed by the cell aspect ratio. In general, the direction of major displacement vectors appeared to be originated from the cell periphery and along the cell long axis throughout different cell aspect ratios. However, fibroblast-liked cells with lower aspect ratio (A.R.= 1.07) did not exhibit preferential deformation along any direction due to the equal boundary sides as shown in Fig. 4.6(b). The displacement vector map shows that the magnitude of deformation vectors was evenly distributed over the radials of cell with low aspect ratio. Moreover, cells were found to generate greater traction forces around the acute corner regions compared to that around the obtuse regions.Hence the resultant force orients along the diagonal axis of the cell. In contrast, cell with moderate aspect ratio (A.R.= 2.10) demonstrated less dominant displacement vectors along the cell diagonal where a notable number of major displacement vectors were shifted towards the direction of cell long axis as shown in Fig. 4.6(d). Increasing number of major displacement vectors were found to be shifted from

the diagonal to the cell long axis against the increase of cell aspect ratio. For instance, significant number of displacement vectors which were parallel to the cell long axis could be observed in the cell with high aspect ratio (A.R.= 4.57) as shown in Fig. 4.6(f). This specific pattern of contractile orientation suggests the possibility of controlling the orientation of tangential traction force against the cell long axis by manipulating the shape of the cell mainly the cellular aspect ratio. This is particularly important in vasoactivity as the vascular SMCs are appeared to be in contractile phenotype with high aspect ratio.

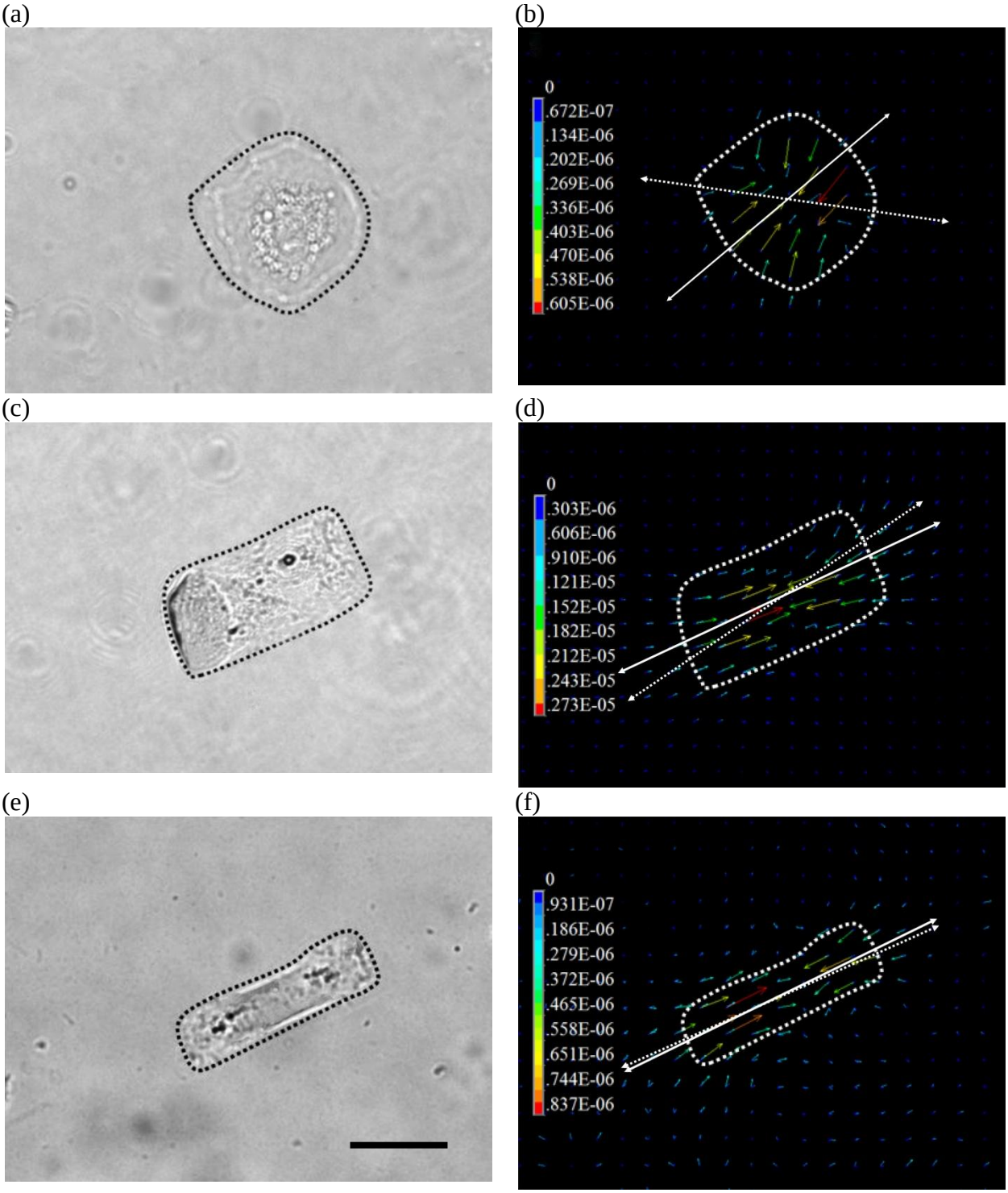

Fig. 4.6 Tangential deformations of PAG surfaces caused by cell traction force on with three distinguish cell aspect ratios. The left column shows the phase contrast image of SMC. (a) SMC with aspect ratio of 1.07 represents the low A.R. group. (c) SMC with

aspect ratio of 2.10 represents the medium A.R. group. (d) SMC with aspect ratio of 4.57 represents the high A.R. group. The right column shows the tangential displacement field induced by the respective SMC from the left column. The scale bar represents 10μm

4.3.4 Lamellipodia formation in the role of spatial distribution of cell traction forces on micropatterned SMCs

By inspecting of the influences of cell shape on the orientation of cell traction force, the broad range of random orientation of cell traction force was found in cells with low aspect ratio as shown in the Fig. 4.5(b). One of the possibilities that had driven this phenomenon could be attributed to the formation of membrane protrusion. Recent studies have shown that cells preferred to form lamellipodia, filopodia, and microspikes from the cell edges with acute geometric features [63, 108]. The extended lamellipodia which is constructed by stress fibers and focal adhesion reoriented the cell traction force and eventually led to the cell membrane protrusion or cell migration [147].

In this study, the lamellipodia formation was observed over a broad range of cell aspect ratio, with a modest preference for corners as the cells acquired rectangular shape on the micropatterned ECM islands. The extension of membrane protrusion at the corners exhibited irregular extension rate and area throughout the observation as shown in the Fig. 4.5(a),Thus the level of contractile force generated by the extended cell membrane fluctuates at the rectangular corners. In consequence, the asymmetrical force balanced was reestablished in order to accommodate the newly extended cell membrane around the cell corners, leading to the reorientation of cell traction force eventually. Even though quadratic cells tend to generate multi-axial forces from the their diagonal axes, the

orientation of tangential force was found to be highlyfluctuated due to the irregular intensity of generated traction forces from the newly formed lamellipodiaas shown in the Fig. 4.7(b) with the aspect ratio of 1.05. The phenomenon as mentioned above is consistent with the random distribution of angular deviation between the orientation of cell and the orientation of the cell-generated traction force found in cells with low aspect ratio. Cells with moderate or high aspect ratio showed similar pattern in lamellipodia formation around the rectangular corners. However, the formation was more ubiquitous along the short edges of the cell. Due to the narrow edges along the cell long axis under the aspect ratio of 1.82, the lamellipodia from the corners paired up at the tips of the elongated cell and extended the cell length along the elongated axis as shown in Fig. 4.7(c). The simultaneous formation of lamellipodia at both ends eventually polarized the cells and constrained the orientation of cell traction force along the cell long axis. Therefore the cells with moderate aspect ratio tend to shift their major deformation vectors from diagonal to the cell long axis with the increasing formation of lamellipodia at both ends as shown in Fig. 4.7(d).

These findings suggest that the orientation of force generated by cells on rectangular ECM pattern is regulated by the cell aspect ratio as well as the spatial lamellipodia protrusion. The alignment of force orientation along the cell long axis against the increase of cell aspect ratio was caused by the formation of two lamellipodia at the short ends of rectangle. While the cell aspect ratio has been identified as the global geometric factor in directing cell migration [105], we hypothesized that the specific migration is modulated by the anisotropic cell-generated contractile force orientation along the cell long axis. It is well known that cell migration is initiated by the formation

of lamellipodia at the moving edge [65]. In addition, by controlling the unilateral distribution of cell traction force using global geometric cue, the direction of vascular SMCs contractility can be controlled via the distinct formation pattern of lamellipodia.

(a) (b)

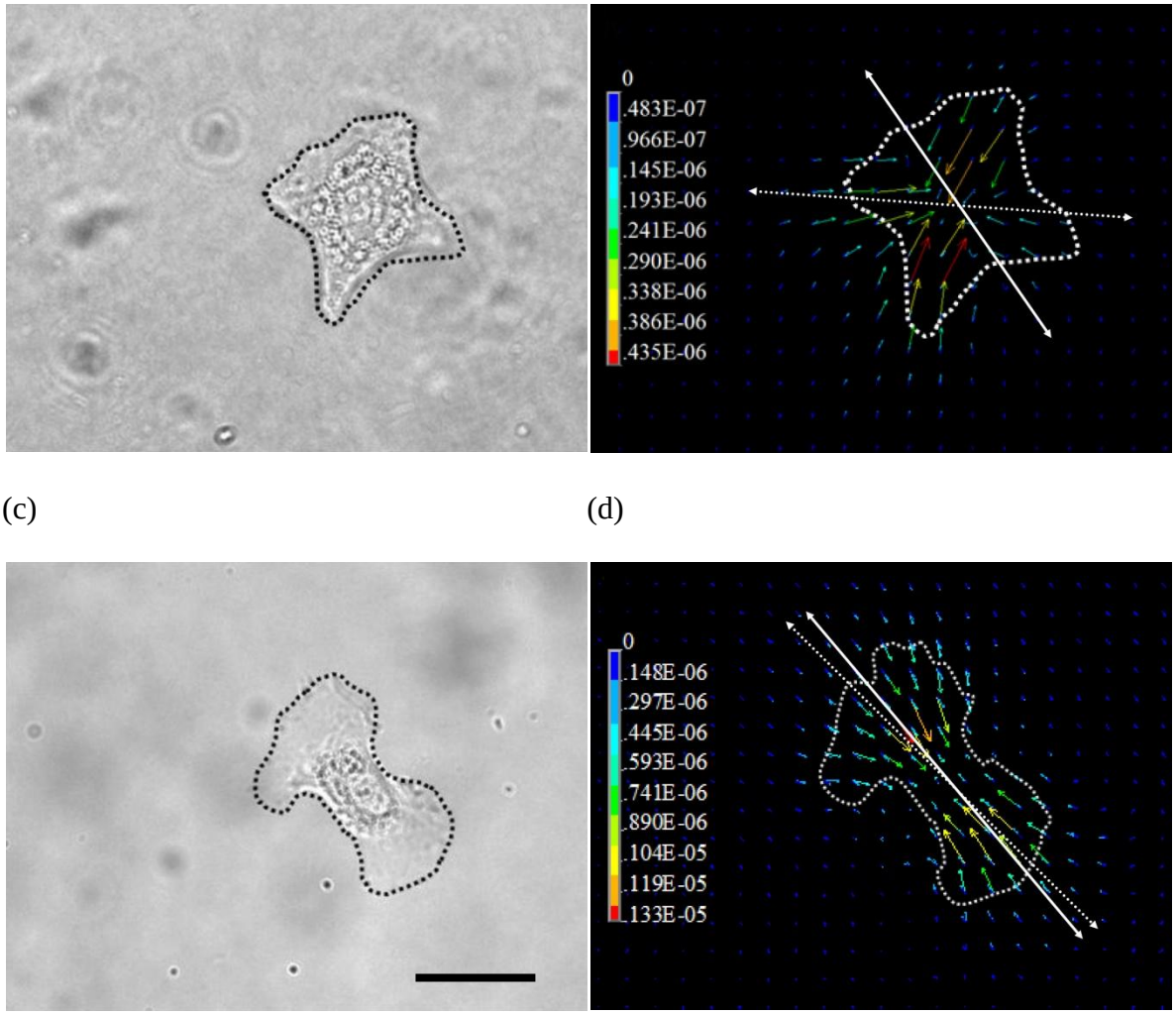

(c) (d)

Fig. 4.7 Patterns of lamellipodia formation in cells with different aspect ratios.The left column shows the phase contrast image of SMC. (a) SMC with aspect ratio of 1.05 represents the low A.R. group. (c) SMC with aspect ratio of 1.82 represents the medium A.R. group. The right column shows the tangential displacement field induced by the respective SMC from the left column. The scale bar represents 10μm

4.3.5 Organization of stress fibers in micropatterned SMCs

We had successfully identified the role of cell aspect ratio and lamellipodia in dictating pattern and orientation of the cell traction force. However, the mechanism that drives this phenomenon is yet to be discovered. It is generally believed the biomechanical responses of cell such as cell traction force are regulated by the multiple intracellular signaling transductions governed by tensegrity principle [5, 6, 26]. The tensegrity principle enables the establishment of force balance between cytoskeletal structure and ECM. In order to establish the force balance to achieve such an isometric tension, cell has to rearrange its cytoskeleton in order to accommodate the spatial constraint provided by the ECM pattern. Therefore, it is important to study the orientation of stress fiber, which is the major component of cytoskeletal structure in order to explore the missing link between the cell aspect ratio and cell traction force orientation.

To study the possible role of stress fiber in dictating the orientation of cell traction force, the fluorescence images of three representative cells for each aspect ratio group taken by confocal microscope were shown in Fig. 4.8.The result showed that fibroblast-liked cells with a low aspect ratio of 1.04 did not exhibit preferential orientation of actin filaments in the cytoplasm. However, bundlesof actin-rich filaments were found to be around the corners of the cells where lamellipodia was extended. This observed pattern of orientated stress fiber for cell with low aspect ratio (Fig. 4.8(b)) was compatible with the spatial distributions of cell traction force, where the major forces were found to be concentrated over the radials of the cells and around the extended cell membrane as shown in Fig. 4.6(b) and Fig. 4.7(b). Most importantly, there is negligible polarization of for cell with low aspect ratio due to the lack of aligned filament in the cytoplasm. The

actin filaments of cell seeded on the ECM pattern with moderate aspect ratio of 1.75 have been aligned with the diagonal axis of the cell as shown in Fig. 4.8(d). As the aspect ratio of the cells increased, the alignment of the actin filaments shifted from the diagonal axis to the cell long axis as shown in Fig. 4.8(f). This cytoskeletal organization as mentioned above suggests that the increases of cell aspect ratio regulate the polarity of the contractile fibers by merging the multiaxial filaments as seen in the cells with low aspect ratio (Fig. 4.8(a-d)) into the uniaxial filaments (Fig. 4.8(f)), and hence contributes to the uniform and directed contraction.

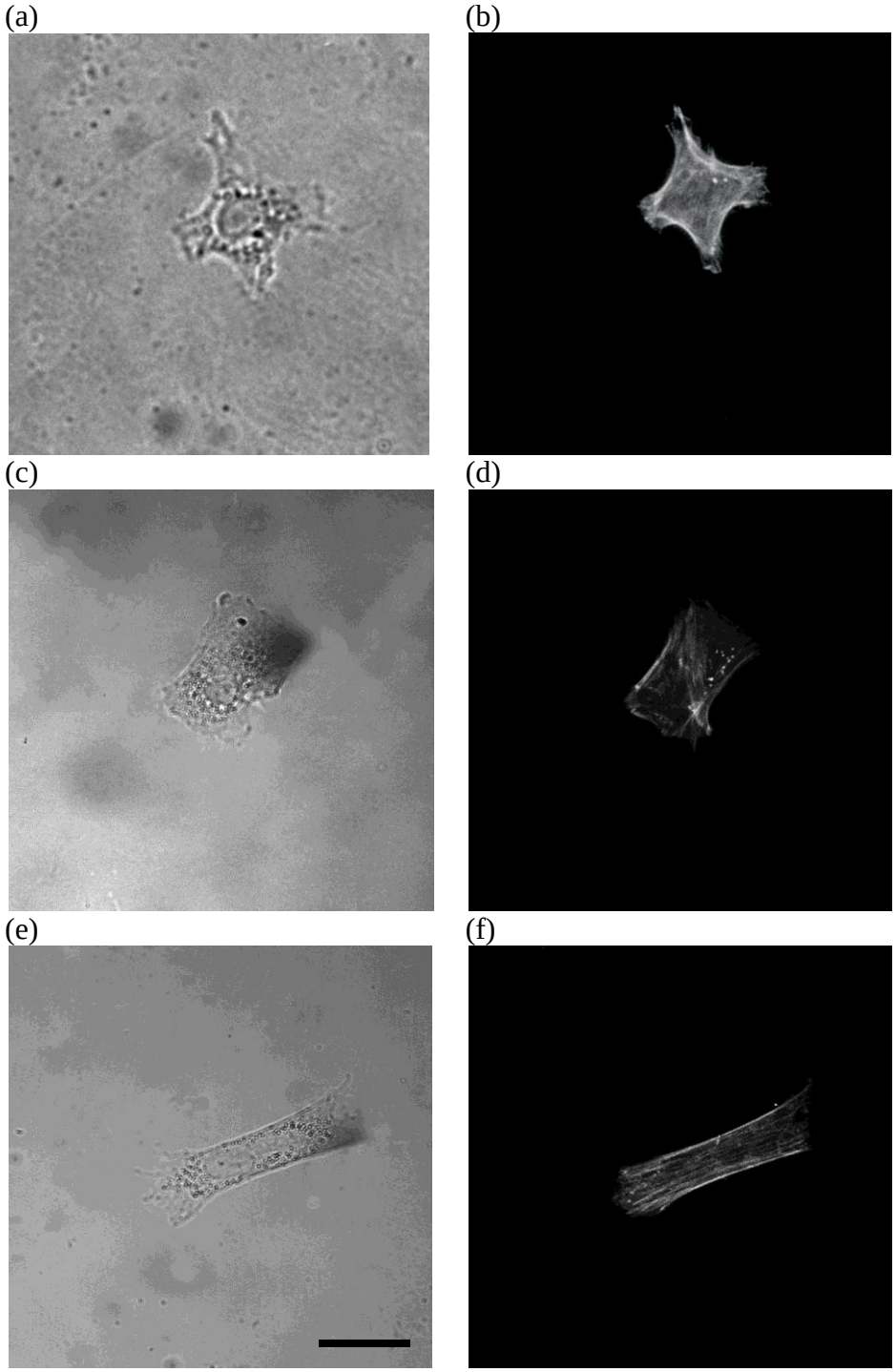

Fig. 4.8 Distribution of stress fibers in cells with different aspect ratios. The left column shows the phase contrast image of SMC. (a) SMC with aspect ratio of 1.04 represents the low A.R. group. (c) SMC with aspect ratio of 1.75 represents the medium A.R. group. (d) SMC with aspect ratio of 4.99 represents the high A.R. group. The right column shows

the confocal microscope images of cells in F-actin. The scale bar represents 10μm

4.3.6 SMC phenotype control in microchannel

It has been shown that uniaxial cell traction force of elongated SMC is the essential indicator of vasoacitivty in cardiovascular tissue engineering. In addition, the elongated SMCs expresses larger amount of contractile proteins such as α-actin, myosin heavy chain, calponin, and smoothelin compared with the cells with low aspect ratio from 1.0 to 1.5 [18-21]. However, the single cell model is insufficient to describe the complete functionality of blood vessels. Therefore, an engineered graft was created to accommodate the circumferentially oriented contractile SMC layer to mimic the cellular assembly and mechanical properties (sufficient burst pressure) of the native vessel wall for promoting specific cardiovascular functions.

To study the collective behaviors of vascular SMCs, we fabricated a microchannel scaffold with discontinuous microwalls that promotes SMCs alignment and contractile phenotype adaptation. This phenotype switch of SMC from synthetic phenotype to contractile phenotype using microchannels was pioneered by Chan-Park et al. [120, 122, 123]. We further modified this scaffold by coating a thin layer of PAG with fluorescent microbeads using argon plasma treatment in order to incorporate the cell traction force microscopy assay. Fig. 4.9(a-b) shows the SEM imaging of the PDMS microchannels with discontinuous microwalls coated with thin layer of PAG, where the smooth surface of PDMS was covered by the wrinkly PAG layer. The homogeneous distribution of fluorescent microbeads images collected by confocal microscope further validated the presence of PAG thin layer over the PDMS surface as shown in Fig. 4.9(c-d).

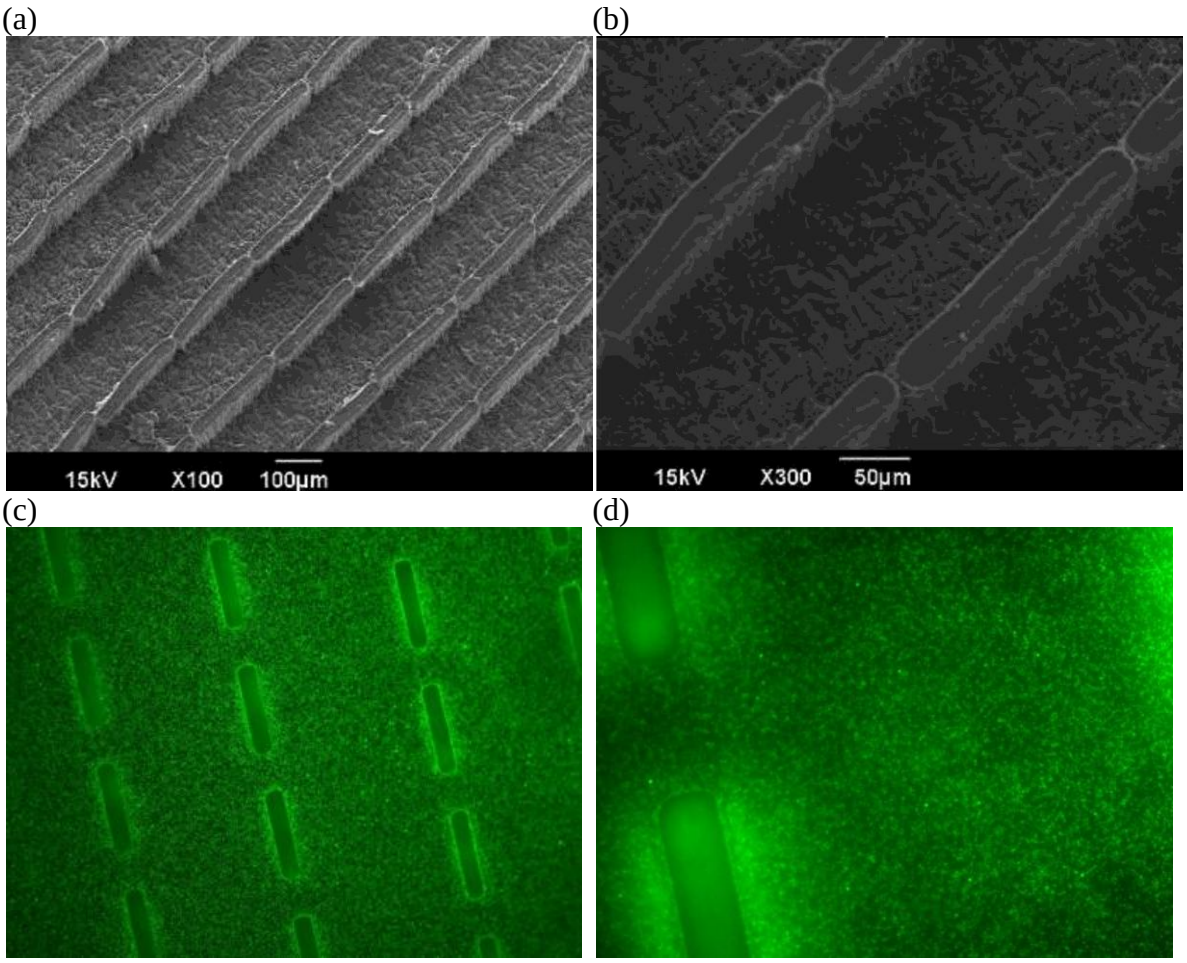

Fig. 4.9 PDMS microchannels with discontinuous microwalls coated with fluorescent embedded PAG. (a-b) Microtopographical structures of PAG coated PDMS microchannels captured by SEM. (c-d) A monolayer of FITC-microbeads distribution on the PDMS surface captured by fluorescent microscope.

As the collective cell behaviors are affected by the 3D topographic cues provided by the discontinuous walls, one would appreciate the influences of mechanical signals in the process of cellular assembly such as cell alignment which eventually contribute to the blood vessel vasoactivity. To observe the role of 3D constraints on the collective mechanical behaviors of cells, we seeded human aorta primary SMC on the PDMS

microchannels that are precoated with a thin layer of fluorescent microbead embedded PAG. With the initial seeding density of $1.5x10^5$ cells/cm^2, the cells started to align along the microwall's long axis after four days incubation. The cell alignment and phenotype changes as shown in Fig. 4.10(a)clearly demonstrated that the inclusion of microtopographical features are influencing the cellular mechano-transduction.

To investigate the collective cell mechanics under the 3D constraints, the surface deformation profile was extracted from the region where the multiple contractile cells were aligned with each other along the microchannels as shown in the dotted red rectangular region in Fig. 4.10(a). Major deformation was found to be originated from the interface between cells and microwalls as shown at the bottom region of Fig. 4.10(b). The cells in direct contact with microwalls exhibited strong contractile ability due to the micro-mechanical interactions between cells and microwalls. This observation was consistent with other studies performed by different cell models such as NIH 3T3 mouse fibroblasts and C2C12 mouse myoblasts [198]. This significant contractile ability and the elongated morphology demonstrated by the SMC adjacent to the microwalls were often accompanied by the cytoskeletal architectural organization as shown in Fig. 4.8, which in turn served as the indicators of changes in cellular activities [199, 200].

While a phenomenological link between cells contractile ability and microwalls is provided in Fig. 4.10(b), the direction of the major displacement vector observed at this region is remained to be elucidated. The results demonstrated in the earlier studies revealed that the direction of the cell traction force was highly regulated along the cell long axis especially for the cells with the aspect ratio of 3.0 and above. However, the surface deformation shown in the region near to the microwalls was perpendicular to the

cell long axis as shown in Fig. 4.10(b). One possibility to elucidate such conflicting findings is that the microwalls provided an extra dimension which was the vertically oriented surface that perpendicular to the direction of microchannelfor cell attachment. The extra dimensionality for cell attachment altered the cytoskeletal organization and the distribution of focal adhesions that correlate with the generation of traction force by providing new anchorage points for stress fibers rearrangement [69, 201]. As the region moving towards the centre of microchannel, the influences of the extra dimensional geometry were dissipating, while the affects of cell aspect ratio were increasingly dominant in the traction force orientation. This can be justified by the shift of the displacement orientation from perpendicular to the cell long axis at the microwall edges to the more aligned orientation to the cell long axis at the middle of microchannel as shown in Fig. 4.10(b). We hypothesized that the shift of displacement pattern at the middle of microchannel was caused by highly elongated and aligned cells that were parallel to the direction of microchannel.

In the analysis of traction stress distribution, the major traction forces were found to be concentrated along the edge of the microwalls and gradually normalized towards the center of the microchannel as shown in Fig. 4.10(c).The combination of this and previous phenomenon indicates that the microwalls served as the topographic cues to regulate the SMC contractile phenotypes and promote cell alignment along the direction of microchannels. Initially, the extra dimensionality for cell attachment provided by microwalls allowed the cell to adapt elongated morphology and to generate greater traction force along the edges of microchannels. As a result, this region of elongated cells with uniform alignment that was profoundly formed at the edges of microchannels

promoted the adjacent cells to adapt the identitical orientation by cell-cell interaction as seen in Fig. 4.10(b) and to provide similar topographic cues like the microwall.

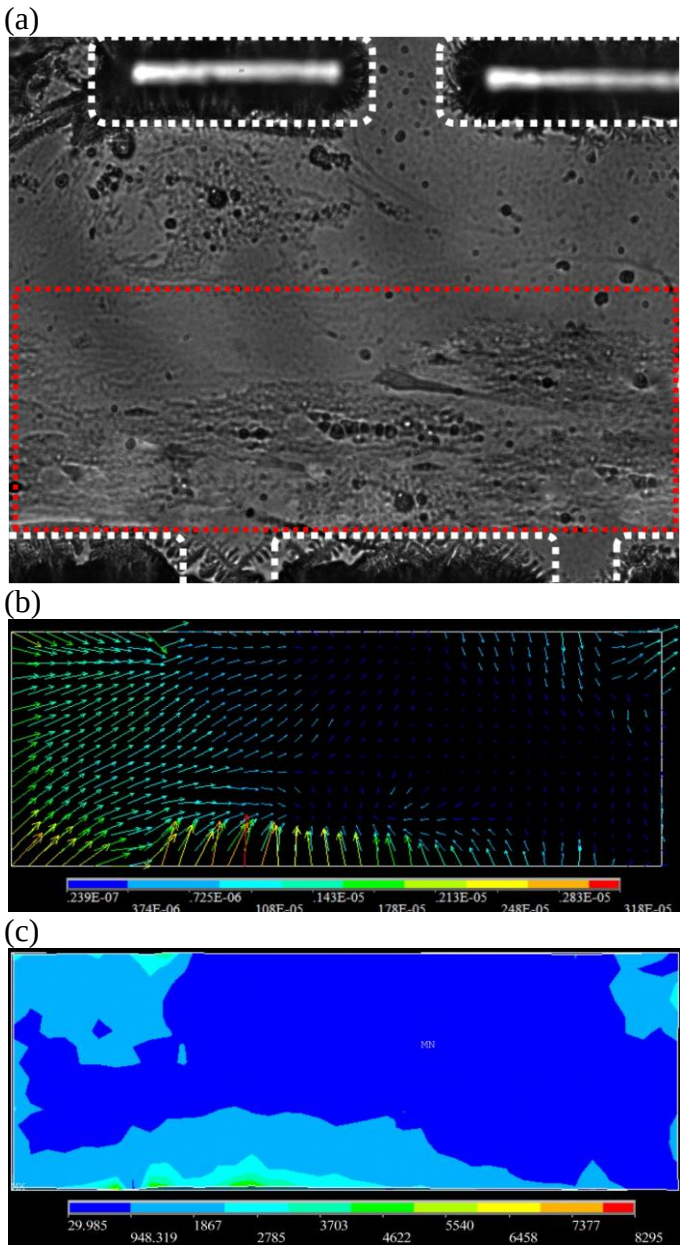

Fig. 4.10. Collective traction force analysis of the elongated SMCs aligned along the microchannels. (a) Phase contrast image of SMCs on microchannels with microwalls represented in white dotted line. The region adjacent to the bottom edge shown in the red dotted rectangle was chosen for displacement and stress analysis. (b) Displacement vector map quantified and analyzed by PIV to represent the PAG surface deformation caused by multiple cells. (c) Stress distribution simulated by FEM analysis.

4.4 Conclusions

In this chapter, the incorporation of μCP technique into our newly developed cell traction force microscopic assay allows us to isolate the role of the cell spreading area and elongation factor from the complex global mechanical cues in order to investigate the respective influences in cell generated traction force. The cell spreading area is found to be the dominant factor in determining the overall magnitude of traction force, where the magnitude of the tangential traction force is increased with the increasing spreading area in a linear relationship manner. The mechanical role in determining the orientation of cell traction force is found to be much more complicating where no major dominant factor can be singled out. First the orientation of cell long axis is found to establish a loose relation with the orientation of cell traction force. Further analysis shows that the force orientation tends to be closely aligned to the cell long axis and exhibits highly restricted angular deviation in SMCs with high aspect ratio. In contrast, SMCs with low aspect ratio tend to express broad range of traction force orientation. The analysis of surface deformation reveals that the alignment of force orientation with cell long axis is regulated by the traction force distribution pattern. The major forces are generally concentrated at the edges with acute geometric features and pointing towards the center of cells, thus cells with high aspect ratio and short edges are more likely to exhibit traction forces along the cell long axis. In addition, due to the preferential lamellipodia formation at the short edges, the extended cell membrane further polarizes the orientation of traction force along the cell long axis. The immunochemical staining of F-actin filaments reveals that the orientation of traction force is governed by the alignment of stress fiber which known

as the generator of traction force. Lastly, the mechanism of SMC elongation and alignment in the microchanneled scaffold is elucidated by investigating the collective traction forces generated by multiple aligned SMCs. Analysis shows that the SMCs establish elongated morphology by adapting the microtopographic cues from the microwalls. The SMCs along the edges of microchannels exhibit greatest traction forces due to the extra dimensionality provided by microwalls. This force is propagated from the edges to the center of microchannel and believed to have played an important role in the subsequent cell alignment. The quantitative measurements of individual and collective cell traction force with respect to their corresponding constraints are expected to facilitate the understanding of SMC physiological behaviors such as vasoactivity that are critical in cardiovascular tissue engineering.

Chapter 5 Bio-mechanistic study on outgrowing phenomenon of encapsulated chondrocytic isogenous groups in surface layer of hydrogel scaffolds for cartilage tissue engineering

5.1 Introduction

Cartilage tissue engineering heavily hinges on the encapsulation of chondrocytes into the 3D scaffold like hydrogels. Recent studies have shown that the microenvironment plays major role in preserving the phenotypes of committed chondrocytes such as spherical morphology and high expressions of collagen II and sulfated glycosaminoglcans (GAGs) [3, 202]. In order to retain the chondrocytic phenotypes in hydrogel such as alginate [203] and agarose [202], a homogenous 3D environment generated from controlled hydrogel synthesis for hosting encapsulated chondrocytes is critical.One primary hurdle for applying hydrogels in cell delivery is their lack of space for fast proliferating therapeutic cells like committed chondrocytes. As the clinical application requires live tissue with high viability, this drawback has to be overcome by providing sufficient space and enhancing cellular proliferation [204]. Thus it is essential to study the cellular activities of the chondrocytes which are encapsulated in various forms of hydrogel in order to discover the optimal cellular microenvironment for the development of alternative tissue engineering strategy to tackle the challenges as mentioned above.

To overcome both steric hindrance for cell growth and lack of cell adhesive moieties, a novel phase transfer cell culture (PTCC) strategy was developed by our collaborator in a recent study [205]. PTCCwas aimed to exploitthe multiple edges produced by the spontaneous formation of microspherical cavities in the hydrogel bulk.

Such multiple edges in the hydrogel bulk facilitated the directed outgrowth of the chondrocytes/isogenous groups from the cell-encapsulating hydrogel phase to the microcavities.This strategy was inspired by the phenomenon where the chondrocytes along the edge of the hydrogel surface exhibited dynamic cellular activities such as higher proliferation and sustainable ECM secretion compared with the chondrocytes located at the bulk region of hydrogel matrix. These specific dynamic cellular activities at the edge of gel were named as "edge flourish" (EF) phenomenon. The defined EF observation was consistent with a number of published works where the phenomenon is commonly occurred in diverse hydrogel studies [206-214]; however, only in the previous paper the EF terminology was defined, discussed, and further applied to a controllable platform [205].

Until now, the mechanism of such encapsulated chondrocyte behaviors in 3D environment is not well understood for further exploitation on the feasibility in applying PTCC strategy in cartilage regeneration. Although the significances of cellular mechanotransduction in 3D culture system are generally recognized, the understanding of such activities is less established due to the difficulties in probing biophysical responses of cells embedded in 3D matrices [215, 216]. Several theoretical simulations were developed using FEM to investigate the interactions between encapsulated chondrocytes, pericellular matrix (PCM), and 3D hydrogel based on the experimentally measured material properties of individual components [217-219]. However, the theoretical modelsas mentioned above did not include the real-time cellular mechanobiological activities of chondrocytes in the 3D system.

Therefore, the goal of this chapter is to substantially discover the biomechanical

nature of EF phenomenon via systematically elucidating the mechanobiological activities of encapsulated chondrocytes in 3D system with the use of biophysical techniques and other quantitative assays. We first evaluated the impacts of EF phenomenon in neo-tissue outgrowth and phenotypic changes along the edge of the agarose hydrogel using histological staining, then we probed the mechanobiological activities of the encapsulated chondrocytes using spatiotemporal studies of cellular distribution and movement in 3D culture system. We determined the micro-mechanical properties of the hydrogel under swelling condition in micro-scale using AFM. We also developed a FEM analysis to characterize and simulate the real-time biomechanical interactions at the interface of encapsulated chondrocytes and the surface of the hydrogel which are induced by EF phenomenon. The results presented here demonstrated that the EF phenomenon was driven by the superior proliferative activities along the edge of hydrogel. The directed growth of chondrocytic isogenous groups spontaneously exhibited asymmetric outwards stress and thus contributed to the emergence of EF layer with superior cell viability and ECM production that are critical in cartilage tissue engineering.

5.2 Materials and methods

5.2.1 Chondrocytes isolation and culture

Primary chondrocytes of each experiment were isolated and harvested from small pieces of cartilage tissues, which were retrieved from the porcine articular cartilage of a 5-month-old pig.The small pieces of cartilage tissues were then incubated in DMEM culture medium supplemented with 10% (v/v) FBS and 1 mg/mL collagenase type II.

After 12 hours of gentle stirring under the 37^{o}C incubation,chondrocytes were centrifuged, and resuspended in chondrocyte culture medium (CCM). The CCM consisted of DMEM supplemented with 20% (v/v) FBS, 0.01 M 4-(2-hydroxyethyl)-piperazine-1-ethanesulfonic acid (HEPES), 0.1 mM nonessential amino acids (NEAA), 0.4 mM proline, 0.05 mg/mL vitamin C, 100 units/mL penicillin and 100 mg/mL streptomycin. The cell suspension was transferred to the 75 mL tissue culture flask (Falcon, seeding density 2 $\times 10^4$ cells/cm^2) and incubated in humidified air with 5% CO_2 at 37 ^{o}C for routine culture.

To observe the histological evaluation of EF phenomenon, 4% paraformaldehyde was used to preserved sample slices. Safranin O and Masson's trichrome dyes were used to stain the sample slices accordingly.

5.2.2 Preparation of agarose hydrogels

Coverslips were first cleaned in Piranha solution (7:3 v/v H_2SO_4: H_2O_2) at 80^{o}C for 2 hours and washed with distilled water. After drying under stream of Nitrogen gas for 15 minutes, the coverslips were immersed in 95% water containing 1% 3-aminopropyltriethoxysilane for 10 minutes and washed three times with acetone, alcohol, and distilled water. The functionalized coverslips were used immediately after dried under 120^{o}C for 45 minutes [220]. 1 x 10^6/ml of Passage I chondrocytes were suspended in agarose hydrogel solution (w/v 0.02g/ml, in PBS) at 37^{o}C and injected into culture dishes with aminosaline functionalized coverslips (ϕ = 30mm) attached at the bottom. After solidification of agarose hydrogel at room temperature in 15 minutes, the cell/gel constructs were cultured in the 5% CO_2 and 37 ^{o}C incubator up to 32 days.

5.2.3 Characterization of mechanical properties of agarose hydrogel

AFM was used to measure linear elastic moduli ofagarose hydrogels with thickness of 600μm under swollen condition. A contact mode with spring constant (*k*) of 34.59 nN/m was applied via the silicon nitride cantilevers (Sharpened Microlevers, Crest Technologies). The indentation (*z*) of hydrogel surface and deflection (*d*) of AFM cantilever were closely monitored throughout the loading and unloading processes as shown in Fig. 5.1(a). The force-indentation relation also known as AFM force curve obeys the following equation[155]. According to the Eq. 3-1 and Eq. 3-2 present in Section 3.3.1, the minimum value of error along the curve in Fig. 5.1(b) represents the minimum least square difference between $z^{experimental}$ and $z^{calculated}$. The Young's modulus of 2% (w/v) agarose hydrogel was found to be around E= 27.83±1.94 kPa.

(a) (b)

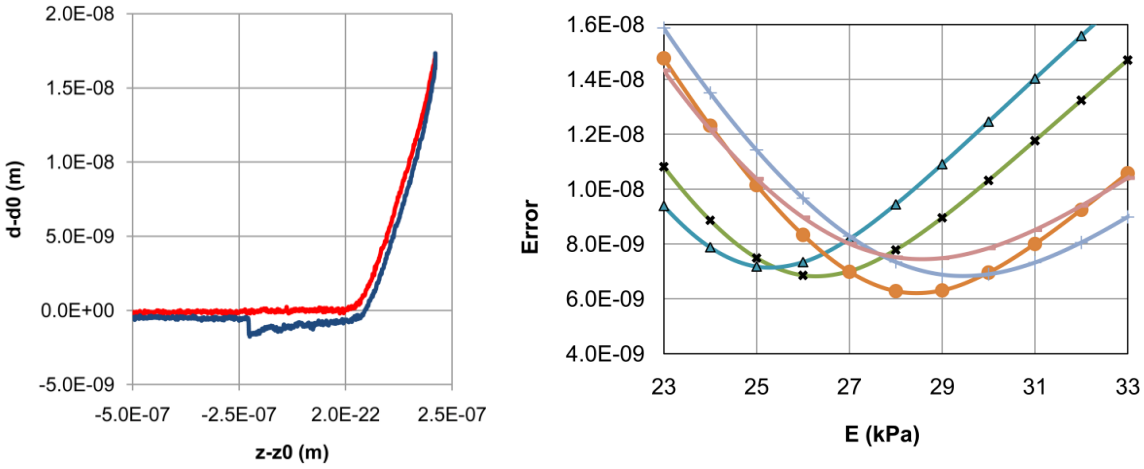

Fig. 5.1Experimental measure of AFM indentation curve for agarose substratum using contact mode. The red and blue curves represent the deflection of AFM cantilever during loading and unloading process, respectively (a). Errors (L_2 norm value) between the calculated and experimental measures of AFM indentation curves, n=5 (b).

5.2.4 Microscopy and characterization of chondrocytes spatiotemporal distribution

Laser scanning confocal microscope (Pascal 5, Carl Zeiss, Germany) with CO_2 incubator (Carl Zeiss, Germany) was employed in the cell imaging. The illumination source in confocal microscope is argon ion laser with maximum power of 1 mW and excitation wavelength of 488 nm. In order to monitor the spatiotemporal distribution of chondrocytes, the sample was transferred to confocal microscopic stage integrated with CO_2 incubator at 37 $^{\circ}$C and 5% CO_2 atmosphere in every alternating day. Confocal microscopy with a transmitted light collector allows us to distinguish individual focal plane with an interval of 100μm. A selected area of 0.849 mm^2 of the sample was captured starting from the bottom (focal plane 100μm)up to the surface of hydrogel (focal plane 700μm) as illustrated in Fig. 5.2(a).At each time point, nine stacked images from three different cell culture samples, eachwith three distinct regions were captured. Image analysis was done by using MetaMorph software (Molecular Devices, Inc. version 7.1.7.0. Sunnyvale, California, United States).

5.2.5 Preparation of microbead embedded-agarose hydrogel

To determine the biomechanical interaction between the edge of hydrogel and the encapsulated chondrocytes, the cell-laden agarose hydrogel was covered with a thin layer of agarose hydrogel embedded with a monolayer of 0.2 μm fluorescent latex microbeads (fluorescein isothiocyanate (FITC)-labeled, Invitrogen). The addition of microbeads served as the displacement markers for the measurement of surface tension of agarose.To prepare a thin sheet of top agarose layer, a 12 μl of mixture was dropped onto the

solidified bottom agarose hydrogel and overlaid with a piece of inert plastic sheet immediately throughout the polymerization process. For all experiments herein, the thickness of top agarose hydrogel is 6.5 μm and the thickness of the cell-laden bottom agarose hydrogel is 500 μm.

5.2.6 Surface tension characterization

Live cell microscopy was performed on an inverted light microscope (Olympus IX71) using a LUCPlanFLN 40x /0.60 Ph2 objective (Olympus) and motorized stage (BioPoint 2, Ludl Electronic Products). Cell-laden agarose hydrogelwith a monolayer of microbeadon the surface was supported on functionalized coverslip. Throughout the experiment, temperature of the chamber was maintained at 37^{o}C using Tempcontrol 37-2 Digital and Heating Unit (Leica). 5% Carbon dioxide and the humidity of the microscope stage were controlled by humidifier system (CTI-Controller 3700, Leica). In order to assess the displacement of microbeads caused by EF phenomenon, photomicrographs of the cells were taken with phase-contrast optics to visualize the cells' morphology and locations offluorescentmicrobeads were illuminated with excitation at 490nm and emission at 515nmat different time points.

PIVwas utilized to calculate the average movement of many nearby particlesinside a small windowdirectly from a *pair* of digital images taken at two different time points [173]. A linear stress-strain relationship was implemented to describe the mechanical behavior of agarose hydrogelfor quantifying the surface stresses generated by the EF phenomenon in the FEM analysis. The mechanical response of agarose hydrogel to the external forces was computed using the following stress-strain relationship:

$$(\varepsilon)=[D]^{-1}(\sigma) \qquad (5\text{-}1)$$

where ε is elastic strain vector and σ is the stress vector. $[D]^{-1}$ is the flexibility or compliance matrix of the material as follows:

$$\begin{pmatrix} \varepsilon_x \\ \varepsilon_y \\ \varepsilon_z \\ \varepsilon_{xy} \\ \varepsilon_{yz} \\ \varepsilon_{xz} \end{pmatrix} = \begin{pmatrix} 1/E_x & -\nu_{xy}/E_x & -\nu_{xz}E_x & 0 & 0 & 0 \\ -\nu_{yx}/E_y & 1/E_y & -\nu_{yz}/E_y & 0 & 0 & 0 \\ -\nu_{zx}/E_z & -\nu_{zy}/E_z & 1/E_z & 0 & 0 & 0 \\ 0 & 0 & 0 & 1/G_{xy} & 0 & 0 \\ 0 & 0 & 0 & 0 & 1/G_{yz} & 0 \\ 0 & 0 & 0 & 0 & 0 & 1/G_{xz} \end{pmatrix} \begin{pmatrix} \sigma_x \\ \sigma_y \\ \sigma_z \\ \sigma_{xy} \\ \sigma_{yz} \\ \sigma_{xz} \end{pmatrix} \quad (5\text{-}2)$$

where:

E_x= Young's modulus in the *x* direction*;* v_{xy}= Poisson's ratio in the *xy* plane*;* G_{xy}= shear modulus in the *xy* plane.The matrix is assumed to be symmetric, so that:

$$\frac{\nu_{yx}}{E_y} = \frac{\nu_{xy}}{E_x}$$

$$\frac{\nu_{zx}}{E_z} = \frac{\nu_{xz}}{E_x} \quad (5\text{-}3)$$

$$\frac{\nu_{zy}}{E_z} = \frac{\nu_{yz}}{E_y}$$

Also, agarose hydrogel is assumed to be an isotropic material. Therefore, $E_x = E_y = E_z$, $v_{xy} = v_{yz} = v_{xz}$, and $G_{xy} = G_{yz} = G_{xz} = \frac{Ex}{2(1+\nu xy)}$.

5.2.7 3D multiple-particle tracking

To characterize the movement of chondrocytic isogenous group, we systematically quantified the local 3D deformation of its surrounding matrix.0.2 μm fluorescent microbeads were evenly distributed throughout the cell-laden agarose hydrogel to serve as the matrix deformation markers. Microbeads adjacent to the target chondrocytes were first identified using the computer-controlled motorized microscope stage. Calibration plot for each identified microbead was then established by capturing a series of images

ranging from -10 μm below to 20 μm above the in-focus plane with the interval of 0.2μm. The intensity profile of the in-focus microbead image (z=0 μm) was sharp and narrow as shown in Fig. 5.3(a). When the microscope stage moved away from the in-focus plane, the pattern of the defocused microbead image deformed against$z$ displacement. At first, the width of microbead image increased and the peak of the intensity profile decreased. Subsequently, a series of ring intensity patterns were formed as the distance of the object from the in-focus plane increased. This assay relies on the change in the fluorescence intensity pattern of microbead against the $z$axisin order to determine the position of microbead caused by the movement of chondrocytes.

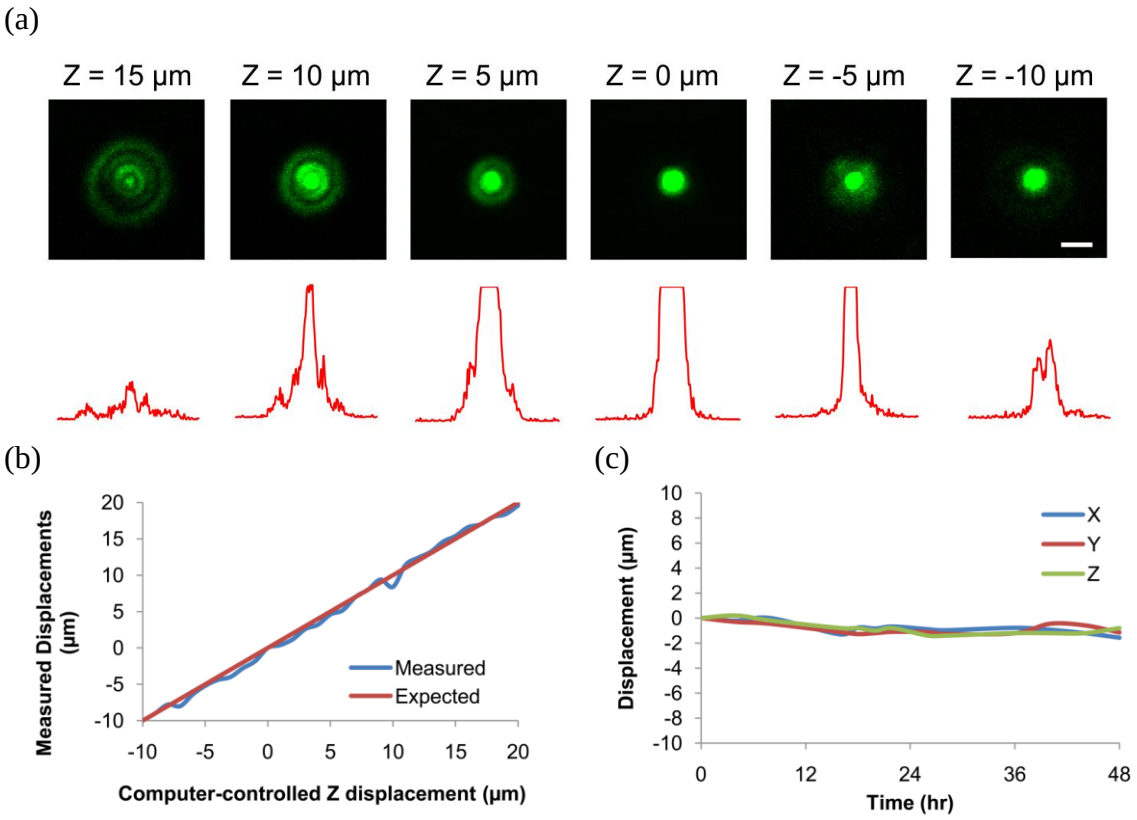

Fig. 5.3Assay to quantify the local 3D deformation of agarose hydrogel caused by chondrocytes. The calibration images set taken from the microbead of interest in the hydrogel. Indicated *z* positions are the relative position of computer-controlled micro stage to the in-focus focal plane, scale bar 3 μm (a). The measurement of *z* displacement is achieved by analyzing the pattern of microbeads gray image. The spatial resolution of the our 3D particle tracking assay was achieved by finding the root-mean-square difference between the position of computer-controlled micro stage and the relative measured displacement from the pattern of microbeads' gray level (b). The resolution of the assay is 0.589 μm, which is in the submicron-meter precision. Negative control of the 3D particle tracking assay (c). The immobilized microbeads were observed over 48 hours duration and the 3D position of microbeads was measured with every 4 hours interval. The passive displacements of microbeads without the presence of chondrocytes were

found to be less than 1 μm in all three directions.

In order to probe the real time deformation of local gel matrix, a set of microbead images spanning across -10 μm to 20μm with 1 μm interval along *z* axis was taken in every two hours. The relative position of the microbeads in *z* direction can be obtained by comparing the individual intensity profile with the respective set of calibration profiles using square error minimization method. This method allowed us to determine the current relative displacement of the microbead in the *z* direction by identifying the minimum value of error among the 150 intensity profiles from the calibration set. The tangential displacements of microbead in agarose hydrogel were obtained by monitoring the intensity-weighted center of mass of the in-focus microbead images using the track-object algorithm provided by MetaMorph.

Fig. 5.3(b) illustrates the relation between the computer-controlled *z* position and the relative *z* displacement measured by our assay. The root-mean-square (RMS) difference between the measured displacement and the imposed position in the *z* direction is 0.589μm. Therefore, the microbead position can be measured up to sub-micrometer precision along the *z* axis spanning from -10 μm to 20 μm away from the in-focus plane of the microbead. The advantage of this 3D particle tracking assay is that the microbead can be tracked over a large rangeof z interval without adjusting the position of motorized microscope stage, by doing so the systematic error can be kept to minimum. In addition, the negative control was carried out by tracking several microbeads in the cell-free agarose hydrogel. As shown in Fig. 5.3(c), over 48 hours of observation, the RMS difference between the measured displacement and the ideal zero movement in cell-free

hydrogel matrix is 0.897μm in *x* direction, 0.966μm in *y* direction, and 0.956μm in *z* direction. The result shows the lack ofself diffusion of the microbeads in gel matrix. In addition, the bulk movement of the agarose hydrogel within the height of500μm does not cause passive displacement of microbead more than 1μm in all three directions.

5.3 Results and Discussion

5.3.1 EF Phenomenon

In our study, the encapsulated chondrocytes were suspended in the homogenous agarose hydrogel and cultured *in vitro* up to 32 days withoutmechanical and biochemical stimulation. Fig. 5.4 illustrates the histological progress of EF phenomenon along the edge of hydrogel. Starting from Day 12 of culture, cellular outgrowth was progressively observed along the edge of the hydrogel. The result indicates that the embedded chondrocytes spontaneously sprout out of the hydrogel and formed a thick layer of neo-tissue known as EF layer on the surface of hydrogel in Day 40 of culture. This newly developed EF layer was rich in chondrocytic ECM such as GAGs and collagen which are visualized by red Safranin O and blue Masson staining, respectively. The formation of such neo-tissue is critical in cartilage tissue engineering where active proliferation of committed chondrocytes is one of the major challenges.

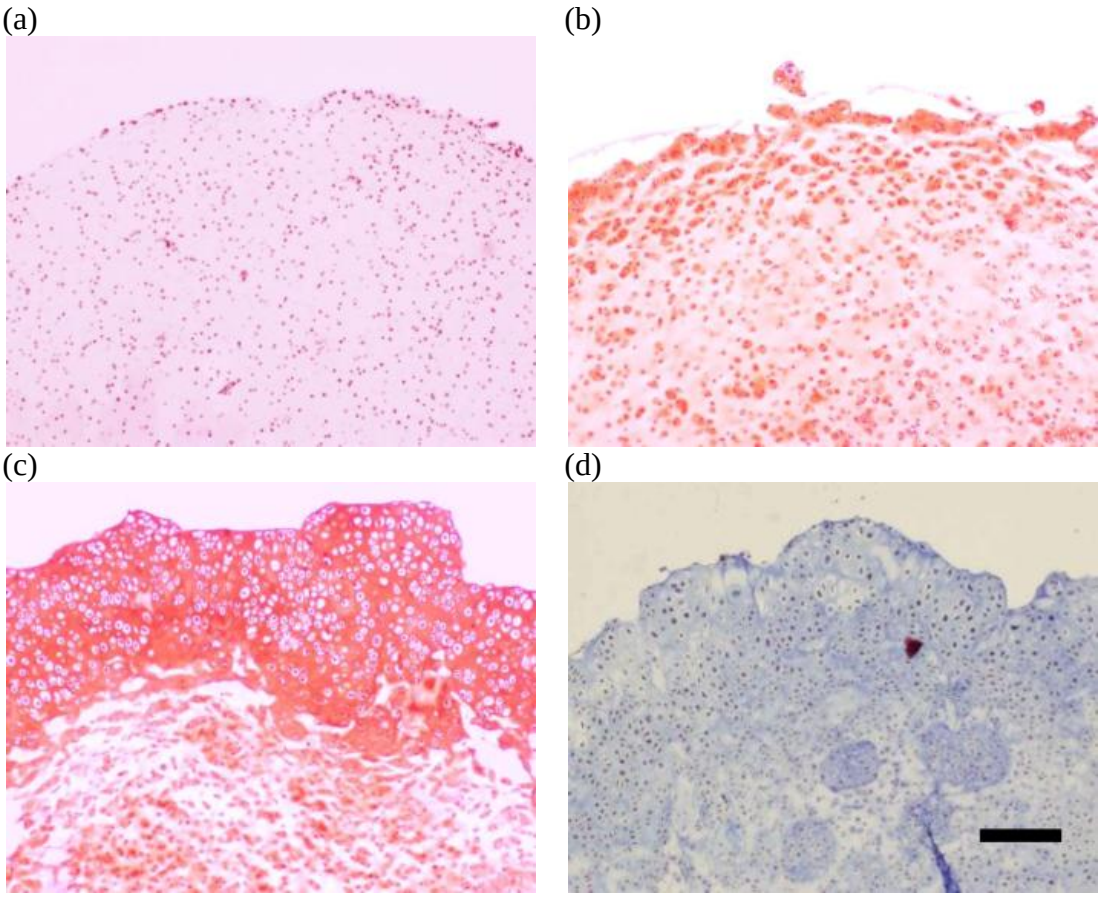

Fig. 5.4Histological illustration of EF phenomenon in agarose hydrogel. The glycosaminoglycan (GAG) and collagen were stained by red Safranin-O and blue masson staining respectively. On Day 3 after cell seeding, the distribution of cell remained homogeneous across the agarose hydrogel (a). On Day 12, the outgrowth of chondrocytes was initiated as a thin layer of rich chondrocytes and GAG was observed along the edge of hydrogel (b). On Day 32, a thick layer of neo-tissue known as EF layer was formed on the surface of hydrogel that is rich in chondrocytic ECM, GAG (c) and collagen (d).Scale bar, 200 μm.

The EF phenomenon has been observed in various *in vitro* systems that involved non-adhesive hydrogeland non-typical anchorage dependent cell types [205, 212]. In

order to facilitate the emergence of this phenomenon, two preconditions have to be fulfilled in the culture system. First, the hydrogel does not support the formation of cellular focal adhesion for attachment in the 3D microenvironment. Second, the encapsulated cell types are capable of preserving high proliferation and viability in the microenvironment with ECM deficiency.When these two preconditions were fulfilled, abundant neo-tissue formation would be observed along the edge of the hydrogel as shown in Fig. 5.4.

5.3.2 Spatiotemporal distribution of chondrocytes in agarose hydrogel.

We began the analysis of chondrocytes activity in agarose hydrogel by characterizingthespatiotemporal distribution of chondrocytes along the z axis.The density of cell increased linearly over time with growth rate of0.0378 x 10^6cells/ml per day as shown in Fig. 5.2(b). Fig. 5.2(c) illustrates the distribution of cell along different focal planes over 19 days of culture.In Day 1, the encapsulated chondrocytes were evenly distributed along all the focal planes in the hydrogel (focal plane 100 μm to 600 μm). For the focal plane closest to the bottom (focal plane 100μm, Fig. 5.2(c), deep blue), the number of cell decreased over time due to the adhesion of chondrocytes. The chondrocytes adhered to the coverslip surface were dedifferentiated and acquired elongated morphology[204]. Therefore none of these dedifferentiated cells were counted in our measurement. The cell number from focal plane 200μm to 500μm remained relatively constant over long period of time. Even though slight deviation in cell number can be observed in this region, yet it was insignificant compared with the overall cell growth. Hence we defined this region as bulk of hydrogel.The region between the hydrogel surface and 100μm below is thus defined as the edge of hydrogel. In contrast to

bulk region, the edge of hydrogel embraces significant cell growth over time. Initially, no cell wasobserved on the surface of hydrogel (focal plane 700µm), the cell number was then increased significantly and surpassed the number of cells from all the individual focal planes in bulk region after Day 17. This focal plane has the highest growth in cell number throughout the hydrogel. Cell number in focal plane 600µm increased linearly overtime and had the maximum number of cell count over all focal planes after Day 7.

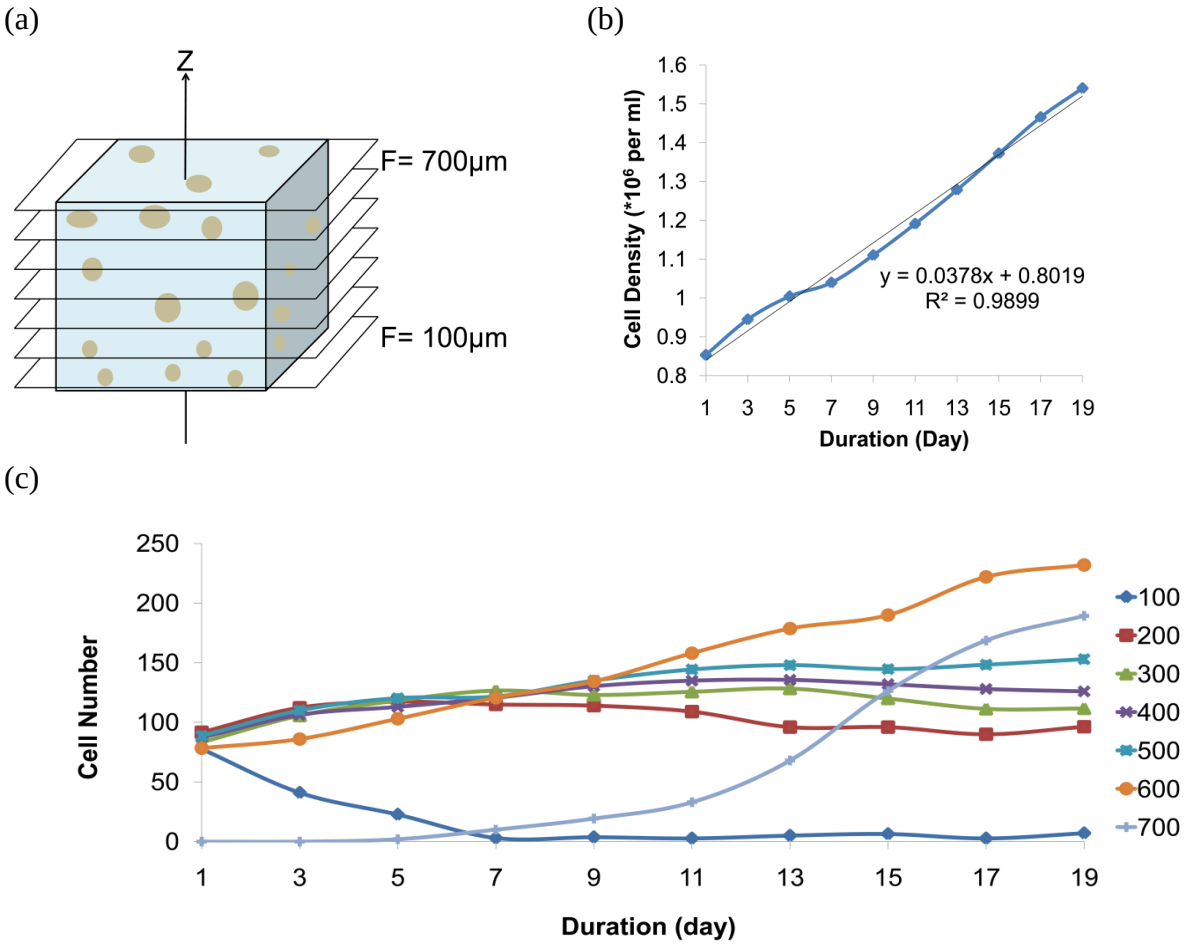

Fig. 5.2Characterization of chondrocytes spatiotemporal distribution along *z* direction in agarose hydrogel. Schematic illustration of the characterization of cellular distribution along different focal planes (a). The overall growth of chondrocytes was quantified by the cell density (per ml) as a function of time (b).Quantification of cellular distribution among different focal planes as a function of time (c).

The spatiotemporal evaluation of cell population along different focal planes showed significant increment of cell number on the edge compared with the bulk of the hydrogel. This spatial variation of cell distribution contributed to the EF phenomenon where substantial neo-tissue outgrowth could be observed at the edge of hydrogel whereby the

bulk region remained relatively stable as shown in Fig. 5.4. This phenomenon can be attributed to either cell migration or directed cell growth towards the surface of hydrogel. The chemotaxis phenomenon where the cells direct their migration towards the surface due to the medium diffusion was insignificant. In fact, the density of agarose used in this study was low and the hydrogel construct was relatively small, hence the permeability of the hydrogel would not contribute to the formation of concentration gradient of important nutrients [221]. Without the external biochemical and mechanical stimulation, such spatial variation was likely caused by the local mechanical interactions between cells and microenvironment. To directly investigate this hypothesis, it would be necessary to study biomechanical activities of cells in the 3D system.

5.3.3 Finite element method analysis of surface tension under 'edge flourish' phenomenon

Based on the above observations, there is a need to probe local mechanical responses of the encapsulated chondrocytes along the edge of the hydrogel. We intergrated the elasticity of agarose hydrogel with experimental measurement of real-time hydrogel deformation in a FEM to examine the local mechanical responses caused by EF phenemenon. A monolayer of fluorescent latex microbeads embeddedon the top layer of agarose hydrogelwere served as the markers to track the surface deformation under the influence of cellular outgrowth. A pair of microbead images was taken from Day 12 and Day 14 of *in vitro* culture to determine the degree of surface deformation induced by cellular outgrowth in EF phenomenon. The quantitative numbers of microbead displacement field were then determined by PIV and served as the input boundary condition for the theoretical prediction of stress distribution in FEM.

A representative chondrocytic isogenous groups located approximately 7μm underneath the monolayer of fluorescent microbead was chosen and captured in phase contrast image as shown in Fig. 5.5(a). The deformation and stress analysis of agarose hydrogel was implemented by the FEM software ANSYS®11. Starting with the geometry of agarose hydrogel, the whole domain (hydrogel) was discretized by isoparametric, 20-node elements. The boundary conditions were specified displacements from PIV resultsat corresponding nodes on the surface of hydrogel, whereas the nodes on the bottom of substrate were fixed because hydrogel was immobilized on the coverslip. The deformation of hydrogel surface on the *xy* plane was reconstructed from the displacement of the microbeads. The hydrogel surface above the chondrocytes experienced significant distortion as shown in the displacement vector map in Fig. 5.5(b). The displacement vectors were pointing away from the center of the isogenous group. This outwards displacement feature initiating from the center of the cells was shown in different durations of time as well as other cells. Displacement located outside the cell boundary could be observed at the top right region, these were probably caused by the adjacent cells located outside the field of view which also contribute to the hydrogel surface distortion.

(a)

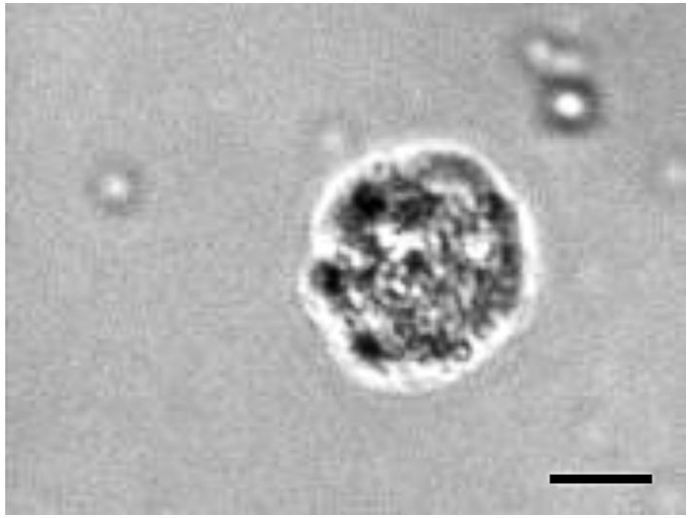

(b)

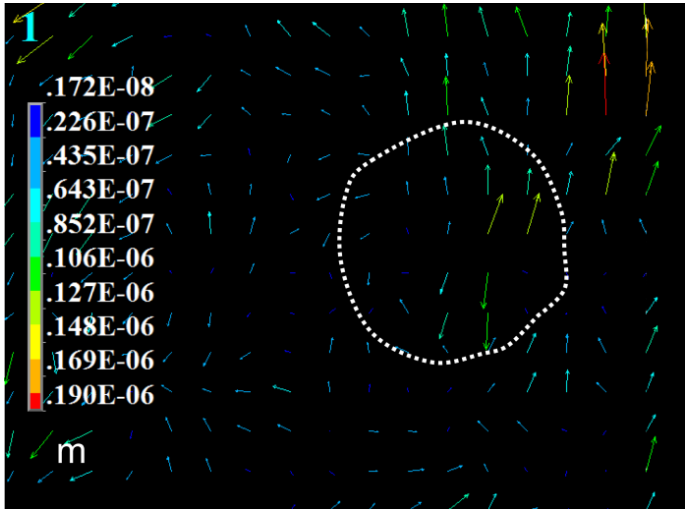
1
.172E-08
.226E-07
.435E-07
.643E-07
.852E-07
.106E-06
.127E-06
.148E-06
.169E-06
.190E-06
m

(c)

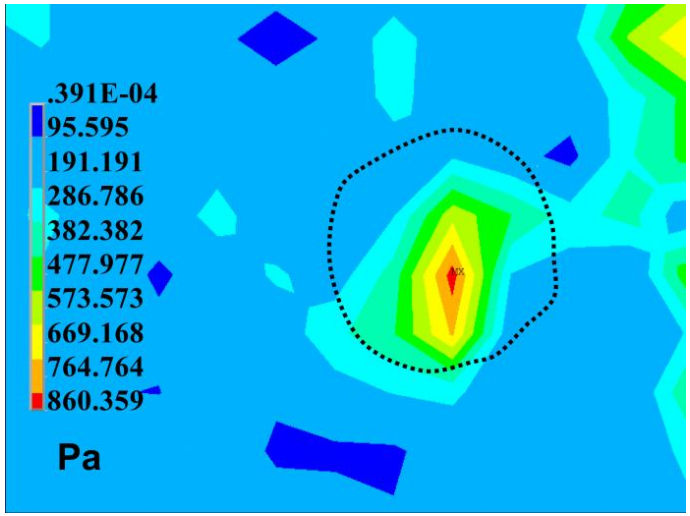
.391E-04
95.595
191.191
286.786
382.382
477.977
573.573
669.168
764.764
860.359
Pa

(d)

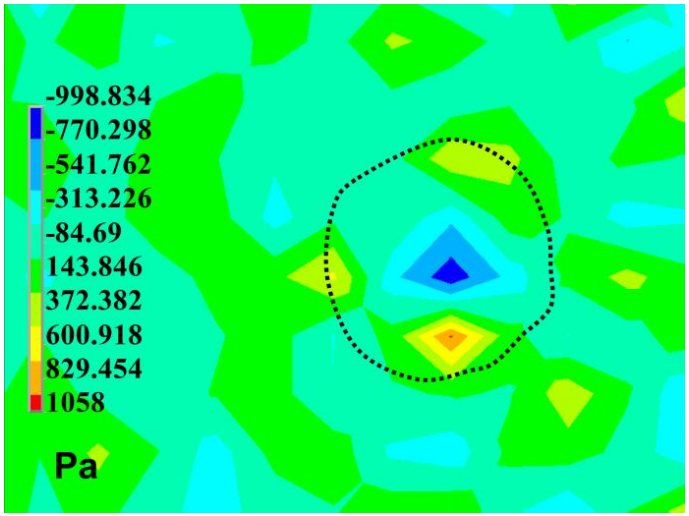
-998.834
-770.298
-541.762
-313.226
-84.69
143.846
372.382
600.918
829.454
1058
Pa

(e) (f)

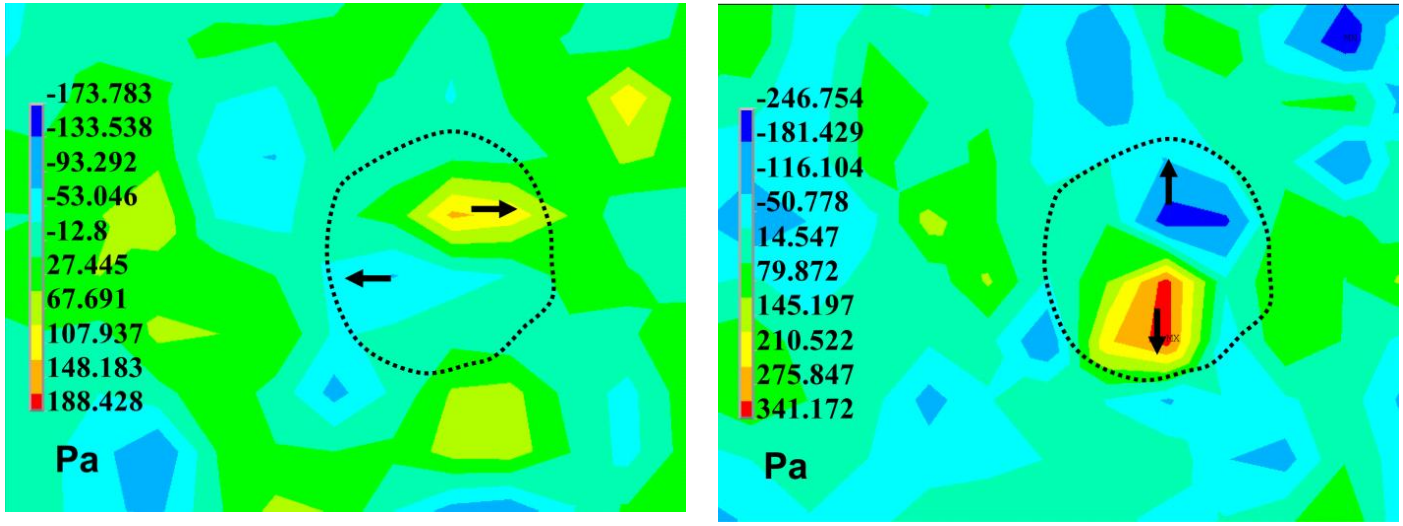

Fig.5.5Displacement field and stress field of agarose hydrogel surface induced by EF phenomenon on Day 12 to Day 14.A phase-contrast image of chondrocytes encapsulated in the 2% w/v agarose hydrogel located approximately 7 μm underneath a monolayer of embedded fluorescent microbeads (a). Tangential (*x*-*y*) displacement field U_{xy}reconstructed from microbeads displacement by FEM analysis (b). The *von Mises* stress (c), *z*-component stress σ_{zz} (d), σ_{xz} shear stress on *x* direction (e), and σ_{yz} shear stress on *y* direction (f). Arrows indicate the directions of net regional stresses.Dotted lines are the boundary of chondrocytes cluster. Scale bar, 10 μm.

Using FEM, the mechanical responses of the agarose hydrogel under the influences of the encapsulated chondrocytes were simulated and investigated. With the specified boundary conditions as mentioned above, the stressescan be analyzed subsequently. Fig. 5.5(c-f)demonstrate the results of four types of stresses on the agarose hydrogel surface. These stresses further supported the described observation of EF phenomenon, where the encapsulated chondrocytes close to the edge of hydrogel have the tendency of protruding out of the hydrogel surface.

Fig. 5.5(c) shows the *von Mises* stress with the presence of chondroytic isogenous group in dotted lines. The FEM model predicted that the agarose hydrogel surface experienced highest degree of stress at the center of group with the maximum stress of 0.86 kPa. The *von Mises* stress gradient demonstrated radial distribution with higher stress values at the center and lower values around the boundary of group. Upon closer inspection of the three components of stress in three-dimensional (Fig. 5.5d-f), it was evident that the maximum *von Mises* stresses at the center of isogenous group were mostly originated from the stresses acting along the normal direction (*z*). The magnitude of normal stress at center region was approximately 3 folds higher than that of tangential stress. It is noticeable that in Fig. 5.5(d), negative normal stress ($-\sigma_{zz}$) is presenting at the center of the group and positive normal stress ($+\sigma_{zz}$) is surrounding the edge of group. Since negative and positiveσ_{zz} represents the upwards and downward stresses, respectively, experienced by the agarose hydrogel surface, the observed pattern demonstrates that the agarose hydrogel surface was bulged right above the encapsulated chondrocytes. This result is consistent with the defined EF phenomenon,where the chondrocytes are believed to have protruded and pushed the hydrogel surface upwards.

The outwards forces experienced by the hydrogel at the center of group were leveled by the inwards forces around the edge of the group in order to maintain the static condition. The corresponding shear stresses σ_{xz} and σ_{yz} are shown in Fig. 5.5(e) and 5F, respectively. Directions of shear stresses are indicated by arrows shown in the figures, which are as expected from the outwards deformation of hydrogel surface and closely related to the displacement vector map obtained from PIV result.

This assay had successfully characterized the surface tension induced by the encapsulated chondrocytes located adjacent to the edge of hydrogel in a quantitative approach. However, the normal stresses were simulated from the tangential displacement using FEM model instead of direct analysis from the experimentally obtained normal displacement vectors. Furthermore, the mechanism of simulated surface tension pointing upward is remained to be studied. The outwards stresses could be originated either from cellmigration or directed cellular growth. Therefore, in order to study the mechanism of EF layer formation and the foundation of asymmetrical-outwards resultant stress from chondrocytic isogenous groups, it is essential to further evaluate the mechanobiological activity of the encapsulated chondrocytes in direct 3D approach.

5.3.4 Patterns of 3D hydrogel deformation caused by encapsulated chondrocytes

The measurement of hydrogel matrix deformation has been performed to understand the interrelationbetween cell adhesion, motility, contractilityand matrix remodeling [222-224]. 3D multiple-particle tracking has been applied to probe the hydrogel local matrix displacement by analyzing the size, intensity, and the diffraction patterns of out-of-focus microbeads[224].We have developed an assay to probe the 3D trajectories of the multiple microbeads adjacent tothe encapsulated chondrocytes inside

hydrogel. This assay allowed us to quantify and understand the 3D movement of the chondrocytes in real time. The 3D trajectories of microbeads were then used to characterize the biomechanical activity of chondrocytes in a spatiotemporal approach.

The analysis of 3D trajectories of microbeads demonstrated that the local deformation of hydrogel matrix varied among different locations. The microbeads located approximately 15 μm away from the edge of cells did not exhibit significant movement over 48 hours of observation. Moreover, the 3D trajectories of microbead located further away from cells resembled the negative control as shown in Fig. 5.3(c). Results revealed that the hydrogel matrix distanced from the cell edge was mechanically decoupled from the cells. The minor displacementsobserved hereinare presumably induced by the thermally excited passive movement of agarose matrix and spontaneous Brownian motion of microbeads. Generally, microbeads that showed significant movement were located within 10 μm away from the boundary of cells. The microbeads located nearby the chondrocytes experienced largest displacement induced by the bulk movement from cells as shown in Fig. 5.6. Furthermore, the normal displacement (z) is significantly higher than the tangential displacements (x, y) as the target microbeads were located above the isogenous group.

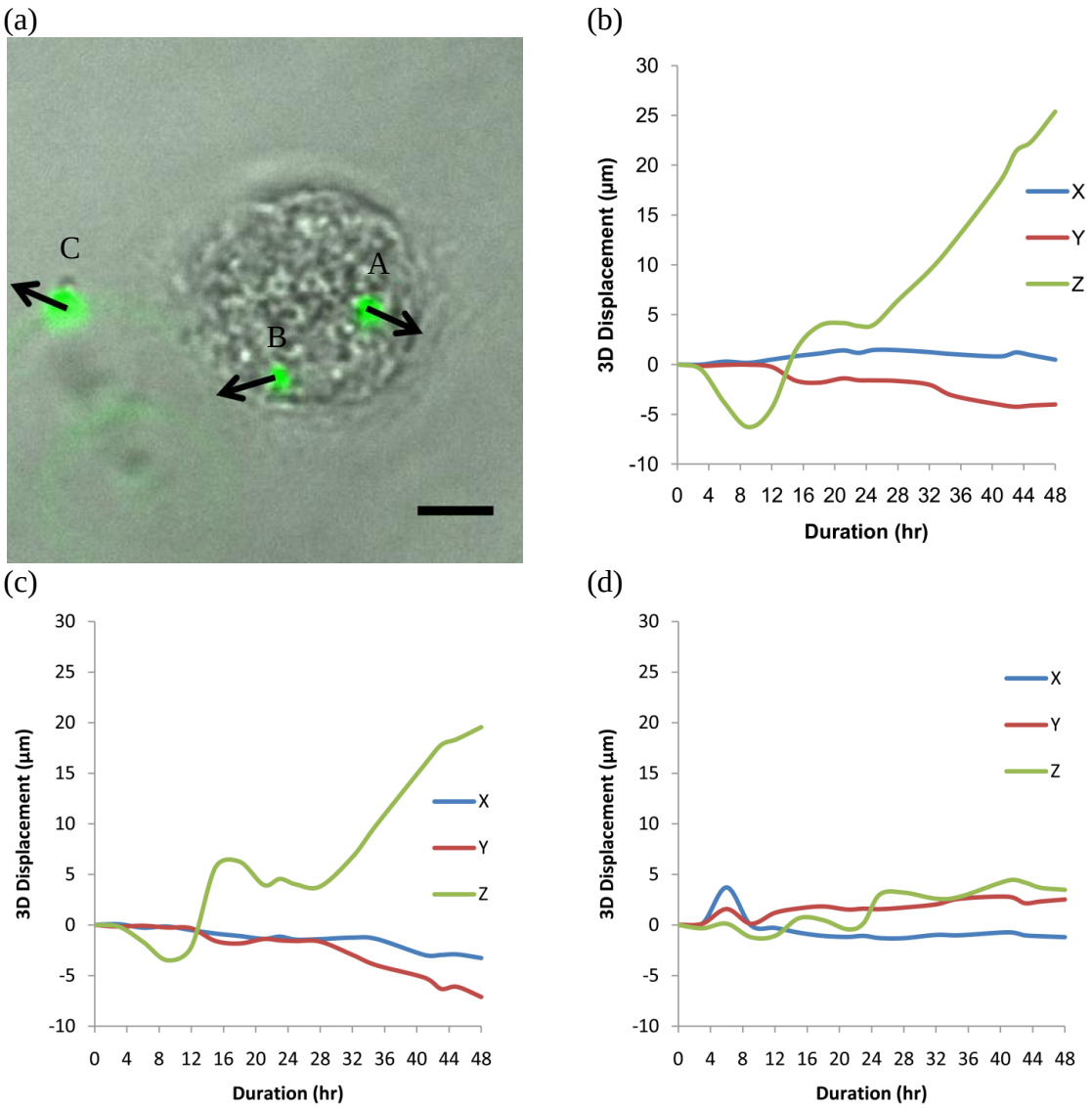

Fig. 5.6 Local 3D deformation of agarose matrix around chondrocytes. Phase contrast image of chondrocytes overlaid with the fluorescent microbeads (a). Microbead B and C located 3.02 μm and 4.91 μm from center respectively, microbead D located 7.92 μm away from the edge of chondrocytes. The arrows represent the direction of tangential displacements of each microbeads. 3D trajectories of microbeads located at three different locations with respect to chondrocytes in (a) are represented in (b) to (d). Scale bar, 10 μm.

Microbead B was immobilized at 3.02 μm and 10 μm away from the center of the chondrocytic isogenous groupsin tangential and normal plane, respectively. The microbeads 3D trajectories revealed the patternof local matrix deformation induced by the encapsulated chondrocytes over 48 hours as shown in Fig. 5.6(b). The local deformation was kept minimal in *x* and *y* directions relative to that along*z* direction. The total magnitude in normal deformation was calculated to be 100 μm higher than the tangential deformation throughout the 48 hours observation. The substantial local deformation in normal direction validated the *in vitro* phenomenon of chondrocytic outgrowths in 3D culture system. During the first 11^{th} hour, the top local matrix the chondrocyteswas first contracted towards the cells and subsequently released to the initial position within an hour. After 12^{th} hour of observation, local matrix expanded with the rate of 0.687 μm per hour along normal axisup until 25 μm above the initial position at 48^{th} hour. Microbead C was immobilized 4.91 μm and 9.852 μm away from the center of the cells in tangential and normal plane, respectively. It exhibited similar 3D trajectories with microbead B as shown in Fig. 5.6(c). The normal displacement was dominant in the local matrix deformation with the total magnitude of 69.213 μm higher than the tangential displacement throughout the 48 hours observation. The *z* and *y* displacement of microbeads C shared similar trajectories in term of direction and relative magnitude. However, the *x* displacement was in opposite directionalthough the magnitude of displacement was kept minimum in both locations with the total displacement two folds lesser than their corresponding *y* displacement. Lastly, microbead D located at 7.92 μm away from the edge of the cells showed little influences from the bulk movement of cells

as shown in Fig. 5.6(d). The statistical fluctuation of the 3D trajectoriesfor this microbead is within 4 μm from the initial position throughout 48 hours observation.

By comparison, the total displacements resulted from the bulk movement of cells were statistically more significant than the passive displacements as shown in Fig. 5.3(c), which is less than 1 μm displacement in all three directions. The characterized 3D trajectories of microbeads at various locations clearly elucidated the local deformation of hydrogel induced by the encapsulated chondrocytic isogenous groups. The significant deformation of surrounding hydrogel matrix revealed that the asymmetric bulk movement of the chondrocytic isogenous groupswas directed to the surface of hydrogel. This was clearly supported by the individual displacement of surrounding microbeads and the outgrowing deformation pattern as shown in Fig. 5.6(a). The arrows in Fig. 5.6(a) represent the direction of local matrix deformation in tangential plane; the magnitude of the displacement was not represented by the length of the arrows.

We further exploited our assay, which allowed us to observe the hydrogel matrix deformation and the cell morphological changes in real time, to investigate the migration mode of cells involved in matrix deformation. The morphology of the chondrocytic isogenous groups remained spheroids throughout 48 hours observation as shown in Fig. 5.7.The result indicated that chondrocytes did not migrate via the mesenchymal mode which establishes cell polarity and proteolytic degradation of the local matrix [225]. This observation is supported by the lack of ECM proteins that work as the adhesion sites for the chondrocytes to generate traction force for the formation of cell polarity. Recent studies have shown that the lack of ECM proteins in hydrogel may convert the mesenchymal motility mode to amoeboid motility mode where the cells remain rounded

in shape [226]. The amoeboid migration in the 3D hydrogel is characterized by contractility-dependent squeezing through the pre-existent pores in the gel matrix. Although some spikes were developed around the boundary of chondrocytes, yet no pseudopod was observed in 48 hours duration as shown in Fig. 5.7(b) (dotted line represents boundary of chondrocytes in Day 12). These findings suggested the local deformation of hydrogel matrix around chondrocytes was not originated from the migration of chondrocytes. In fact, the radial expansion of isogenous group revealed that the asymmetrical-outwards resultant stress experienced by the superficial hydrogel was driven by the superior directed outgrowth of encapsulated chodrocytes adjacent to the edge of hydrogel.

(a) (b)

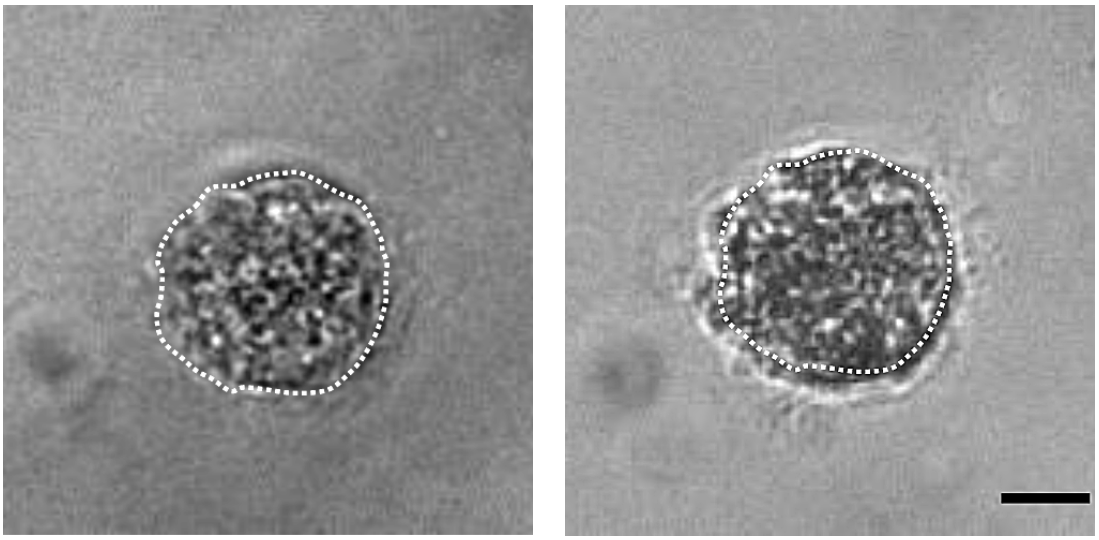

Fig. 5.7 Morphologicalchangesof chodrocytic isogenous group fromDay 12 (a) toDay 14 (b) of *in vitro* culturein the 3D multiple-particle tracking assay. The maximum cellular projected areas are 137.57 μm^2 and 1764.86μm^2 respectively. Scale bar, 10 μm.

5.4 Conclusion

In our current study, we successfully characterized the mechanism of EF phenomenon in 3D culture system with a novel approach combining surface tension microscopy and multiple-particle tracking assays. Under the real-time microscopic observation and histological staining, the encapsulated chondrocytes located along the edge of hydrogel exhibited superior proliferative and secretive activities than those in the bulk of hydrogel. The surface tension microscopy assay revealed significant surface tension on the interface of agarose hydrogel and medium under the outgrowing influences of encapsulated chondrocytic isogenous groups, which was driven by an asymmetrical-outwards resultant stress. The outwards (i.e. upwards) stresses appeared to be originated from the directed outgrowth and superior proliferative rate of chondrocytic isogenous groups rather than bulk migration. The observed spontaneous outwards stress contributed to the dynamic outgrowth of chondrocytes from the cell-laden hydrogel bulk to the surface of hydrogel. The emergence of EF layer that rich in cell viability and ECM production is critical in the tissue engineering, as it is the fundamental elementof vibrant neo-tissue formation. The findings from the EF phenomenon study are expected to facilitate the development of more innovative and robust tissue engineered scaffoldsthat provide substantial platforms for higher efficiency in tissue formation.

Chapter 6 Conclusions

Mechanobiology focuses on the physical forces that contribute to the physiology of cells and tissue. In contrast to the reductionism that has been practiced for decades, mechanobiology is an emerging field in cell biology that adopts an integrative paradigm where the collective interactions among multiple components are put into consideration. Therefore, intrinsic studies on biomechanistic behaviours of cells towards the microenvironment are essential in the quest of discovering discrete events that contribute to the cellular activity as well as developing seamless engineered tissue. However, the study of mechanobiology is significant impaired due to the practical difficulties in fabricating mechanical signals and probing cellular mechanical responses in sub-cellular level.

In this dissertation, cell traction force microscopy (CTFM) assay was first developed to evaluate the cellular mechanical responses via the hydrogel deformation caused by cell adhesion. Cell traction force is the direct representative parameter of cell contractility established by the dynamic force equilibrium between cytoskeletal architecture and ECM through the tensegrity principal [187]. The direct quantitative measurement of cell traction allowed us to evaluate the prestress or isometric tension of the individual cell that serves as the predominant factor in mechanobiology. In Chapter 3, polyacrylamide gel (PAG) was first prepared to a desired elasticity by optimizing the concentration ratio of monomers and cross-linkers. The mechanical property of the hydrogel substrate is one of the important factors in determining the feasibility of this assay. Therefore, atomic force microscope (AFM) was introduced to perform

microscopic elasticity characterization which has never been incorporated in previous reported models. It was concluded that the used of AFM rather than the conventional macroscopic characterization is more relevant to the actual cell-substrate physical interactions. A new hyperelastic model that obeys Mooney-Rivlin constitution law was proposed based on the experimental mechanical behaviour of PAG and tested with the linear elastic model which was generally assumed in the study of CTFM. Mooney-Rivlin model was better in representing the mechanical response of PAG under compressive stress compared to the linear elastic model. From the numerical results of bead displacements and stresses, the Mooney-Rivlin model provided more favorable predictions on PAG's mechanical responses induced by cell traction forces.

The implementation of finite element method (FEM) in the computation of cellular traction stress on three-dimensional (3D) PAG was shown to be more convenient and efficient than the conventional cellular traction force computations which require intensive iteration to solve the regularized inverse problem. Our results highlighted that the unique combination of microscopic mechanical characterization, Mooney-Rivlin model, and 3D FEM in traction force computation helped to improve the accuracy and simplicity of CTFM assay.Lastly, the total traction forces in all three directions were calculated from FEM analyses to provide valuable insights into the cell traction microscopy.

In Chapter 4, micro-contact printing technique (μCP) was incorporated into the newly developed CTFM assay in the aim of investigating the effects of cell shape on cell traction force. The cell spreading area was found to be the major factor in determining the overall intensity of cell traction force. This observation was consistent with the previous

studies where the degree of cell spreading regulates the cell proliferation and apoptosis [102, 106]. In additional to overall intensity of force, the implementation of the newly developed CTFM assay allows us to evaluate the orientation of cell traction forces. We discovered that the orientation of cell traction force was closely related to the orientation of cell long axis. Further analyses had shown that the cell elongation factor played an important role in traction force orientation, where the highly elongated cells tended to exhibit major traction forces along cell long axis in a highly controlled manner. In contrast, the fibroblast-like cells with low aspect ratio revealed broad range of traction force orientation with respect to the cell long axis. The combination of CTFM assay with immunochemical staining revealed that the direction of individual generated traction force was governed by the alignment of stress fibers which are known to be the generator of cell contractility. In addition, due to the preferential lamellipodia formation at acute geometric features, the orientation of cell traction force was further polarized by the extended cell membrane at both short edges. The highly regulated traction force that aligns with cell long axis is an important characteristic for contractile vascular smooth muscle cells (SMCs) in the functionality of tissue-engineered blood vessel.

The collective cell traction force study based on the multiple vascular SMCs in the microchanneled scaffold revealed the role of microtopographic features in controlling the phenotype and alignment of vascular SMCs. Initially, SMCs adjacent to the edges of microchannel exhibited significant traction force and adopted highly elongated morphology due to the extra dimensionality provided by the microwalls for cell attachment. The collective cell traction force demonstrated that the high traction forces along the edges were propagated to the center of microchannel and served as the physical

cues in mediating the morphology and alignment of the entire SMCs sheet. In addition, the phenotype changes were identical with the previous studies where the contractile gene expression was significantly higher when SMCs reached confluence [122]. This phenomenon is particularly important in the cardiovascular tissue engineering where the SMCs sheet must established elongated morphology with circumferentially alignment towards the blood flow in order to generate collective contractile forces to perform normal vascular function like vasoactivity.

The biomechanistic studies of cells were extended from the two-dimensional (2D) geometry to the 3D microenvironment. As highlighted in the studies demonstrated in the microchanneled scaffold, the extra dimensionality provided by the microwalls can be served as the physical cue in determining the functionality of cardiovascular engineered tissues. Therefore, cells in 3D matrix are expected to embrace unique biomechanical behaviors which are different from 2D environment. This study is particularly important for the tissue formation that is initiated and developed in 3D environment such as cartilage tissue engineering. In Chapter 5, we investigated the biomechanical behaviors that contributed to the newly discovered "edge flourish" (EF) phenomenon observed in the encapsulated chondrocytes in 3D agarose hydrogel [205]. This EF phenomenon was utilized in the phase transfer cell culture (PTCC) strategy to overcome the major hurdles in for applying hydrogels in cartilage tissue engineering. The spatiotemporal evaluation of cell population along different focal planes revealed significant increment in cell number on the hydrogel edge compared with the bulk of the hydrogel. This trend was consistent with the substantial neo-tissue formation at the edge of the hydrogel with higher cell density and ECM secretion.

Without the external stimulation, the EF phenomenon was likely driven by the local mechanical interactions between cells and 3D matrix. Therefore, intrinsic study of cellular biophysical activities in the hydrogel is essential in determining the mechanism of EF phenomenon. We first characterized the real-time hydrogel surface tension caused by the EF phenomenon in order to investigate the local mechanical responses of the encapsulated chondrocyte. The newly developed FEM surface stress analysis demonstrated that the encapsulated chondrocytes located along the edge of hydrogel exhibited outwards stresses towards the interface of hydrogel and medium. To investigate the driven force of such outwards stresses generated by chondrocytes, 3D multiple-particle tracking assay was implemented to track the individual isogenous group in the agarose matrix. The 3D trajectories of chondrocytes revealed that the cells adjacent to the edge of hydrogel were consistently moving upwards to the surface with insignificant movement in other two directions. We further exploited this tracking assay to observe the morphological changes of chondrocytes during the upwards movement and found neither mesenchymal nor amoeboid motility mode was established. Therefore, it is concluded that the asymmetrical-outwards resultant stress experienced by the superficial hydrogel was driven by the superior directed outgrowth of encapsulated chondrocytes adjacent to the edge of hydrogel. In conclusion, the EF phenomenon was driven by the directed outgrowth of isogenous groupsthat eventual contributed to the substantial upwards surface tension on the hydrogel surface and ultimatelyled to the formation of neo-tissue with rich proliferative and chondrocytic extracellular matrix secretion rate at the surface of hydrogel.

The future project which can be based on this disertation will be the determination

of cellular mechanobiological behavior in different cell culture systems. It is widely known that the establishment of cell or tissue physiology and the development of tissue engineering are heavily relied on insoluble ECM molecules and mechanical forces. The development of *in vitro* culture system that mimic the native microenvironment is a promising approach in the study of tissue engineering, drug delivery, toxicology, virology, etc. This is because the clinical trial of such experimental studies one human body is expensive, time consuming, and potentially hazardous. Therefore, new approaches in characterizing and manipulating cells or tissues in microenvironment are needed to investigate the intrinsic interactions among cells with the surroundings that trigger biocomplexity.

The spatial heterogeneity regulated by μCP, topographic features, and 3D microenvironment facilitates the study of biomechanical behaviors of cells. It can also be served as the critical parameter in determining the formation of engineered tissue. The importance of microenvironment in regenerative medicine is well studied.The cell critical behaviors were found to be closely controlled by the physical signals from the surroundings. Therefore, a systematic approach in mapping the influences of spatial factors in cell behaviors is essential in establishing the standardization of engineering artificial tissue. This systematic mapping involves multi-disciplinary field such as systems biology, microarray technology, statistical analysis, synthetic biology, etc.

In addition, the newly developed cell traction force microscopy assay in this dissertation enables us to characterize the forces in three-directional based on the simplified 2D platform. In order to achieve higher precision, it is inevitable that the boundary condition from the third dimension is highly demanded. The displacement

quantification along *z*-axis is challenging because of the resolution restrictiondue to the current imaging system. However, with the incorporation of PIV assay and 3D multiple-particle tracking assay developed in Chapter 5.2.7, it is feasible to provide 3D boundary condition in the FEM simulation.

REFERENCES

1. Chan-Park MB, Shen JY, Cao Y, Xiong Y, Liu YX, Rayatpisheh S, et al. Biomimetic control of vascular smooth muscle cell morphology and phenotype for functional tissue-engineered small-diameter blood vessels. Journal of Biomedical Materials Research Part A 2009 Mar;88A(4):1104-1121.
2. Dermenoudis S, Missirlis YF. Bioreactors in Tissue Engineering. Advanced Engineering Materials Nov;12(11):B592-B608.
3. Cindy Chung, Burdick JA. Engineering cartilage tissue. Advanced Drug Delivery Reviews 2008;60(2):243-262.
4. Frixione E. Recurring views on the structure and function of the cytoskeleton: A 300-year epic. Cell Motility and the Cytoskeleton 2000 Jun;46(2):73-94.
5. Ingber DE. Tensegrity II. How structural networks influence cellular information processing networks. Journal of Cell Science 2003 Apr;116(8):1397-1408.
6. Ingber DE. Tensegrity I. Cell structure and hierarchical systems biology. Journal of Cell Science 2003 Apr;116(7):1157-1173.
7. Chicurel ME, Chen CS, Ingber DE. Cellular control lies in the balance of forces. Current Opinion in Cell Biology 1998 Apr;10(2):232-239.
8. Martin P. Wound healing - Aiming for perfect skin regeneration. Science 1997 Apr;276(5309):75-81.
9. Schmeichel KL, Weaver VM, Bissell MJ. Structural cues from the tissue microenvironment are essential determinants of the human mammary epithelial cell phenotype. Journal of Mammary Gland Biology and Neoplasia 1998 Apr;3(2):201-213.
10. Watson PA. FUNCTION FOLLOWS FORM - GENERATION OF INTRACELLULAR SIGNALS BY CELL-DEFORMATION. Faseb Journal 1991 Apr;5(7):2013-2019.
11. Barcelloshoff MH, Aggeler J, Ram TG, Bissell MJ. Functional-differentiation and alveolar morphogenesis of primary mammary cultures on reconstituted basement-membrane. Development 1989 Feb;105(2):223-&.
12. Pirone DM, Chen CS. Strategies for engineering the adhesive microenvironment. Journal of Mammary Gland Biology and Neoplasia 2004 Oct;9(4):405-417.
13. Stamenovic D, Ingber DE. Tensegrity-guided self assembly: from molecules to living cells. Soft Matter 2009;5(6):1137-1145.
14. Liu WF, Chen CS. Cellular and multicellular form and function. Advanced Drug Delivery Reviews 2007 Nov;59(13):1319-1328.
15. Lazarides E. Actin, alpha-actinin, and tropomyosin interaction in structural organization of actin-filaments in nonmuscle cells. Journal of Cell Biology 1976;68(2):202-219.
16. Rathke PC, Osborn M, Weber K. Immunological and ultrastructural characterization of microfilament bundles- polygonal nets and stress fibers in an established cell-line. European Journal of Cell Biology 1979;19(1):40-48.
17. Ingber DE. Mechanobiology and diseases of mechanotransduction. Annals of Medicine 2003;35(8):564-577.
18. Ingber DE. Tensegrity-based mechanosensing from macro to micro. Prog Biophys

Mol Biol 2008 Jun-Jul;97(2-3):163-179.
19. Ferkiss V. Synergetics- explorations in geometry of thinking- Fuller, RB. Technology and Culture 1976;17(1):104-108.
20. Kumar S, Maxwell IZ, Heisterkamp A, Polte TR, Lele TP, Salanga M, et al. Viscoelastic retraction of single living stress fibers and its impact on cell shape, cytoskeletal organization, and extracellular matrix mechanics. Biophysical Journal 2006 May;90(10):3762-3773.
21. Lopez JI, Mouw JK, Weaver VM. Biomechanical regulation of cell orientation and fate. Oncogene 2008 Nov;27(55):6981-6993.
22. Patel AA, Thakar RG, Chown M, Ayala P, Desai TA, Kumar S. Biophysical mechanisms of single-cell interactions with microtopographical cues. Biomedical Microdevices Apr;12(2):287-296.
23. Gallant ND, Michael KE, Garcia AJ. Cell adhesion strengthening: Contributions of adhesive area, integrin binding, and focal adhesion assembly. Molecular Biology of the Cell 2005 Sep;16(9):4329-4340.
24. Li F, Li B, Wang QM, Wang JHC. Cell shape regulates collagen type I expression in human tendon fibroblasts. Cell Motility and the Cytoskeleton 2008 Apr;65(4):332-341.
25. Janmey PA. The cytoskeleton and cell signaling: Component localization and mechanical coupling. Physiological Reviews 1998 Jul;78(3):763-781.
26. Ingber DE. Engineering cell shape and function through control of substrate adhesion. Antec 95 - the Plastics Challenger: a Revolution in Education, Conference Proceedings, Vols I-Iii - Vol I: Processing; Vol Ii: Materials; Vol Iii: Special Areas 1995:2849-2851.
27. Singhvi R, Kumar A, Lopez GP, Stephanopoulos GN, Wang DIC, Whitesides GM, et al. Engineering Cell-Shape and Function. Science 1994 Apr;264(5159):696-698.
28. Chen CS, Mrksich M, Huang S, Whitesides GM, Ingber DE. Micropatterned surfaces for control of cell shape, position, and function. Biotechnology Progress 1998 May-Jun;14(3):356-363.
29. Crisp M, Liu Q, Roux K, Rattner JB, Shanahan C, Burke B, et al. Coupling of the nucleus and cytoplasm: role of the LINC complex. Journal of Cell Biology 2006 Jan;172(1):41-53.
30. Haque F, Lloyd DJ, Smallwood DT, Dent CL, Shanahan CM, Fry AM, et al. SUN1 interacts with nuclear lamin A and cytoplasmic nesprins to provide a physical connection between the nuclear lamina and the cytoskeleton. Molecular and Cellular Biology 2006 May;26(10):3738-3751.
31. Wang N, Tytell JD, Ingber DE. Mechanotransduction at a distance: mechanically coupling the extracellular matrix with the nucleus. Nature Reviews Molecular Cell Biology 2009 Jan;10(1):75-82.
32. Fey EG, Wan KM, Penman S. Epithelial cytoskeletal framework and nuclear matrix intermediate filament scaffold- 3-dimensional organization and protein-composition. Journal of Cell Biology 1984;98(6):1973-1984.
33. Maniotis AJ, Chen CS, Ingber DE. Demonstration of mechanical connections between integrins cytoskeletal filaments, and nucleoplasm that stabilize nuclear structure. Proc Natl Acad Sci U S A 1997 Feb;94(3):849-854.
34. Jaalouk DE, Lammerding J. Mechanotransduction gone awry. Nature Reviews Molecular Cell Biology 2009 Jan;10(1):63-73.

35. Albrechtbuehler G. Role of cortical tension in fibroblast shape and movement. Cell Motility and the Cytoskeleton 1987;7(1):54-67.
36. Evans E, Yeung A. Apparent viscosity and cortical tension of blood granulocytes determined by micropipet aspiration. Biophysical Journal 1989 Jul;56(1):151-160.
37. Leucht P, Kim JB, Currey JA, Brunski J, Helms JA. FAK-Mediated Mechanotransduction in Skeletal Regeneration. Plos One 2007 Apr;2(4).
38. Rice KM, Desai DH, Kinnard RS, Harris R, Wright GL, Blough ER. Load-induced focal adhesion mechanotransduction is altered with aging in the Fischer 344/NNiaHSd x Brown Norway/BiNia rat aorta. Biogerontology 2007 Jun;8(3):257-267.
39. Klossner S, Durieux AC, Freyssenet D, Flueck M. Mechano-transduction to muscle protein synthesis is modulated by FAK. European Journal of Applied Physiology 2009 Jun;106(3):389-398.
40. Foster CD, Varghese LS, Gonzales LW, Margulies SS, Guttentag SH. The Rho Pathway Mediates Transition to an Alveolar Type I Cell Phenotype During Static Stretch of Alveolar Type II Cells. Pediatric Research Jun;67(6):585-590.
41. Provenzano PP, Keely PJ. Mechanical signaling through the cytoskeleton regulates cell proliferation by coordinated focal adhesion and Rho GTPase signaling. Journal of Cell Science Apr;124(8):1195-1205.
42. Villa J, Warshel A. Energetics and dynamics of enzymatic reactions. Journal of Physical Chemistry B 2001 Aug;105(33):7887-7907.
43. Ingber DE. Cellular mechanotransduction: putting all the pieces together again. Faseb Journal 2006 May;20(7):811-827.
44. Sytina OA, Heyes DJ, Hunter CN, Alexandre MT, van Stokkum IHM, van Grondelle R, et al. Conformational changes in an ultrafast light-driven enzyme determine catalytic activity. Nature 2008 Dec;456(7224):1001-U1089.
45. Benkovic SJ, Hammes-Schiffer S. A perspective on enzyme catalysis. Science 2003 Aug;301(5637):1196-1202.
46. Hammes GG. Multiple conformational changes in enzyme catalysis. Biochemistry 2002 Jul;41(26):8221-8228.
47. Taneja KL, Lifshitz LM, Fay FS, Singer RH. Poly(A) RNA codistribution with microfilaments- Evaluation by in situ hybridization and quantitative digital imaging microscopy. Journal of Cell Biology 1992 Dec;119(5):1245-1260.
48. Bassell GJ, Powers CM, Taneja KL, Singer RH. Single messenger-RNAs visualized by ultrastructural in-situ hybridization are principally localized at actin filament intersections in fibroblasts. Journal of Cell Biology 1994 Aug;126(4):863-876.
49. Chicurel ME, Singer RH, Meyer CJ, Ingber DE. Integrin binding and mechanical tension induce movement of mRNA and ribosomes to focal adhesions. Nature 1998 Apr;392(6677):730-733.
50. Huang S. Gene expression profiling, genetic networks, and cellular states: an integrating concept for tumorigenesis and drug discovery. Journal of Molecular Medicine-Jmm 1999 Jun;77(6):469-480.
51. Mooney DJ, Cima L, Langer R, Johnson L, Hansen LK, Ingber DE, et al. Principles of tissue engineering and reconstruction using polymer-cell constructs.In: Cima LG, Ron ES, editors. Tissue-Inducing Biomaterials, 1992. p. 345-352.
52. Cima LG, Vacanti JP, Vacanti C, Ingber D, Mooney D, Langer R. TISSUE ENGINEERING BY CELL TRANSPLANTATION USING DEGRADABLE

POLYMER SUBSTRATES. Journal of Biomechanical Engineering-Transactions of the Asme 1991 May;113(2):143-151.
53. Langer R, Vacanti JP. Tissue Engineering. Science 1993 May;260(5110):920-926.
54. Estes BT, Gimble JM, Guilak F. Mechanical signals as regulators of stem cell fate. Stem Cells in Development and Disease, 2004. p. 91-126.
55. Bershadsky A, Kozlov M, Geiger B. Adhesion-mediated mechanosensitivity: a time to experiment, and a time to theorize. Current Opinion in Cell Biology 2006 Oct;18(5):472-481.
56. Paulsson M. Basement-membrane proteins- Structure, assembly, and cellular interactions. Critical Reviews in Biochemistry and Molecular Biology 1992;27(1-2):93-127.
57. Leivo I. Structure and composition of early basement-membranes- Studies with early embryos and teratocarcinoma cells. Medical Biology 1983;61(1):1-30.
58. Nogawa H, Morita K, Cardoso WV. Bud formation precedes the appearance of differential cell proliferation during branching morphogenesis of mouse lung epithelium in vitro. Developmental Dynamics 1998 Oct;213(2):228-235.
59. Farge E. Mechanical induction of twist in the Drosophila foregut/stomodeal primordium. Current Biology 2003 Aug;13(16):1365-1377.
60. Kauffman SA. The Sciences of Complexity and Origins of Order. Psa 1990, Vol 2 1991;2:299-322.
61. Bischoff F, Bryson G. CARCINOGENESIS THROUGH SOLID STATE SURFACES. Progress in Experimental Tumor Research 1964;5:85-&.
62. Chen CS, Mrksich M, Huang S, Whitesides GM, Ingber DE. Geometric control of cell life and death. Science 1997 May;276(5317):1425-1428.
63. Parker KK, Brock AL, Brangwynne C, Mannix RJ, Wang N, Ostuni E, et al. Directional control of lamellipodia extension by constraining cell shape and orienting cell tractional forces. Faseb Journal 2002 Aug;16(10).
64. Engler AJ, Griffin MA, Sen S, Bonnetnann CG, Sweeney HL, Discher DE. Myotubes differentiate optimally on substrates with tissue-like stiffness: pathological implications for soft or stiff microenvironments. Journal of Cell Biology 2004 Sep;166(6):877-887.
65. Lo CM, Wang HB, Dembo M, Wang YL. Cell movement is guided by the rigidity of the substrate. Biophysical Journal 2000 Jul;79(1):144-152.
66. Folkman J, Watson K, Ingber D, Hanahan D. Induction of angiogenesis during the transition from hyperplasia to neoplasia. Nature 1989 May;339(6219):58-61.
67. Ingber DE. Can cancer be reversed by engineering the tumor microenvironment? Seminars in Cancer Biology 2008 Oct;18(5):356-364.
68. Ellison ML, Ambrose EJ, Easty GC. Differentiation in a transplantable rat tumour maintained in organ culture. Experimental Cell Research 1969;55(2):198-&.
69. Balaban NQ, Schwarz US, Riveline D, Goichberg P, Tzur G, Sabanay I, et al. Force and focal adhesion assembly: a close relationship studied using elastic micropatterned substrates. Nature Cell Biology 2001 May;3(5):466-472.
70. Gillespie PG, Walker RG. Molecular basis of mechanosensory transduction. Nature 2001 Sep;413(6852):194-202.
71. Wang HB, Dembo M, Hanks SK, Wang YL. Focal adhesion kinase is involved in mechanosensing during fibroblast migration. P Natl Acad Sci 2001 Sep;98(20):11295-

11300.
72. Schwarz US, Balaban NQ, Riveline D, Bershadsky A, Geiger B, Safran SA. Calculation of forces at focal adhesions from elastic substrate data: The effect of localized force and the need for regularization. Biophysical Journal 2002 Sep;83(3):1380-1394.
73. Polte TR, Eichler GS, Wang N, Ingber DE. Extracellular matrix controls myosin light chain phosphorylation and cell contractility through modulation of cell shape and cytoskeletal prestress. American Journal of Physiology-Cell Physiology 2004 Mar;286(3):C518-C528.
74. Chen CS. Mechanotransduction - a field pulling together? Journal of Cell Science 2008 Oct;121(20):3285-3292.
75. Schwarz U. Soft matters in cell adhesion: rigidity sensing on soft elastic substrates. Soft Matter 2007;3(3):263-266.
76. Ghibaudo M, Saez A, Trichet L, Xayaphoummine A, Browaeys J, Silberzan P, et al. Traction forces and rigidity sensing regulate cell functions. Soft Matter 2008;4(9):1836-1843.
77. Harris AK, Wild P, Stopak D. Silicone-Rubber Substrata - New Wrinkle in the Study of Cell Locomotion. Science 1980;208(4440):177-179.
78. Lee J, Leonard M, Oliver T, Ishihara A, Jacobson K. Traction Forces Generated by Locomoting Keratocytes. Journal of Cell Biology 1994 Dec;127(6):1957-1964.
79. Burton K, Taylor DL. Traction forces of cytokinesis measured with optically modified elastic substrata. Nature 1997 Jan;385(6615):450-454.
80. Dembo M, Wang YL. Stresses at the cell-to-substrate interface during locomotion of fibroblasts. Biophysical Journal 1999 Apr;76(4):2307-2316.
81. Chen YW, Dokholyan NV. Insights into allosteric control of vinculin function from its large scale conformational dynamics. J Biol Chem 2006 Sep;281(39):29148-29154.
82. Defilippi P, Di Stefano P, Cabodi S. p130Cas: a versatile scaffold in signaling networks. Trends Cell Biol 2006 May;16(5):257-263.
83. Clark EA, King WG, Brugge JS, Symons M, Hynes RO. Integrin-mediated signals regulated by members of the Rho family of GTPases. J Cell Biol 1998 Jul;142(2):573-586.
84. Cox EA, Sastry SK, Huttenlocher A. Integrin-mediated adhesion regulates cell polarity and membrane protrusion through the Rho family of GTPases. Mol Biol Cell 2001 Feb;12(2):265-277.
85. Chaturvedi LS, Marsh HM, Basson MD. Src and focal adhesion kinase mediate mechanical strain-induced proliferation and ERK1/2 phosphorylation in human H441 pulmonary epithelial cells. Am J Physiol-Cell 2007 May;292(5):C1701-C1713.
86. Beningo KA, Wang YL. Flexible substrata for the detection of cellular traction forces. Trends in Cell Biology 2002 Feb;12(2):79-84.
87. Vogel V, Sheetz M. Local force and geometry sensing regulate cell functions. Nature Reviews Molecular Cell Biology 2006 Apr;7(4):265-275.
88. Harris AK. Tissue-culture cells on deformable substrata- Biomechanical implications. Journal of Biomechanical Engineering-Transactions of the Asme 1984;106(1):19-24.
89. Pelham RJ, Wang YL. Cell locomotion and focal adhesions are regulated by

substrate flexibility. Proceedings of the National Academy of Sciences of the United States of America 1997 Dec;94(25):13661-13665.
90. Pelham RJ, Wang YL. High resolution detection of mechanical forces exerted by locomoting fibroblasts on the substrate. Mol Biol Cell 1999;10(4):935-945.
91. Butler JP, Tolic-Norrelykke IM, Fabry B, Fredberg JJ. Traction fields, moments, and strain energy that cells exert on their surroundings. American Journal of Physiology-Cell Physiology 2002 Mar;282(3):C595-C605.
92. Yang ZC, Lin JS, Chen JX, Wang JHC. Determining substrate displacement and cell traction fields - a new approach. Journal of Theoretical Biology 2006 Oct;242(3):607-616.
93. Dong Y R, Lin JT, Bhattacharyya D. Determination of critical material parameters for numerical simulation of acrylic sheet forming. Journal of Materials Science 2005;40:399-410.
94. Kawamura T, Urayama K, Kohjiya S. Multiaxial deformations of end-linked poly(dimethylsiloxane) networks 5. Revisit to Mooney-Rivlin approach to strain energy density function. Journal of the Physical Society of Japan 2003;31(4):213-217.
95. Pearson I, Pickering M. The determination of a highly elastic adhesive's material properties and their representation in finite element analysis. Finite Elements in Analysis and Design 2001 Mar;37(3):221-232.
96. Sasso M, G. P, Chiappini G, Amodio D. Characterization of hyperelastic rubber-like materials by biaxial and uniaxial stretching tests based on optical methods. Polymer Testing 2008;27:995-1004.
97. Subhani PMR, K. KR. A New Stored Energy Function for Rubber Like Materials for Low Strains. Mechanics of Advanced Materials and Structures 2009;16:402-416.
98. Yu YS, Zhao YP. Deformation of PDMS membrane and microcantilever by a water droplet: Comparison between Mooney-Rivlin and linear elastic constitutive models. Journal of Colloid and Interface Science 2009 Apr;332(2):467-476.
99. Boudou T, Ohayon J, Picart C, Pettigrew RI, Tracqui P. Nonlinear elastic properties of polyacrylamide gels: Implications for quantification of cellular forces. Biorheology 2009;46(3):191-205.
100. Moore KA, Polte T, Huang S, Shi B, Alsberg E, Sunday ME, et al. Control of basement membrane remodeling and epithelial branching morphogenesis in embryonic lung by Rho and cytoskeletal tension. Developmental Dynamics 2005 Feb;232(2):268-281.
101. Benzeev A, Robinson GS, Bucher NLR, Farmer SR. Cell cell and cell matrix interactions differentially regulate the expression of hepatic and cytoskeletal genes in primary cultures of rat hepatocytes. Proc Natl Acad Sci U S A 1988 Apr;85(7):2161-2165.
102. Huang S, Ingber DE. Shape-dependent control of cell growth, differentiation, and apoptosis: Switching between attractors in cell regulatory networks. Experimental Cell Research 2000 Nov;261(1):91-103.
103. Lee KM, Tsai KY, Wang N, Ingber DE. Extracellular matrix and pulmonary hypertension: control of vascular smooth muscle cell contractility. American Journal of Physiology-Heart and Circulatory Physiology 1998 Jan;274(1):H76-H82.
104. Mochitate K, Pawelek P, Grinnell F. Stress-relaxation of contracted collagen gels-Disruption of actin filament bundles, release of cell-surface fibronectin, and down-

regulation of DNA and protein-synthesis. Experimental Cell Research 1991 Mar;193(1):198-207.
105. Jiang XY, Bruzewicz DA, Wong AP, Piel M, Whitesides GM. Directing cell migration with asymmetric micropatterns. Proc Natl Acad Sci U S A 2005 Jan;102(4):975-978.
106. Thakar RG, Cheng Q, Patel S, Chu J, Nasir M, Liepmann D, et al. Cell-Shape Regulation of Smooth Muscle Cell Proliferation. Biophysical Journal 2009 Apr;96(8):3423-3432.
107. Geisse NA, Sheehy SP, Parker KK. Control of myocyte remodeling in vitro with engineered substrates. In Vitro Cellular & Developmental Biology-Animal 2009 Aug;45(7):343-350.
108. Wang N, Ostuni E, Whitesides GM, Ingber DE. Micropatterning tractional forces in living cells. Cell Motility and the Cytoskeleton 2002 Jun;52(2):97-106.
109. Tolic-Norrelykke IM, Wang N. Traction in smooth muscle cells varies with cell spreading. Journal of Biomechanics 2005 Jul;38(7):1405-1412.
110. Bray MA, Sheehy SP, Parker KK. Sarcomere alignment is regulated by myocyte shape. Cell Motility and the Cytoskeleton 2008 Aug;65(8):641-651.
111. Lehnert D, Wehrle-Haller B, David C, Weiland U, Ballestrem C, Imhof BA, et al. Cell behaviour on micropatterned substrata: limits of extracellular matrix geometry for spreading and adhesion. Journal of Cell Science 2004 Jan;117(1):41-52.
112. Thery M, Racine V, Piel M, Pepin A, Dimitrov A, Chen Y, et al. Anisotropy of cell adhesive microenvironment governs cell internal organization and orientation of polarity. Proc Natl Acad Sci U S A 2006 Dec;103(52):19771-19776.
113. Estevez M, Fernandez-Ulibarri I, Martinez E, Egea G, Samitier J. Changes in the internal organization of the cell by microstructured substrates. Soft Matter 2010;6(3):582-590.
114. Cukierman E, Pankov R, Yamada KM. Cell interactions with three-dimensional matrices. Current Opinion in Cell Biology 2002 Oct;14(5):633-639.
115. Hahn C, Schwartz MA. Mechanotransduction in vascular physiology and atherogenesis. Nature Reviews Molecular Cell Biology 2009 Jan;10(1):53-62.
116. Lusis AJ. Atherosclerosis. Nature 2000 Sep;407(6801):233-241.
117. Owens GK. Regulation of differentiation of vascular smooth-muscle cells. Physiological Reviews 1995 Jul;75(3):487-517.
118. Ra HJ, Picart C, Feng HS, Sweeney HL, Discher DE. Muscle cell peeling from micropatterned collagen: direct probing of focal and molecular properties of matrix adhesion. Journal of Cell Science 1999 May;112(10):1425-1436.
119. Thakar RG, Ho F, Huang NF, Liepmann D, Li S. Regulation of vascular smooth muscle cells by micropatterning. Biochemical and Biophysical Research Communications 2003 Aug;307(4):883-890.
120. Feng J, Chan-Park MB, Shen JY, Chan V. Quick layer-by-layer assembly of aligned multilayers of vascular smooth muscle cells in deep microchannels. Tissue Engineering 2007 May;13(5):1003-1012.
121. Sarkar S, Dadhania M, Rourke P, Desai TA, Wong JY. Vascular tissue engineering: microtextured scaffold templates to control organization of vascular smooth muscle cells and extracellular matrix. Acta Biomaterialia 2005 Jan;1(1):93-100.
122. Cao Y, Poon YF, Feng J, Rayatpisheh S, Chan V, Chan-Park MB. Regulating

orientation and phenotype of primary vascular smooth muscle cells by biodegradable films patterned with arrays of microchannels and discontinuous microwalls. Biomaterials 2010 Aug;31(24):6228-6238.
123. Shen JY, Chan-Park MB, Zhu AP, Zhu X, Beuerman RW, Yang EB, et al. Three-dimensional microchannels in biodegradable polymeric films for control orientation and phenotype of vascular smooth muscle cells. Tissue Engineering 2006 Aug;12(8):2229-2240.
124. Cukierman E, Pankov R, Stevens DR, Yamada KM. Taking cell-matrix adhesions to the third dimension. Science 2001 Nov;294(5547):1708-1712.
125. Ishii I, Tomizawa A, Kawachi H, Suzuki T, Kotani A, Koshushi I, et al. Histological and functional analysis of vascular smooth muscle cells in a novel culture system with honeycomb-like structure. Atherosclerosis 2001 Oct;158(2):377-384.
126. Aigner T, Stöve J. Collagens - Major component of the physiological cartilage matrix, major target of cartilage degeneration, major tool in cartilage repair. Advanced Drug Delivery Reviews 2003;55(12):1569-1593.
127. Bryant SJ, Anseth KS. Hydrogel properties influence ECM production by chondrocytes photoencapsulated in poly(ethylene glycol) hydrogels. Journal of Biomedical Materials Research 2002;59(1):63-72.
128. Mann BK, Gobin AS, Tsai AT, Schmedlen RH, West JL. Smooth muscle cell growth in photopolymerized hydrogels with cell adhesive and proteolytically degradable domains: Synthetic ECM analogs for tissue engineering. Biomaterials 2001;22(22):3045-3051.
129. Wang DA, Williams CG, Li Q, Sharma B, Elisseeff JH. Synthesis and characterization of a novel degradable phosphate-containing hydrogel. Biomaterials 2003;24(22):3969-3980.
130. Elisseeff J. Injectable cartilage tissue engineering. Expert Opinion on Biological Therapy 2004;4(12):1849-1859.
131. Elisseeff J, McIntosh W, Anseth K, Riley S, Ragan P, Langer R. Photoencapsulation of chondrocytes in poly(ethylene oxide)-based semi- interpenetrating networks. Journal of Biomedical Materials Research 2000;51(2):164-171.
132. Elsdale T, Bard J. Collagen substrata for studies on cell behavior. Journal of Cell Biology 1972;54(3):626-&.
133. Von Der Mark K, Gauss V, Von Der Mark H, Mueller P. Relationship between cell shape and type of collagen synthesised as chondrocytes lose their cartilage phenotype in culture. Nature 1977;267(5611):531-532.
134. Benya PD, Padilla SR, Nimni ME. Independent regulation of collagen types by chondrocytes during the loss of differentiated function in culture. Cell 1978;15(4):1313-1321.
135. Wang Y, Kim UJ, Blasioli DJ, Kim HJ, Kaplan DL. In vitro cartilage tissue engineering with 3D porous aqueous-derived silk scaffolds and mesenchymal stem cells. Biomaterials 2005;26(34):7082-7094.
136. Benya PD, Shaffer JD. Dedifferentiated chondrocytes reexpress the differentiated collagen phenotype when cultured in agarose gels. Cell 1982;30(1):215-224.
137. Bonaventure J, Kadhom N, Cohen-Solal L, Ng KH, Bourguignon J, Lasselin C, et al. Reexpression of cartilage-specific genes by dedifferentiated human articular chondrocytes cultured in alginate beads. Experimental Cell Research 1994;212(1):97-

104.
138. Stevens MM, Qanadilo HF, Langer R, Shastri VP. A rapid-curing alginate gel system: Utility in periosteum-derived cartilage tissue engineering. Biomaterials 2004;25(5):887-894.
139. Chaipinyo K, Oakes BW, Van Damme MPI. The use of debrided human articular cartilage for autologous chondrocyte implantation: Maintenance of chondrocyte differentiation and proliferation in type I collagen gels. Journal of Orthopaedic Research 2004;22(2):446-455.
140. Takahashi T, Ogasawara T, Asawa Y, Mori Y, Uchinuma E, Takato T, et al. Three-dimensional microenvironments retain chondrocyte phenotypes during proliferation culture. Tissue Engineering 2007;13(7):1583-1592.
141. Malemud CJ, Stevenson S, Mehraban F, Papay RS, Purchio AF, Goldberg VM. The proteoglycan synthesis repertoire of rabbit chondrocytes maintained in type II collagen gels. Osteoarthritis and Cartilage 1994;2(1):29-41.
142. Ulijn RV, Bibi N, Jayawarna V, Thornton PD, Todd SJ, Mart RJ, et al. Bioresponsive hydrogels. Materials Today 2007;10(4):40-48.
143. Munevar S, Wang YL, Dembo M. Traction force microscopy of migrating normal and H-ras transformed 3T3 fibroblasts. Biophysical Journal 2001 Apr;80(4):1744-1757.
144. Harris AK. Tissue-culture cells on deformable substrata- Biomechanical implication. J Biomech Eng-T ASME 1984;106(1):19-24.
145. Dembo M, Oliver T, Ishihara A, Jacobson K. Imaging the traction stresses exerted by locomoting cells with the elastic substratum method. Biophysical Journal 1996 Apr;70(4):2008-2022.
146. Chu TC, Ranson WF, Sutton MA. Applications of digital-image-correlation techniques to experimental mechanics. Exp Mech 1985;25(3):232-244.
147. Brock A, Chang E, Ho CC, LeDuc P, Jiang XY, Whitesides GM, et al. Geometric determinants of directional cell motility revealed using microcontact printing. Langmuir 2003 Mar;19(5):1611-1617.
148. Berfield TA, Patel JK, Shimmin RG, Braun PV, Lambros J, Sottos NR. Micro- and Nanoscale Deformation Measurement of Surface and Internal Planes via Digital Image Correlation. Experimental Mechanics 2007;47:51-62.
149. Ghosh K, Pan Z, Guan E, Ge SR, Liu YJ, Nakamura T, et al. Cell adaptation to a physiologically relevant ECM mimic with different viscoelastic properties. Biomaterials 2007 Feb;28(4):671-679.
150. Wang JHC, Lin JS. Cell traction force and measurement methods. Biomechanics and Modeling in Mechanobiology 2007 Nov;6(6):361-371.
151. Alpin JD, Hughes C. Protein-derivatised glass coverslips for the study of cell-to-substratum adhesions. Anal Biochem 1981;113:144.
152. Wang YL, Pelham RJ. Preparation of a flexible, porous polyacrylamide substrate for mechanical studies of cultured cells. Molecular Motors and the Cytoskeleton, Pt B, 1998. p. 489-496.
153. Kandow CE, Georges PC, Janmey PA, Beningo KA. Polyacrylamidc hydrogels for cell mechanics: Steps toward optimization and alternative uses. Cell Mechanics, 2007. p. 29-+.
154. Beningo KA, Lo CM, Wang YL. Flexible polyacrylamide substrata for the analysis of mechanical interactions at cell-substratum adhesions. Methods in Cell-Matrix

Adhesion, 2002. p. 325-339.
155. Domke J, Radmacher M. Measuring the elastic properties of thin polymer films with the atomic force microscope. Langmuir 1998 Jun;14(12):3320-3325.
156. Engler AJ, Richert L, Wong JY, Picart C, Discher DE. Surface probe measurements of the elasticity of sectioned tissue, thin gels and polyelectrolyte multilayer films: Correlations between substrate stiffness and cell adhesion. Surface Science 2004 Oct;570(1-2):142-154.
157. Johnson KL. Contact Mechanics. Cambridge University Press 1985.
158. Damljanovic V, Lagerholm BC, Jacobson K. Bulk and micropatterned conjugation of extracellular matrix proteins to characterized polyacrylamide substrates for cell mechanotransduction assays. Biotechniques 2005 Dec;39(6):847-851.
159. Sun YJ, Akhremitchev B, Walker GC. Using the adhesive interaction between atomic force microscopy tips and polymer surfaces to measure the elastic modulus of compliant samples. Langmuir 2004 Jul;20(14):5837-5845.
160. Yeung T, Georges PC, Flanagan LA, Marg B, Ortiz M, Funaki M, et al. Effects of substrate stiffness on cell morphology, cytoskeletal structure, and adhesion. Cell Motility and the Cytoskeleton 2005 Jan;60(1):24-34.
161. A-Hassan E, Heinz WF, Antonik MD, D'Costa NP, Nageswaran S, Schoenenberger CA, et al. Relative microelastic mapping of living cells by atomic force microscopy. Biophysical Journal 1998 Mar;74(3):1564-1578.
162. Ludwig T, Kirmse R, Poole K, Schwarz US. Probing cellular microenvironments and tissue remodeling by atomic force microscopy. Pflugers Archiv-European Journal of Physiology 2008 Apr;456(1):29-49.
163. Pearson I, Pickering M. The determination of a highly elastic adhesive's material properties and their representation in finite element analysis. Finite Elem Anal Des 2001 Mar;37(3):221-232.
164. Yu YS, Zhao YP. Deformation of PDMS membrane and microcantilever by a water droplet: Comparison between Mooney-Rivlin and linear elastic constitutive models. J Colloid Interf Sci 2009 Apr;332(2):467-476.
165. Sasso M, G. P, Chiappini G, Amodio D. Characterization of hyperelastic rubber-like materials by biaxial and uniaxial stretching tests based on optical methods. Polym Test 2008;27:995-1004.
166. Subhani PMR, K. KR. A New Stored Energy Function for Rubber Like Materials for Low Strains. Mech Adv Mater Struct 2009;16:402-416.
167. Kawamura T, Urayama K, Kohjiya S. Multiaxial deformations of end-linked poly(dimethylsiloxane) networks 5. Revisit to Mooney-Rivlin approach to strain energy density function. J Rhel Soc Jap 2003;31(4):213-217.
168. Dong Y R, Lin JT, Bhattacharyya D. Determination of critical material parameters for numerical simulation of acrylic sheet forming. J Mater Sci 2005;40:399-410.
169. Sabass B, Gardel ML, Waterman CM, Schwarz US. High resolution traction force microscopy based on experimental and computational advances. Biophysical Journal 2008 Jan;94(1):207-220.
170. Ingber DE. Cellular mechanotransduction: putting all the pieces together again. FASEB 2006 May;20(7):811-827.
171. Ananthakrishnan R, Allen Ehrlicher A. The Forces Behind Cell Movement. Int J Biol Sci 2007;3(5):303-317.

172. Guo W-H, Wang Y-L. Retrograde Fluxes of Focal Adhesion Proteins in Response to Cell Migration and Mechanical Signals. Mol Biol Cell 2007;18(4519-4527).
173. Mori N, Chang K-A. Introduction to mPIV: PIV toolbox in MATLAB version 0.96. 2004.
174. Jensen A, Sveen JK, Grue J, Richon JB, Gray C. Accelerations in water waves by extended particle image velocimetry. Exp Fluids 2001;30:500-510.
175. Sveen JK, E. Cowen A. Quantitative imaging techniques and their application to wavy flow. PIV and Water Waves. World Scientific 2004.
176. Gui L, Merzkirch W. Generating arbitrarily sized interrogation windows for correlation-based analysis of particle image velocimetry recordings. Exp Fluids 1996;21:465-468.
177. Gui L, Merzkirch W. A comparative study of the mqd method and several correlation-based PIV evaluation algorithms. Exp Fluids 2000;28:36-44.
178. Krige DG. A statistical approach to some mine valuations and allied problems at the Witwatersrand [Master's thesis]: University of Witwatersrand; 1951.
179. Matheron G. Principles of Geostatistics. Econ Geol 1963;58:1246-1266.
180. Matheron G. The intrinsic random functions, and their applications. Adv Appl Prob 1973;5:439-468.
181. Hur SS, Zhao Y, Li Y-S, Botvinick E, Chien S. Live Cells Exert 3-Dimensional Traction Forces on Their Substrata. Cell Mol Bioeng 2009 SEP 2009 2(3):425-436.
182. Xia N, Thodeti CK, Hunt TP, Xu Q, Ho M, Whitesides GM, et al. Directional control of cell motility through focal adhesion positioning and spatial control of Rac activation. FASEB 2008;22(6):1649-1659
183. Tan JL, Tien J, Pirone DM, Gray DS, Bhadriraju K, CS C. Cells lying on a bed of microneedles: An approach to isolate mechanical force. PROCEEDINGS OF THE NATIONAL ACADEMY OF SCIENCES OF THE UNITED STATES OF AMERICA 2003 FEB 18 2003 100(4):1484-1489.
184. Hur SS, Zhao YH, Li YS, Botvinick E, Chien S. Live Cells Exert 3-Dimensional Traction Forces on Their Substrata. Cellular and Molecular Bioengineering 2009 Sep;2(3):425-436.
185. Gerald CF, Wheatley PO. Applied Numerical Analysis. 3rd ed. California: Addison- Wesley Publishing Company, 1984.
186. Thery M, Racine V, Pepin A, Piel M, Chen Y, Sibarita JB, et al. The extracellular matrix guides the orientation of the cell division axis. Nature Cell Biology 2005 Oct;7(10):947-U929.
187. Chen CS, Ingber DE. Tensegrity and mechanoregulation: from skeleton to cytoskeleton. Osteoarthritis and Cartilage 1999 Jan;7(1):81-94.
188. Dahl KN, Booth-Gauthier EA, Ladoux B. In the middle of it all: Mutual mechanical regulation between the nucleus and the cytoskeleton. Journal of Biomechanics Jan;43(1):2-8.
189. Li B, Lin M, Tang Y, Wang B, Wang JHC. A novel functional assessment of the differentiation of micropatterned muscle cells. Journal of Biomechanics 2008 Dec;41(16):3349-3353.
190. Tolic-Nørrelykke IM, Wang N. Traction in smooth muscle cells varies with cell spreading. Journal of Biomechanics 2005;38(7):1405-1412.
191. Thery M, Pepin A, Dressaire E, Chen Y, Bornens M. Cell distribution of stress

fibres in response to the geometry of the adhesive environment. Cell Motility and the Cytoskeleton 2006 Jun;63(6):341-355.
192. Kang ET, Zhang Y. Surface modification of fluoropolymers via molecular design. Advanced Materials 2000 Oct;12(20):1481-1494.
193. Yang MR, Chen KS. Wettability and lubrication of polytetrafluorethylene (PTFE) by UV-induced graft copolymerization on plasma-treated surface. Materials Chemistry and Physics 1997 Aug;50(1):11-14.
194. Yang GH, Zhang Y, Lee KS, Kang ET, Neoh KG. Thermal imidization of poly(pyromellitic dianhydride-4, 4 '-oxydianiline) precursors on fluoropolymers modified by surface graft-copolymerization with glycidyl methacrylate. Journal of Fluorine Chemistry 2003 Feb;119(2):151-160.
195. Reinhart-King CA, Dembo M, Hammer DA. The dynamics and mechanics of endothelial cell spreading. Biophysical Journal 2005 Jul;89(1):676-689.
196. Sukkar MB, Stanley AJ, Blake AE, Hodgkin PD, Johnson PRA, Armour CL, et al. 'Proliferative' and 'synthetic' airway smooth muscle cells are overlapping populations. Immunology and Cell Biology 2004 Oct;82(5):471-478.
197. Moussallem MD, Olenych SG, Scott SL, Keller TCS, Schlenoff JB. Smooth Muscle Cell Phenotype Modulation and Contraction on Native and Cross-Linked Polyelectrolyte Multilayers. Biomacromolecules 2009 Nov;10(11):3062-3068.
198. Thakar RG, Chown MG, Patel A, Peng L, Kumar S, Desai TA. Contractility-dependent modulation of cell proliferation and adhesion by microscale topographical cues. Small 2008 Sep;4(9):1416-1424.
199. Lang A, Brenner DA. Gene regulation in hepatic stellate cell. Italian Journal of Gastroenterology and Hepatology 1999 Mar;31(2):173-179.
200. Pelletier S, Julien C, Popoff MR, Lamarche-Vane N, Meloche S. Cyclic AMP induces morphological changes of vascular smooth muscle cells by inhibiting a Rac-dependent signaling pathway. Journal of Cellular Physiology 2005 Aug;204(2):412-422.
201. Tan JL, Tien J, Pirone DM, Gray DS, Bhadriraju K, Chen CS. Cells lying on a bed of microneedles: An approach to isolate mechanical force. Proc Natl Acad Sci U S A 2003 Feb;100(4):1484-1489.
202. Buschmann MD, Gluzband YA, Grodzinsky AJ, Kimura JH, Hunziker EB. Chondrocytes in agarose culture synthesize a mechanically functional extracellular-matrix. Journal of Orthopaedic Research 1992 Nov;10(6):745-758.
203. Homicz MR, Chia SH, Schumacher BL, Masuda K, Thonar EJ, Sah RL, et al. Human septal chondrocyte redifferentiation in alginate, polyglycolic acid scaffold, and monolayer culture. Laryngoscope 2003 Jan;113(1):25-32.
204. Francioli SE, Candrian C, Martin K, Heberer M, Martin I, Barbero A. Effect of three-dimensional expansion and cell seeding density on the cartilage-forming capacity of human articular chondrocytes in type II collagen sponges. Journal of Biomedical Materials Research Part A Dec;95A(3):924-931.
205. Gong YH, Su K, Lau TT, Zhou RJ, Wang DA. Microcavitary Hydrogel-Mediating Phase Transfer Cell Culture for Cartilage Tissue Engineering. Tissue Engineering Part A 2010 Dec;16(12):3611-3622.
206. Ladet SG, Tahiri K, Montembault AS, Domard AJ, Corvol MTM. Multi-membrane chitosan hydrogels as chondrocytic cell bioreactors. Biomaterials 2011;32(23):5354-5364.

207. Wang DA, Varghese S, Sharma B, Strehin I, Fermanian S, Gorham J, et al. Multifunctional chondroitin sulphate for cartilage tissue-biomaterial integration. Nature Materials 2007;6(5):385-392.
208. Pescosolido L, Vermonden T, Malda J, Censi R, Dhert WJA, Alhaique F, et al. In situ forming IPN hydrogels of calcium alginate and dextran-HEMA for biomedical applications. Acta Biomaterialia 2011;7(4):1627-1633.
209. Appelman TP, Mizrahi J, Elisseeff JH, Seliktar D. The influence of biological motifs and dynamic mechanical stimulation in hydrogel scaffold systems on the phenotype of chondrocytes. Biomaterials 2011;32(6):1508-1516.
210. Park H, Temenoff JS, Holland TA, Tabata Y, Mikos AG. Delivery of TGF-β1 and chondrocytes via injectable, biodegradable hydrogels for cartilage tissue engineering applications. Biomaterials 2005;26(34):7095-7103.
211. Klein TJ, Rizzi SC, Schrobback K, Reichert JC, Jeon JE, Crawford RW, et al. Long-term effects of hydrogel properties on human chondrocyte behavior. Soft Matter 2010;6(20):5175-5183.
212. Gong YH, Wang CM, Lai RC, Su K, Zhang F, Wang DA. An improved injectable polysaccharide hydrogel: modified gellan gum for long-term cartilage regeneration in vitro. Journal of Materials Chemistry 2009;19(14):1968-1977.
213. Ladet S, Tahiri K, Montembault A, Domard A, Corvol M. Multi-membrane chitosan hydrogels as chondrocytic cell bioreactors. Biomaterials 2011 May 5;32(23):5354-5364.
214. Park H, Temenoff JS, Holland TA, Tabata Y, Mikos AG. Delivery of TGF-beta 1 and chondrocytes via injectable, biodegradable hydrogels for cartilage tissue engineering applications. Biomaterials 2005 Dec;26(34):7095-7103.
215. Pedersen JA, Swartz MA. Mechanobiology in the third dimension. Annals of Biomedical Engineering 2005 Nov;33(11):1469-1490.
216. Pampaloni F, Reynaud EG, Stelzer EHK. The third dimension bridges the gap between cell culture and live tissue. Nature Reviews Molecular Cell Biology 2007 Oct;8(10):839-845.
217. Kim EJ, Guilak F, Haider MA. The Dynamic Mechanical Environment of the Chondrocyte: A Biphasic Finite Element Model of Cell-Matrix Interactions Under Cyclic Compressive Loading. Journal of Biomechanical Engineering-Transactions of the Asme 2008 Dec;130(6).
218. Guilak F, Mow VC. The mechanical environment of the chondrocyte: a biphasic finite element model of cell-matrix interactions in articular cartilage. Journal of Biomechanics 2000 Dec;33(12):1663-1673.
219. Alexopoulos LG, Setton LA, Guilak F. The biomechanical role of the chondrocyte pericellular matrix in articular cartilage. Acta Biomaterialia 2005 May;1(3):317-325.
220. Yu W, Gu N, Zhang HQ, Wu JG, Wang YH, Wesche KD. Microarray preparation based on oxidation of agarose-gel and subsequent enzyme immunoassay. Sensors and Actuators B-Chemical 2004 Mar;98(1):83-91.
221. Lin CC, Anseth KS. PEG Hydrogels for the Controlled Release of Biomolecules in Regenerative Medicine. Pharmaceutical Research 2009 Mar;26(3):631-643.
222. Fraley SI, Feng YF, Krishnamurthy R, Kim DH, Celedon A, Longmore GD, et al. A distinctive role for focal adhesion proteins in three-dimensional cell motility. Nature Cell Biology 2010 Jun;12(6):598-U169.

223. Bloom RJ, George JP, Celedon A, Sun SX, Wirtz D. Mapping local matrix remodeling induced by a migrating tumor cell using three-dimensional multiple-particle tracking. Biophysical Journal 2008 Oct;95(8):4077-4088.
224. Toprak E, Balci H, Blehm BH, Selvin PR. Three-dimensional particle tracking via bifocal imaging. Nano Letters 2007 Jul;7(7):2043-2045.
225. Decaestecker C, Debeir O, P VH. Can anti-migratory drugs be screened in vitro? A review of 2D and 3D assays for the quantitative analysis of cell migration MEDICINAL RESEARCH REVIEWS 2007 MAR 2007 27(2):149-176.
226. Wolf K, Mazo I, Leung H, Engelke K, von Andrian UH, Deryugina EI, et al. Compensation mechanism in tumor cell migration: mesenchymal-amoeboid transition after blocking of pericellular proteolysis. Journal of Cell Biology 2003 Jan;160(2):267-277.

Appendix: Publication

1. Xi Li, Huixing Feng, Beiyi Chen, Soon Seng Ng, Wei Ning Chen, Vincent Chan. "Epigallocatechin-3-gallate induced modulation of cell deadhesion and migration on thermosensitive poly(N-isopropylacrylamide)". **Journal of Biomedical Materials Research Part A 2011** September; 98A(3): 450-460.
2. Soon Seng Ng, Chuan Li, Vincent Chan. "Experimental and numerical determination of cellular traction force on polymeric hydrogels". **Interface Focus. 2011**doi: 10.1098/ rsfs.2011.0036. *In press*
3. Soon Seng Ng, Kai Su, Chuan Li, Mary B. Chan-Park, Dong-An Wang , Vincent Chan. "Bio-mechanical study on edge outgrowing phenomenon of encapsulated chondrocytic isogenous groups in surface layer of hydrogel scaffolds for cartilage tissue engineering". **Acta Biomaterialia. 2011**. *In press*.
4. Tao He, Soon Seng Ng, Vincent Chan. "Bio-selective Adhesion Surface Based on an Anti-adhesive Dextran Sulfate/Chitosan Multilayer and Specific Adhesive Ligand RGD". *Submitted*
5. Soon Seng Ng, Xi Li, Chuan Li, Mary B. Chan-Park, Vincent Chan. "The effect of two-dimensional and topographic characteristics on cellular traction force". 2011. *In writing*.